Studies on high-power and rare-metal-free nickel-metal hydride batteries for industrial applications

Nishimura, Kazuya

(Degree)
博士（工学）

(Date of Degree)
2014-03-25

(Date of Publication)
2015-03-01

(Resource Type)
doctoral thesis

(Report Number)
甲第6097号

(URL)
https://hdl.handle.net/20.500.14094/D1006097

博　士　論　文

Studies on high-power and rare-metal-free nickel-metal hydride batteries for Industrial applications

(産業用ニッケル水素電池の高出力化とレアメタルフリー化に関する研究)

平成２６年１月

神戸大学大学院工学研究科

西　村　　和　也

Contents

Chapter 4. Development of fiber-type Ni(OH)2 electrodes for Ni-MH battery

Chapter 1

General introduction

1.1 Scope

After the industrial revolution, mankind invented a method to get electrical energy from fossil fuels. Energy consumption has then exponentially increased by the shift to industrialization with mass-production and mass-consumption and the information-oriented society with the development of the IT technique, that caused various environmental problems such as limited fossil fuels, air pollution and global warming.

The development of alternative energy sources is indispensable to control the occurrence of environmental problems and to continue economic development. Moreover, it is important to minimize the consumption of fossil fuels by pushing forward the development of energy-saving techniques. These new technologies have attracted much interest by the global deployment of a new fiscal policy “Green New Deal”. As an alternative energy source, a method to convert natural energy sources, such as solar, wind and tidal powers, into electric energy has been energetically investigated. For the natural power sources, the quantity of generation easily fluctuates dependent on the local weather and time. A stable electricity supply is required in order to use these energy sources as a social power supply network. Energy storage devices can effectively improve the noticeable fluctuations in the generated power. Large-sized energy storage systems, such as secondary batteries, should be developed and widely used for renewable energy applications.

Currently, Pb-acid batteries have been widely used as the battery for industrial applications. The reason why this battery has been widely used is because it is economical and inexpensive [1]. However, the Pb-acid battery has a low energy-density and power, and the Pb causes environmental problems.

The R&D studies of secondary batteries are now focused on applications for use in a

hybrid electric vehicle (HEV) and electric vehicle (EV). The HEV, which realizes on energy-savings by combining the gasoline engine and battery, has been commercialized and widely used [2-7]. Over 3 million of the HEV “Prius” commercialized by Toyota were sold during the past 15 years [8]. The nickel-metal hydride (Ni-MH) battery is generally used as the battery of HEVs.

In the near future, a smart grid, which is a method of controlling the renewable energies with large load-fluctuations by secondary batteries and IT technology, will be developed and applied on a global scale. In this situation, requirements for further high-performance rechargeable batteries would be increased [9 - 11]. The total energy management, which performs energy storage and supply between a plug-in hybrid electric vehicle (PHEV) and the power grid (smart grid), is examined and introduced.

As the larger-scale battery applications, a battery-driven light rail vehicle (LRV) and wayside energy storage system for railways, which stores regenerative energy and supplies the stored power to other trains, has been developed [12-21]. The large-scale battery systems capable of delivering several hundreds of kWhs are necessary for the railway applications [15-19, 22, 23]. Verification tests have been carried out for both the Ni-MH battery [12-19] and the Li-ion battery [20-21]. However, their expensive costs have to be reduced for the widespread use of these applications. The development of these high-performance large-scale battery systems would promote penetration into the social-infrastructure of future large-scale grid systems.

The Ni-MH battery does not contain elements which have a significant impact on the environment, and uses hydrogen as the active material. Hydrogen is a clean energy source. However, large containers are necessary to store the gaseous hydrogen. Therefore, a hydrogen storage material is necessary as the medium to store gaseous hydrogen at a normal pressure and ambient temperature [24-26]. In this battery, an

alkaline aqueous solution is used as the electrolyte thus it exhibits a superior safety to the lithium-ion (Li-ion) battery, which uses a combustible organic electrolyte. For the Li-ion battery, safety is one of the most important subjects in the development of a large-sized cell. Energetic research by many groups has remarkably improved the safety of the Li-ion battery [27, 28], but the development of a large-sized Ni-MH battery, which uses a noncombustible electrolyte, plays a significant role in ensuring the widespread use of energy-storage devices for industrial applications.

1.2 Background of this research

A device picking up electric energy using the oxidation-reduction reaction of materials is called a chemical battery. Chemical batteries are classified into three groups, namely, the primary battery, secondary battery and fuel cell. For the secondary battery, a reverse current needs to flow through the battery which has discharged in order to return it to its original state before the discharge again. In other words, a secondary battery may be called a rechargeable battery because it is a battery which can be charged [29, 30].

The first secondary battery was the Pb-acid battery invented by R.L.G. Planté in 1859. In 1899, Swedish W. Junger developed the nickel-cadmium (Ni-Cd) secondary battery, and in 1900, American T. Edison developed the nickel-iron (Ni-Fe) secondary battery. Edison's Ni-Fe battery was used as a power source of an electric vehicle which was able to travel 160km on one charge. Junger's Ni-Cd battery was commercialized in 1946, and was widely used as a small consumer battery.

In 1990, the nickel-metal hydride (Ni-MH) battery was developed using a combination of hydrogen storage alloys and battery technologies [2]. This battery has a two times higher energy density and fewer environmental problems, but is much more

expensive than the conventional Ni-Cd battery. As the legal regulations for the disposal of Ni-Cd batteries became very strict, replacing Ni-Cd batteries with Ni-MH batteries in the small rechargeable battery market rapidly expanded. The Ni-MH batteries are widely used as the power sources of hybrid electric vehicles (HEVs) as well as consumer electronic devices. The demand for the Ni-MH batteries is increasing due to the increasing focus on the environment and its sustainability.

In the 1950s, the development of a battery using metallic lithium (Li) as the anode, which can provide a higher energy density than other anode materials, occurred [31]. In the 1970s, the lithium primary cell was commercialized [32]. Moreover, in 1991, the first Li-ion battery, which uses $LiCoO_2$ and carbon as the cathode and anode materials, respectively, was developed and commercialized [33, 34]. The Li-ion batteries have been used as the power source of consumer electric devices, such as mobile phones, laptop computers and power tools because of its superior high energy density.

1.3 General concept of the nickel-metal hydride battery

The nickel-metal hydride (Ni-MH) battery has emerged from the conventional alkaline secondary battery using a different negative-electrode material. The principle of the Ni-MH battery is explained in the Fig. 1.1. Nickel hydroxide ($Ni(OH)_2$) and a metal hydride (MH) are used as the positive and negative electrode materials, respectively. As the electrolyte, a potassium hydroxide-based aqueous solution is used.

The metal hydride (MH) is a hydrogen absorbed alloy, and $LaNi_5H_6$ is one of the representative examples. For the commercialized Ni-MH batteries, Mm (mish metal) has been used instead of La because of its performance and cost. Part of the Ni is replaced by several other transition metals such as cobalt (Co), manganese (Mn) and aluminum (Al).

The charge and discharge reactions are expressed as follows [35].

Positive: $Ni(OH)_2 + OH^- \leftrightarrow NiOOH + H_2O + e^-$ (1.1)

Negative: $M + H_2O \leftrightarrow MH + OH^-$ (1.2)

Overall reaction: $Ni(OH)_2 + M \leftrightarrow NiOOH + MH$ (1.3)

As shown by reaction (1.3), the water does not contribute to the battery reaction. Therefore, the electrolyte density is constantly maintained. The theoretical electromotive force, the real working voltage and the operating temperature are almost the same as those of a nickel-cadmium battery.

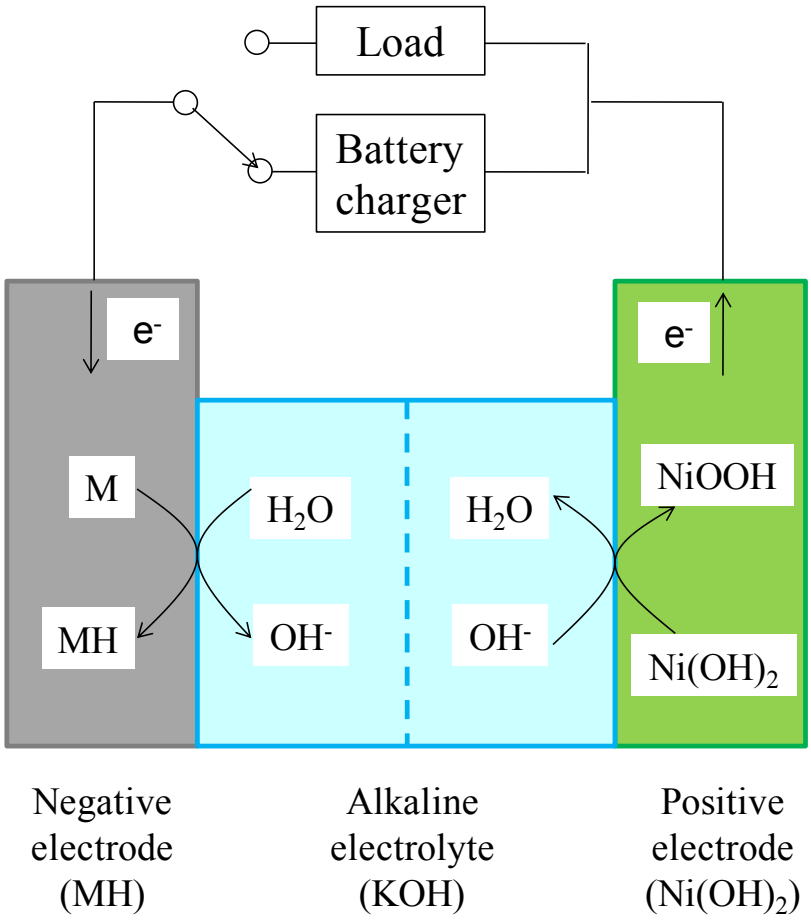

Figure 1.1: Schematic view of charge reaction for Ni-MH battery.

During the charging process, the positive $Ni(OH)_2$ is converted to nickel oxy-hydroxide (NiOOH), and hydrogen is electrochemically absorbed by the negative electrode alloy. Moreover, during the overcharging process, oxygen is generated in the positive electrode by water-electrolysis. This oxygen changes into a hydroxyl group at the negative alloy surface as shown by reactions (1.4) and (1.5).

$$\text{Positive:} \quad 4OH^- \rightarrow 2H_2O + O_2 + 4e^- \qquad (1.4)$$

$$\text{Negative:} \quad 2H_2O + O_2 + 4e^- \rightarrow 4OH^- \qquad (1.5)$$

1.4 Components for Ni-MH battery

1.4.1 Positive electrode

The nickel hydroxide, $Ni(OH)_2$, is used as the positive-electrode material. This material is a layered compound with a CdI_2-type crystal structure [36, 37]. As shown in Fig. 1.2, the nickel-ion is sandwiched between the hexagonally closed packed hydroxide-ion layers, corresponding to the octahedral coordinated layered-structure. The OH bonding arranges in the *c*-axis direction that is perpendicular to the layer. The interlayer distance is approximately 4.6Å, and the layers are connected by van der Waals forces, meaning that the hydrogen ion (proton) can easily move. This crystal structure is called β-$Ni(OH)_2$, and its density is 3.97g/cm^3. The interlayer distance increases to 7Å upon water-molecule intercalation. This structure is called α-$Ni(OH)_2$, and its density is 2.82g/cm^3.

The β-$Ni(OH)_2$ has been generally used as the positive active material of alkaline secondary battery. Its layered structure is maintained during the charge and discharge processes, and the proton goes in and out between the layers. The nickel valence is transformed between 2^+ and 3^+ during the typical charging and discharging.

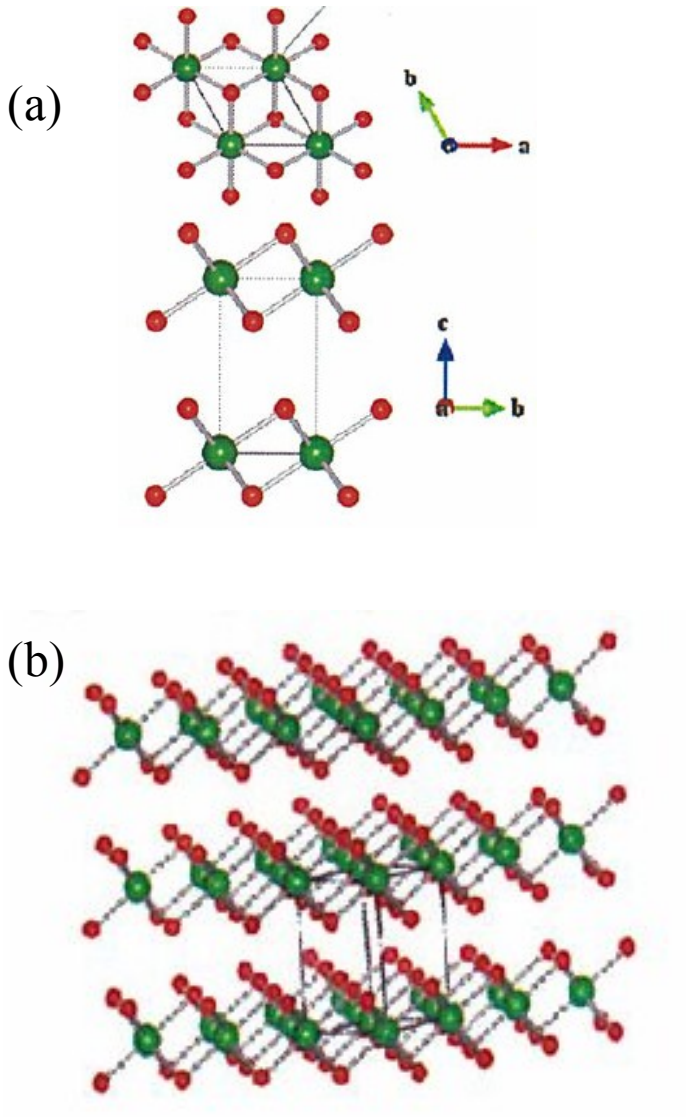

Figure 1.2: Crystal structure of β-$Ni(OH)_2$, (a) primitive lattice, (b) outline of atomic arrangement

The α-$Ni(OH)_2$, involving the α-$Ni(OH)_2$/γ-NiOOH transition, has received much attention as a high-capacity active material for the positive electrode of advanced Ni-MH batteries. In this reaction, the nickel valence would be increased to 3.3 – 3.7. In general, the pure α-$Ni(OH)_2$ is unstable in an alkali electrolyte, being easily transformed

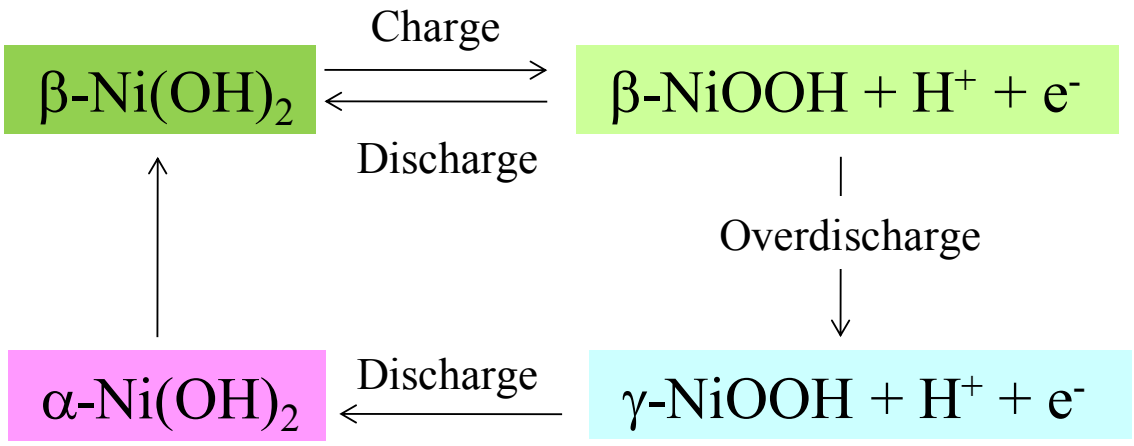

Figure 1.3: Charge and discharge behavior of nickel hydroxide (Bode diagram).

into β-$Ni(OH)_2$ as shown in Fig.1.3. To stabilize the α-$Ni(OH)_2$ structure, partial substitution of the nickel in the $Ni(OH)_2$ by other elements, such as Co [38], Fe [39], Mn [40-42], Al [43], and Zn [44], have been carried out. Substitution by trivalent Al ions over 20mol% stabilizes the α-$Ni(OH)_2$ structure. In recent studies, several new Al-substituted materials, such as the α-$Ni(OH)_2$ thin film [45] and α-$Ni(OH)_2$/carbon composite [46], were developed by a liquid phase deposition method.

However, the α-$Ni(OH)_2$/γ-NiOOH transformation produces a 30% volume change, causing the active-material separation from the substrate and capacity decay. Furthermore, the γ-NiOOH would be formed during the overcharge of the β-$Ni(OH)_2$. The expanded γ-NiOOH absorbs electrolyte, and then causes dry out of the battery. Generally, zinc or magnesium are coprecipitated with the $Ni(OH)_2$ to prevent the formation of γ-NiOOH [47]. In order to create a greater high-capacity positive electrode, the utilization of the α-$Ni(OH)_2$/γ-NiOOH transformation is expected.

A paste-type electrode is generally used for the Ni-MH battery in order to increase the energy density of the nickel positive electrode [48-50]. This electrode is comprised of a spherical $Ni(OH)_2$ powder which is loaded on a porous nickel foam substrate. In

order to improve the low electrical conductivity of $Ni(OH)_2$ and increase the active-material utilization, the addition of a conductive agent is required. In general, the surface of the $Ni(OH)_2$ particle is coated with cobalt materials such as $Co(OH)_2$, CoO and CoOOH [48,49,51,52]. The cobalt materials are transformed into CoOOH having a high electrical conductivity during the charging process.

1.4.2 Negative electrode

The negative electrode alloy is required to have a high reversible hydrogen capacity at room temperature and long cycle-life performance in an alkaline electrolyte. In order to satisfy these requirements, the material consisting of light elements with a reversible hydrogen storage property at room temperature, alkaline resistance and oxidation resistance is required. There are few materials meeting these specifications in spite of many hydrogen storage materials.

In general, the AB_5 type $Mm(Ni,Co,Mn,Al)_5$ (Mm: misch-metal, A: Mm, B: transition metals and Al) alloys have been used as the negative material. In these types of alloys, cobalt (Co) is added to improve the cycle-life performance of the alloy electrode. The manganese (Mn) and aluminum (Al) are added to regulate the hydrogen equilibrium pressure (EP). The Mn can regulate the EP without reducing the hydrogen storage capacity. However, the Co and manganese (Mn) cause an increased self-discharge [53-55]. In the 1970s, the $MmNi_5$ and $MmNi_{5-x}M_x$ (M = Co, Mn and Al) base materials had already been developed and their hydrogen storage properties investigated [56, 57]. In the 1980s, these alloys were developed as the negative materials of an alkaline secondary battery [58, 59]. In the 1990s, these materials were used for commercialized Ni-MH batteries [1, 60].

The AB_2-type alloys (A: Ti, Zr, B:Ni, V, Mn, Co, Cr, Al, etc.) were also used as the

negative alloy [61 - 64]. The theoretical capacity of this alloy is greater than that of the AB_5-type one. However, these alloys are not used because of the difficulty of activation and the various battery performance deteriorations such as cycle-life, power and self-discharge.

In 1997, the $REMg_2T_9$ (AB_3; RE = rare earth, T = transition metals) with the high discharge capacity of 370mAh/g was discovered [65-71], and this discovery has led to the development of various RE-Mg-Ni based alloys ($AB_{3.0\text{-}3.7}$; A = La, Pr, Nd and Mg, B = Ni, Al, Co, Mn) [72-75]. In these crystal structures, the AB_5 lattice and AB_2 one are alternately stacked in the c-axis direction. The stacked structure would maintain a good cycle-life performance in spite of the Co-less or Co-free composition. Dependent on the stacking numbers, various crystal structures, such as the $PuNi_3$-type、Ce_2Ni_7-type and Pr_5Co_{19}-type ones, exist as shown in Fig. 1.4.

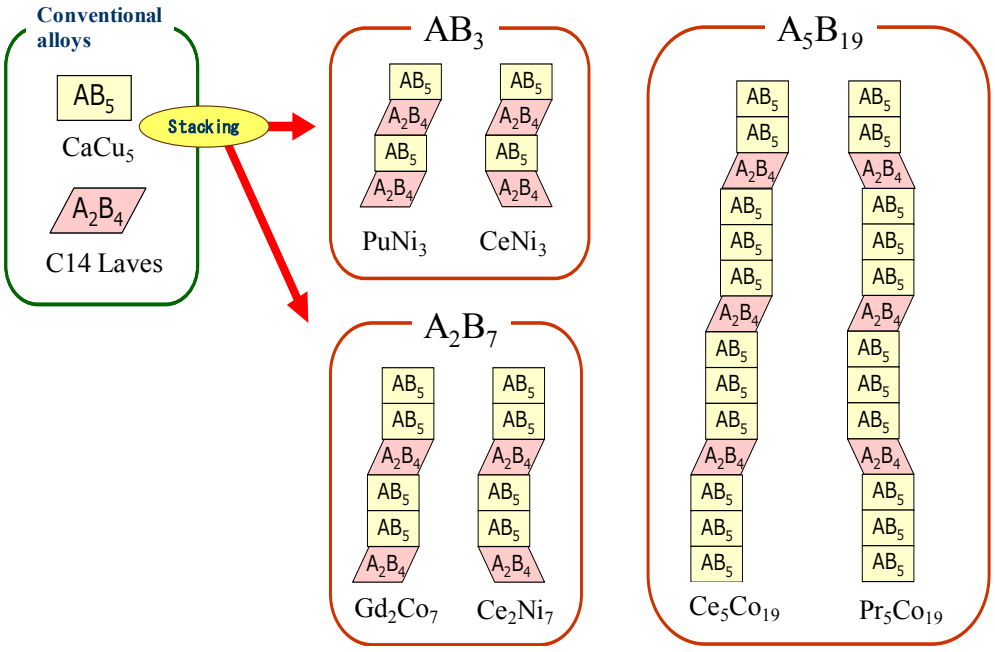

Figure 1.4: Schematic view (perpendicular to c-axis direction) of stacking structure observed in RE-Mg-Ni based alloys.

1.4.3 Separator [76]

The role of the separator is to separate both electrodes so that the positive one does not make electrical contact with the negative one. Moreover, various functions, such as electrolyte retention between both electrodes, gas permeability, absorbing the volume changes in the electrodes and trapping the deposit are required to maintain the battery performance.

Previously, a nonwoven nylon fabric was used as the separator of an alkaline secondary battery [53]. However, the nylon easily decomposed during the overcharge process or the dried out, and poor safety was a problem. Currently, a polyolefin fabric, such as the nonwoven fabric of polypropylene fibers is generally used. In order to improve the hydrophilicity of the polyolefin fiber, a hydrophilic processing with fuming sulfuric acid is carried out.

A thinner separator is generally desirable to preserve the battery capacity and increase the power capability. Meanwhile, a thin separator can cause short-circuiting during the battery manufacturing process and reduced electrolyte storage between both electrodes. A thin separator, which is hard to short-circuit and hold the electrolyte, needs to be developed.

1.4.4 Electrolyte [77]

As the electrolyte of the Ni-MH battery, a caustic alkaline aqueous solution, such as KOH, NaOH and LiOH, is used. Of these three materials, the ionic conductivity becomes higher in order of LiOH, NaOH and KOH. In particular, the 7mol/L KOH exhibits the best ionic conductivity.

Meanwhile, in the alkaline battery, a side-reaction of oxygen gas generation occurs during the charging process, and the charge efficiency is decreased. In order to increase

the oxygen overpotential and improve the charge efficiency, NaOH and/or LiOH is generally added to the KOH aqueous solution.

1.4.5 Design and structure of alkaline secondary battery

Ni-MH batteries for consumer applications consist of spirally wound electrodes and a cylinder-type container as shown in Fig. 1.5. In this type of battery, a current-collecting tab is welded on the electrode terminal.

The battery performances such as power, capacity and cycle-life, depend on the internal resistance, current-correcting resistance, reaction resistance, ion-diffusion resistance and electrical conducting resistance. These resistance factors are connected in series and determine the internal resistance. In order to decrease the internal resistance, it is necessary to reduce each factor. One representative measure is to thin the electrode. For the high-power type batteries, thin electrodes are generally used.

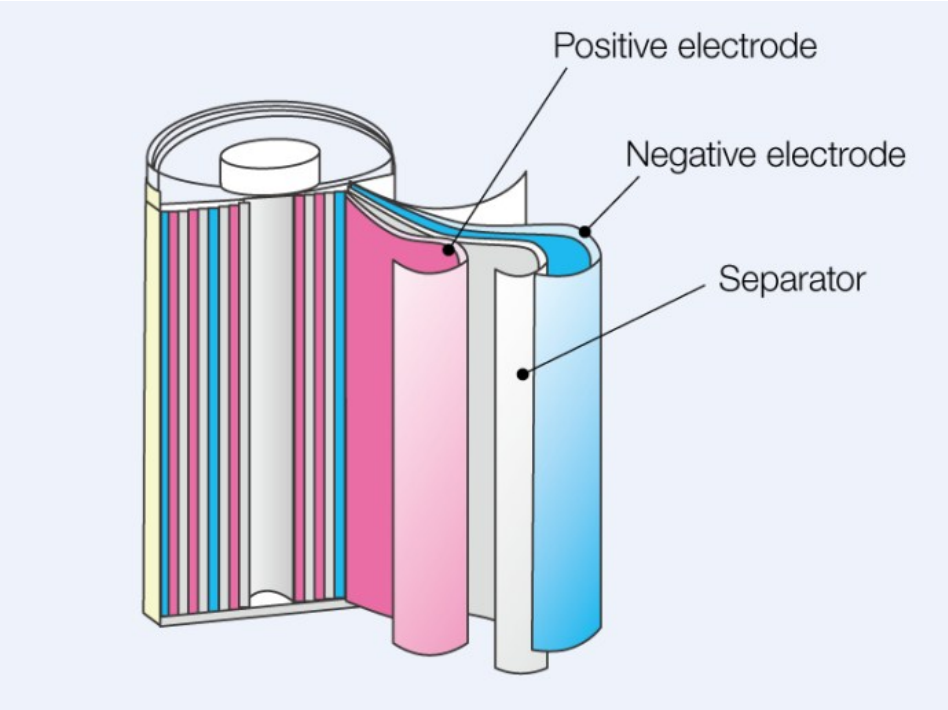

Figure 1.5: Schematic view of the cylinder-type structure for consumer Ni-MH battery.

1.5 Purpose and subject of this research

The consumer-type Ni-MH battery with the spirally wound structure is already a mature product. However, there would be many factors that should be improved so that the large-sized Ni-MH battery can be used for industrial applications. In these applications, safe and low-cost materials, which can be stably supplied, are indispensable. The Ni-MH battery using an aqueous electrolyte is safer than the Li-ion one using an organic electrolyte. Moreover, the Ni-MH battery exhibits a superior battery performance such as energy density, power and low environmental load performance in comparison to the Pb-acid battery, which has already been used for industrial applications. As for the high-performance Ni-MH battery, the spread to the social infrastructure is expected.

On the other hand, the Ni-MH battery is very expensive because both electrodes consist of rare metals such as transition metals and rare-earth elements. In particular, as for Co, which is added to both electrodes as an essential element, the components are unevenly distributed, and the price is easily increased based on the influence of the local government. For example, only about 10% Co in the alloys accounts for half of the total alloy cost [78]. Moreover, the cost of Co has exhibited a noticeable fluctuation and has often increased over the past three decades. In 2008, the highest price (> 110 US$/t) in history was recorded for some unexplained reason. After 2010, its price has had a stable transition due to an excess supply. However, the concern about a stable supply in the future still remains. The development of Co-free materials is an important subject for reducing the cost of the Ni-MH battery.

It is necessary to manage the battery in kW not the conventional kWh in order to make a profit based on current economic indicators. It is essential to improve the power and cycle-life of the battery. Based on these commitments, the problems to be solved are

enumerated.

1.5.1 Electrode and battery structure for industrial applications

For industrial applications, the single-cell capacity is generally greater than that of the consumer one. A number of single cells are stacked in series to assemble a high-voltage battery module. It is necessary to provide a battery structure with a low internal resistance and an efficient heat releasing system in order to suppress the battery deterioration due to the heat generated during the charge and discharge process. For the conventional battery structure as shown in Fig. 1.5, the resistance around the current collecting tub would be increased with increasing the electrode size. The resistance causes increased heat and voltage reduction, therefore, the current collector should be improved.

As for the battery for industrial applications, the long-term durability of 15 years is required. In this case, it is necessary to increase the electrolyte quantity compared to a consumer battery to prevent electrolyte loss. However, for the conventional paste-type electrode, if there is too much electrolyte, the $Ni(OH)_2$ particles would be easily separated from the nickel-foam substrate. A binder material, which exhibits a good adhesion, is necessary.

Verification tests have to be conducted for future industrial applications, such as a battery-driven light rail vehicle (LRV), Battery Power System (BPS) for railways and power generation and stabilization of the Power Grid.

1.5.2 Development of Co-free-type electrodes

As already described, Co is essential for both electrodes of the Ni-MH battery. However there are serious problems when using Co additives for industrial applications.

For the positive electrode, the CoOOH conductive network is easily reduced by an overdischarge and thus disruption of the conductive network is a concern. To realize the long cycle-life and manage the battery safely, the overdischarge resistance of the battery must be improved. Furthermore, a high amount of $Co(OH)_2$ with a thick deposition layer not only has a low specific area, but also hinders the diffusion of protons from the surface to the interior of the $Ni(OH)_2$ particles [79]. A new conductive agent, which replaces the CoOOH, has to be developed in order to design a Co-free positive electrode for the Ni-MH battery.

For the single-cell stacked battery module, each of the cells are equally charged and discharged during the initial cycles. However, the increasing self-discharge in some cells causes a difference in the state-of-charge (SOC) among the cells, and these cells would be degraded by any overdischarge. When the conventional AB_5 or AB_2 alloys are used as the negative materials, various elements, such as Co and Mn, are eluted into the alkaline electrolyte, and cause self-discharge of the cells. As a conventional provision, the alkaline immersion of the alloy powder before battery construction would be an effective way to suppress the self-discharge during the initial cycles. As for the industrial battery with long-term use, development of Co and Mn-free alloys with no self-discharge is desirable.

1.5.3. Development of high-power type electrodes

Large-sized batteries are needed to fabricate large-scale energy storage systems for industrial applications. Conventionally, the Pb-acid battery has been used in these applications. Performance of this battery is inferior to the Ni-MH ones, but the cost is much lower. It would be difficult for the expensive Ni-MH batteries to be used in the social infrastructure even if the batteries exhibited high performances. Although unit

cost per kWh for the battery has been reduced by the efforts of many battery makers, there is no-prospect that a drastic price reduction realizes. This is because the theoretical battery capacity is limited by the battery materials. Moreover, the price of the rare metals, which consists of the electrode materials has shown a noticeable fluctuation and often increased over the three decades. Concern about a stable supply in the future still remains. The development of rare-metal-free electrodes is an important subject for reducing the cost of the Ni-MH battery.

Here, the unit price of a battery is defined as the battery price divided by the energy storage capacity (Japanese-yen(JY)/kWh). For the commercialized electrical power, the unit price is 10 ~ 30 JY/kWh, while for the battery, 100,000 ~ 300,000 JY/kWh. From an economical point of view, 10,000 cycles of charge and discharge are necessary for equivalent use.

Meanwhile, if the battery costs were considered based on kW, instead of kWh, the battery would be useful in the social infrastructure. Based on this point of view, when the battery with 300,000 JY/kWh is charge and discharged at the 1C-rate, the battery price becomes 300,000 JY/kW. If the rate was increased to the 20C-rate, the price would be reduced to 1/20, that is 15,000 JY/kW. Increasing the rate decreases the battery capacity and cost.

In particular, when the battery is used for a large load change (charge and discharge by a momentary large current), the output is more important than the capacity of the battery. This is easy to understand when the EV and HEV are compared. In other words, a lot of kWh is necessary for an EV to provide the mileage, but the charge and discharge rate can be reduced because the battery capacity is high. On the other hand, an HEV is equipped with a small-sized high-power battery. This battery is used to obtain the power rather than the mileage, and a high-rate charge and discharge capability (kW) is required.

For further large-scale industrial applications, improving the high-power performance is desirable. Furthermore, improving the cycle-life performance of the battery will reduce the running costs.

1.6 Outline of this thesis

The outline of this thesis is as follows. For a large-sized Ni-MH battery, a low internal resistance and long-term durability are the key points.

In chapter 2, I present and discuss the new concepts for industrial battery components. A new low-internal resistance battery structure was developed, and the battery performance was confirmed. This concept has been applied to Kawasaki's battery product, called the "GIGACELL®". I have conducted various verification tests using the GIGACELL® applications and confirmed its high-performances in LRV, BPS, wind-power and solar-power applications. In addition, I have developed a high-capacity electrode with a long cycle-life performance. In this electrode, the active material was granulated along with a binder and conductive materials, and the granulated particles were collected with nickel foam substrates.

In chapter 3, I present and discuss the development of Co-free materials for a Co-free Ni-MH battery. As the negative materials, $RE_{0.9}Mg_{0.1}Ni_xAl_{0.2}$ (x = 3.9 ~ 4.3, $AB_{4.1\text{-}4.5}$) alloys are prepared. These alloys are characterized by X-ray diffraction and transmission electron microscopy measurements. Furthermore, the battery performance with an improved self-discharge capability was investigated. For the positive electrode, an oxidation-resistant carbon was used as a substitute for the conventional conductive material, CoOOH. In order to develop a conductive network among the $Ni(OH)_2$ particles, the carbon-coated $Ni(OH)_2$ was prepared by spraying a carbon dispersion onto the $Ni(OH)_2$ particles using a fluid-bed coating technique. A Co-free Ni-MH battery

with a 205Ah rating was constructed and tested.

In chapter 4, I present and discuss the development of high-power carbon fiber-type electrodes. The β-$Ni(OH)_2$ is electrodeposited on the carbon fiber in a nickel nitrate solution. The α-$Ni(OH)_2$ can be prepared by the 20%Al addition to the nickel nitrate solution. Super high-rate charge and discharge performances of these fiber-type electrodes were investigated. The charge and discharge mechanisms are investigated by a synchrotron XRD analysis. Furthermore, the fiber-type electrode manufacturing technology and cell with a fiber electrode having a 350mAh rating was developed.

References

[1] 2012 Battery-related market actual situation total investigation, Fuji-Keizai

[2] T. Sakai, I. Uehara and H. Ishikawa, *J. Alloys. Compd*., **293-295**, 762 (1999).

[3] A. Taniguchi, N. Fujioka, M. Ikoma and A. Ohta, *J. Power Sources*, **100**, 117 (2001).

[4] T. Sakai, N. Sato, "*Development of large scale rechargeable batteries for vehicles*", CMC Publishing, Tokyo, 2003 (in Japanese).

[5] K. Shinyama, Y. Magari, K. Kumagae, H. Nakamura, T. Nohma, M. Takee and K. Ishiwa, *J. Power Sources*, **141**, 193 (2005).

[6] T. Sakai, *Funtai Gijutsu,* **2(3)**, 17 (2010) (in Japanese).

[7] M. Watada, *Funtai Gijutsu,* **2(3)**, 25 (2010) (in Japanese).

[8] http://car.watch.impress.co.jp/docs/news/20130703_606305.html

[9] T. Teratani, "*Battery system technology -Energy storage application for electric-vehicle, Railway-*", chapter 1, p.1, Ohmsha, Ltd., Tokyo, Japan (2012).

[10] B. S. M.C. Borba, A. Szklo, R. Schaeffer, *Energy,* **37**, 469 (2012).

[11] M. Esteban, Q. Zhang, A. Utama, *Energy Policy*, **47**, 22 (2012).

[12] K. Nishimura, K. Tsutsumi, A wet synthesis sealing up battery, Powder Science and Engineering, **39(7)**, 1 (2007).

[13] K. Tsutsumi, Journal of the Japan Institute of Energy, **87(7)**, 506 (2008).

[14] Y. Oku, *Kawasaki Technical Review,* **169**, 10 (2009).

[15] K. Tsutsumi, T. Matsumura, Science & Technology in Japan, **26**, 21 (2009).

[16] H. Yamazaki, S. Akiyama, T. Hirashima, M. Kataoka, K. Matsuo, Urban Transportation that is friendly for people and the environment, Kawasaki Technical Review. **170**, 16 (2010).

[17] K. Ogura, T. Matsumura, C. Tonda, K. Nishimura, M. Kataoka, Kawasaki Technical Review. **170**, 24 (2010).

[18] K. Ishikawa, *Large scale secondary battery for electrical power storage,* chapter 4, p. 113, Nikkan Kogyo Shinbun, Ltd., Tokyo, Japan (2011).

[19] *Nikkel Monozukuri*, **3**, 36 (2008) (in Japanese).

[20] M. Shimada, R. Oishi, D. Araki, Y. Nakamura, *Hitachi-Hyoron,* **92(2)**, 32 (2010) (in Japanese).

[21] T. Hashimoto, *Large scale secondary battery for electrical power storage,* chapter 5, p. 155, Nikkan Kogyo Shinbun, Ltd., Tokyo, Japan (2011) (in Japanese).

[22] A. Okui, S. Hase, H. Shigeeda, T. Konishi, T. Yoshi, International Power Electronics Conference (IPEC2010), p. 3117, (2010).

[23] H. Lee, E. Joung, G. Kim, C. An, International Conference on Information and Multimedia Technology (ICIMT2009), p. 28, (2009).

[24] J.J. Reilly, R.H. Wiswall Jr, *Inorg. Chem.* **7**, 2254 (1968).

[25] H. Zijlstra, F.F. Westendorp, *Solid St. Commun.* **7**, 857 (1969).

[26] G. Sandrock, *J. Alloys Compd.* **293-295**, 877 (1999).

[27] Z. Ogumi, A. Nishio, "*All of innovation type batteries*", Ohm Publishing, Tokyo, (2011) (in Japanese).

[28] T. Miyuki, Y. Okuyama, T. Sakamoto, Y. Eda, T. Kojima, T. Sakai, *Electrochemistry*, **80(6)**, 401 (2012).

[29] S. U. Falk, A. J. Salkind, *Alkaline Storage Batteries*, John Wiley & Sons, Inc, New York, (1969).

[30] T. Watanabe, Y. Katayama, "*Introduction to electrochemistry to understand batteries*", Ohm Publishing, Tokyo, (2011) (in Japanese).

[31] J. M. Tarascon, in "*Recent Advances in Rechargeable Li Batteries*", special issue of Solid State Ionics., eds. M. S. Whittingham, **69**, No.3-4 (1994).

[32] H. Ikeda, T. Saito, H. Tamura, in Proc. Manganese Dioxide Symp. Vol.1, eds. A.

Kozawa and R. B. Brodd (IC sample Office, Cleveland. OH. 1975).

[33] T. Nagaura, K. Tozawa, *Prog. Bastte. Solar cells,* **9**, 209 (1990).

[34] A. Yoshino, K. Sanechika, T. Nakashima, Japan Kokai Shou 62-90863 (1987).

[35] "*Series on functional chemistry of electrons and ions: Everything about the nickel-metal hydride secondary batteries attracting attention*", eds. H. Tamura, NTS Inc. Tokyo, Japan (2001). (in Japanese)

[36] P. Oliva, J. Leonaridi, J.F. Laurent, C. Delmas, J.J. Braconnier, M. Figlarz, F. Fievet and A. De Guibert, *J. Power Sources,* **8**, 229 (1982).

[37] F.P. Kober, *J. Electrochem. Soc.,* **112**, 1064 (1965).

[38] C. Delmas, J.J. Braconnier, Y. Borthomieu, P. Hagenmuller, *Mat. Res. Bull.,* **22**, 741 (1987).

[39] L. Demourgues-Guerlou, C. Delmas, *J. Power Sources,* **45**, 281 (1993).

[40] L. Demourgues-Guerlou, C. Denage, C. Delmas, *J. Power Sources,* **52**, 269 (1994).

[41] L. Demourgues-Guerlou, C. Delmas, *J. Power Sources,* 52, 275 (1994).

[42] L. Guerlou-Demourgues, C. Delmas, *J. Electrochem. Soc.,* **143**, 561 (1996).

[43] P. V. Kamath, M. Dixit, L. Indira, A. K. Shukla, V. Ganesh Kumar, N. Munichandraiah, *J. Electrochem. Soc.,* **141**, 2956 (1994).

[44] M. Dixit, P. V. Kamath, J. Gopalakrishnan, *J. Electrochem. Soc.,* 146, 72 (1999).

[45] S. Deki, A. Hosokawa, A.B. Béléké and M. Mizuhata, *Thin Solid Films,* **517**, 1546 (2009).

[46] A.B. Béléké, A. Hosokawa, M. Mizuhata and S. Deki, *J. Ceram. Soc. Japan,* **117**, 392 (2009).

[47] M. Oshitani, M. Watada, H. Yufu and Y. Matsumaru, *Denki Kagaku oyobi Kogyo Buturi Kagaku*, **57**, 480 (1989).

[48] I. Matsumoto, M. Ikeyama, T. Iwaki and H. Ogawa, *Denki Kagaku oyobi Kogyo*

Buturi Kagaku, **54**, 159 (1986).

[49] M. Oshitani, H. Yufu, K. Takashima, S. Tsuji and Y. Matsumaru, *J. Electrochem. Soc.*, **136**, 1590 (1989).

[50] M. Yao, K. Okuno, T. Iwaki, M. Kato, K. Harada, J.J. Park, S. Tanase, T. Sakai, *Electrochem. Solid-State Lett.,* **10(3)** A56 (2007).

[51] M. Yano, T. Ogasawara, Y. Baba, M. Tadokoro and S. Nakahori, *Electrochemistry,* **69**, 858 (2001).

[52] E. Higuchi, T. Mizuta and H. Inoue, *Electrochemistry,* **78**, 420 (2010).

[53] M. Ikoma, Y. Hoshina, I. Matsumoto, C. Iwakura, *J. Electrochem. Soc,* **143**, 1904 (1996).

[54] K. Shinyama, Y. Magari, H. Akita, K. Kumagae, H. Nakamura, S. Matsuta, T. Nohma, M. Takee, K. Ishiwa, *J. Power Sources,* **143**, 265 (2005).

[55] M. Kanemoto, T. Ozaki, T. Kakeya, D. Okuda, M. Kodama, R. Okuyama, *GS-Yuasa Technical Report,* **8**, 22 (2011).

[56] Y. Osumi, H. Suzuki, A. Kato, M. Nakane, Y. Miyake, *Nippon Kagaku Kaishi,* **11**, 1472 (1978).

[57] Y. Osumi, A. Kato, H. Suzuki, M. Nakane, Y. Miyake, *J. Less-Common Met.* **66**, 67 (1979).

[58] M. Kanda, ”*Development and materials for Advanced Storage Battery*”, CMC Publishing, Tokyo, 2002 (in Japanese).

[59] T. Sakai, H. Miyamura, N. Kuriyama, A. Kato, K. Oguro, H. Ishikawa, *J. Electrochem. Soc.,* **137(3)**, 795 (1990).

[60] T. Sakai, H. Yoshinaga, H. Miyamura, N. Kuriyama, H. Ishikawa, *J. Alloys. Compd.,* **180** (1992) 37.

[61] H. Yayama, O. Ichinomiya, K. Hirakawa, *Jpn. J. Appl. Phys.*, **22**, L621 (1983).

[62] M. A. Fetcenko, S. Venkatesan, K. C. Hong, B. Richman, *Power Souces,* **12**, 411 (1989).

[63] Y. Moriwaki, T. Gamo, H. Seri, T. Iwaki, *J. Less-Commun Met.,* **172-174**, 1211 (1991).

[64] T. Gamo, Y. Tsuji, Y. Moriwaki, The Electrocom, Soc. Proc., **94-97**, 155 (1994).

[65] K. Kadir, T. Sakai, I. Uehara, J. Alloys. Compd., **257** (1997) 115.

[66] K. Kadir, N. Kuriyama, T. Sakai, I. Uehara, J. Alloys. Compd., **284** (1999) 145.

[67] K. Kadir, T. Sakai, I. Uehara, J. Alloys. Compd., 287 (1999) 264.

[68] K. Kadir, H. Tanaka, T. Sakai, I. Uehara, J. Alloys. Compd., **289** (1999) 66.

[69] K. Kadir, T. Sakai, I. Uehara, J. Alloys. Compd., 302 (2000) 112.

[70] T. Sakai, K. Kadir, M. Nagatani, H. Takeshita, H. Tanaka, N. Kuriyama, I. Uehara, Abstract of the 40th Battery Symposium, Kyoto, Japan, 1999, p. 133.

[71] J. Chen, N. Kuriyama, H. Takeshita, H. Tanaka, T. Sakai, M. Haruta, Electrochem. Solid State Lett. **3(6)** (2000) 304.

[72] T. Kohno, H. Yoshida, F. Kawashima, T. Inaba, I. Sakai, M. Yamamoto, M. Kanda, J. Alloys. Compd., **311** (2000) L5.

[73] S. Yasuoka, Y. Magari, T. Murata, T. Tanaka, J. Ishida, H. Nakamura, T. Nohma, M. Kihara, Y. Baba, H. Teraoka, J. Power Sources, **156** (2006) 662.

[74] T. Ozaki, M. Kanemoto, T. Kakeya, Y. Kitano, M. Kuzuhara, M. Watada, S. Tanase, T. Sakai, J. Alloys. Compd, **446-447** (2007) 620.

[75] T. Ozaki, M. Kanemoto, T. Kakeya, Y. Kitano, M. Kuzuhara, M. Watada, S. Tanase, T. Sakai, ITE-letters on Batteries, New Technologies & Medicine, **8(4)**, 394 (2007).

[76] "*Series on functional chemistry of electrons and ions: Everything about the nickel-metal hydride secondary batteries attracting attention*", chapter 2 Section 4, p.117,eds. H. Tamura, NTS Inc. Tokyo, Japan (2001). (in Japanese).

[77] "*Series on functional chemistry of electrons and ions: Everything about the nickel-metal hydride secondary batteries attracting attention*", chapter 2 Section 3, p.99,eds. H. Tamura, NTS Inc. Tokyo, Japan (2001). (in Japanese)

[78] T. Sakai, J. Jpn. Inst. Energy, **89**, 420 (2010) (in Japanese).

[79] C. Shao-an, W. Leng, Z. Jianqing and C. Chunan, *J. Power Sources,* **101,** 248 (2001).

Chapter 2

Development of high-power and large-sized Ni-MH battery

2.1 Development of high-capacity $Ni(OH)_2$ electrode using granulation process

2.1.1 Introduction

After the industrial revolution, mankind invented a method to get electrical energy from fossil fuels. The energy consumption has exponentially increased by the shift to industrialization with mass-production and mass-consumption and the information-oriented society with the development of the IT technique, causing various environmental problems such as limited fossil fuel resources, air pollution and global warming.

In Japan, new technologies such as alternative energy and energy savings have attracted much interest by the global deployment of a new fiscal policy called the "Green New Deal". In the near future, the ratio of power generation using a renewable energy, such as solar and wind, would be increased. Moreover, the energy savings using a battery is promoted not only for cars (Sakai, 2010; Sakai and Sato, 2003), but also for public transportation such as trains (Nishimura and Tsutumi, 2007; Tsusumi, 2008; Tsutsumi and Matsumura, 2009; Yamazaki et al., 2010; Ogura et al., 2010). A large battery with a high-capacity and long cycle-life is indispensable to absorb the load fluctuations of generation and railways. In order to meet this requirement, the development of a higher-capacity electrode than the conventional one would be one of the effective ways.

For industrial applications, a number of single cells are stacked to assemble a high voltage battery. A difference in the state of charge gradually increases during the charge and discharge cycles, and some cells could be overcharged and overdischarged. For the conventional positive electrode containing a CoOOH conductive material, the overdischarge causes degradation of the battery performance as well as disruption of the CoOOH conductive network (Takasaki et al., 2013). In addition, cobalt is an expensive

rare metal, and its price has often noticeably fluctuated. The securing of a stable supply is a serious concern. Therefore, the Co-free $Ni(OH)_2$ electrode is an important subject for the Ni-MH battery.

Furthermore, as for the battery for industrial applications, the long-term durability of 15 years is required. In this case, it is necessary to increase the electrolyte quantity compared to a consumer battery to prevent electrolyte loss. However, for the conventional paste-type electrode, if there is too much electrolyte, the $Ni(OH)_2$ particles would be easily separated from the nickel-foam substrate. A binder material, which exhibits a good adhesion, is necessary.

In this study, a high-capacity positive electrode with the long-term durability was prepared by granulating the $Ni(OH)_2$ with conductive and binder materials. The battery performances dependent on this addition were investigated and the optimum addition was investigated. A small-sized test cell consisting of a structure that is equivalent to a large-sized Ni-MH battery, called the GIGACELL® (Nishimura and Tsutumi, 2007; Tsusumi, 2008; Tsutsumi and Matsumura, 2009; Yamazaki et al., 2010; Ogura et al., 2010), was constructed, and the contact pressure between the electrode and separator was measured and the correlation among the electrode-expansion, the electrolyte-loss and cycle-life performance was investigated.

2.1.2. Experimental

As the positive material, spherical $Ni(OH)_2$ particles with an approximate 10 μ m ϕ size were used. An oxidation-resistant carbon (CB) and Ni-plated carbon fiber (PAN) were used as the conductive materials. The oxidation-resistant carbon was prepared by annealing carbon black at approximately 2500K in an inert-gas atmosphere. Ethylene vinyl acetate (EVA), which exhibits a good oxidation-resistance, is alkali-proof and has

a good binding strength, was also used.

The CB, PAN and EVA were added to a xylene solvent at the weight ratio of 1 : 1 : 1, then stirred while heating to 333K to obtain a uniform slurry. The positive granulated particles were formed by adding $Ni(OH)_2$ powder, and mixing it with a high-speed LFS-2 mixer (Earthtechnica Co., Ltd., Japan) while heating. In addition, the $MmNi_{3.7}Co_{0.7}Mn_{0.3}Al_{0.3}$ alloy with an approximate 50 μ m ϕ was used as the negative material, and negative granulated particles were made using a manufacturing method equivalent to the positive one.

The granulated particles were molded as electrodes for the battery test by maintaining them at 333K for 10 minutes while compacting them by at 6MPa after sandwiched between two pieces of nickel-foam with 0.04g/cm^2 of the weight per area. The GIGACELL-type single cells (Nishimura and Tsutumi, 2007; Tsusumi, 2008; Tsutsumi and Matsumura, 2009; Yamazaki et al., 2010; Ogura et al., 2010) with a 15Ah rating were constructed using the granulated electrodes. Inside the cells, pre-formed stripes of positive and negative electrodes are inserted into the respective sides of the pleat-folded separator. The separator thickness was 0.4mm. The electrolyte was 6mol/L KOH.

As a probe to measure the pressure change between the electrode and separator during the charge/discharge process, three small-sized LM-100KA-P load-cells (Kyowa Electronic Instruments Co., Ltd., Japan) were sandwiched between two pieces of stainless steel boards with the same size as the electrode and fixed in place. The entire probe was sealed in a plastic bag and inserted into a separator with the electrodes. The average of the measured values of the 3 load-cells was divided by the electrode area to obtain the pressure (kgf/cm^2). An autograph AG-100kNG (Shimadzu Corporation) was used for measuring the repulsive force during the separator compression.

2.1.3. Results and discussion

2.1.3.1. Electrode preparation and performance

The obtained granulated particles were shifted, and the particles with an approximate 3mm ϕ were sorted as shown in Fig. 1. The CB and PAN dispersed around the $Ni(OH)_2$ particles could contribute to improving the electrical conductivity, while the EVA plays a role to maintain the shape of the granulated particles as binder.

Figure 1: Photograph of the granulated $Ni(OH)_2$ particles.

In the electrode molding process, the granulated particles were sandwiched between two nickel-foam pieces and pressed while heating as shown in Fig. 2(a). Figure 2(b) shows a photograph of the molded electrodes. The thickness of the electrodes was approximately 1.2mmt, and the density of the granulated particles was approximately 1.8 ~ 2.0g/cm^3. In addition, it was difficult to mold the electrode at room temperature because the EVA does not work as an adhesive at this temperature.

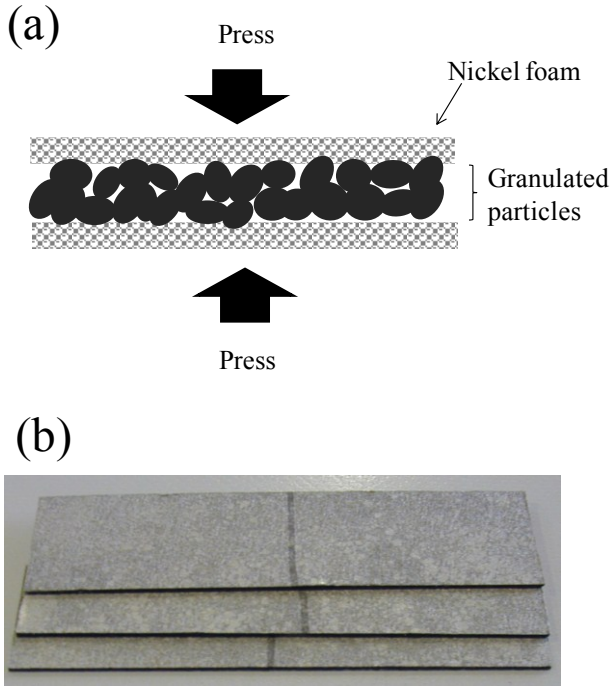

Figure 2: (a)Schematic view of electrode molding process, (b) granulated particles sandwiched between nickel foams and pressed while heating at 333K.

Table 1 shows the energy density of the granulated electrode compared to that of the various conventional sintered (Fleischer, 1948; Falk and Salkind, 1969; Ng and Schneider, 1986) and paste-type (Oshitani et al., 1989; Yao et al., 2007) ones. The capacity per unit volume (mAh/cm^3) was comparable or greater than that of the sintered electrode, while the capacity per unit area (mAh/cm^2) , which was estimated by dividing the capacity per unit volume in the electrode thickness, was 1.5 ~ 2 times greater than the paste-type one using Ni-foam substrate.

Table1: Energy density for various electrodes

Electrode type	Energy density		Electrode thickness
	mAh/cm^2	mAh/cm^3	mm
Granulated particle	54	450	1.2
Ni-foam	36	600	0.6
sintered	20	400	0.5

As shown in Table 2, the electrical resistance of the positive electrode decreased with the increasing conductive additives. The conductive materials would improve the low electrical conductivity of the $Ni(OH)_2$. However, the high-rate discharge performances of electrode #p1, which exhibited the best electrical conductivity, were inferior to those of electrode #p2. This result indicates that a large amount of the conductive material would reduce the $Ni(OH)_2$/electrolyte interface, and prevent the electrochemical reaction by ionic diffusion. The high-rate performances of electrode #p3 suggest that the electrical conductivity was not sufficiently improved even if the $Ni(OH)_2$/electrolyte interface is sufficient. The amount of additives for electrode #p2 is the most suitable for improving the electrode performance.

For the negative electrode, two electrodes were tested. Electrode #n1 with higher amount of additives exhibited the better performance. The higher amount of EVA would improve the adhesion of the alloy particles to the nickel-foam substrate. The amount of additives in the negative electrodes was lower than that of the positive ones. This would be related to the good metallic conductivity of the negative alloy compared to the $Ni(OH)_2$. In the following battery tests, electrodes p#2 and n#1 were used.

Table 2: The weight ratio of active materials and additives, resistance of electrode and high-rate performance

	No.	$Ni(OH)_2$	EVA	CB	PAN	Resistance (Ω)	Discharge capacity (mAh/g)		
							0.1C	1C	5C
Positive electrode	#1	100	10	10	10	7.0	230	195	52
	#2	100	5	5	5	8.2	248	230	69
	#3	100	2.5	2.5	2.5	103	151	38	1

	No.	MH	EVA	CB	PAN	Resistance (Ω)	Discharge capacity (mAh/g)		
							0.1C	1C	5C
Negative electrode	#1	100	2.5	2.5	2.5	0.27	270	244	55
	#2	100	1.25	1.25	1.25	0.25	236	217	21

2.1.3.2. Pressure variation between the electrode and separator

The test batteries, which had a structure equivalent to the GIGACELL® (Nishimura and Tsutsumi, 2007; Tsutsumi, 2008; Tsutsumi and Matsumura, 2009; Yamazaki et al., 2010; Ogura et al., 2010), were constructed using electrodes p#2 and n#1 as shown in Fig. 3. The pressure upon a unit area between the electrode and separator was monitored using the inserted load-cells. The value of separator thickness was designed to be 0.4mmt, which is equal to the original thickness.

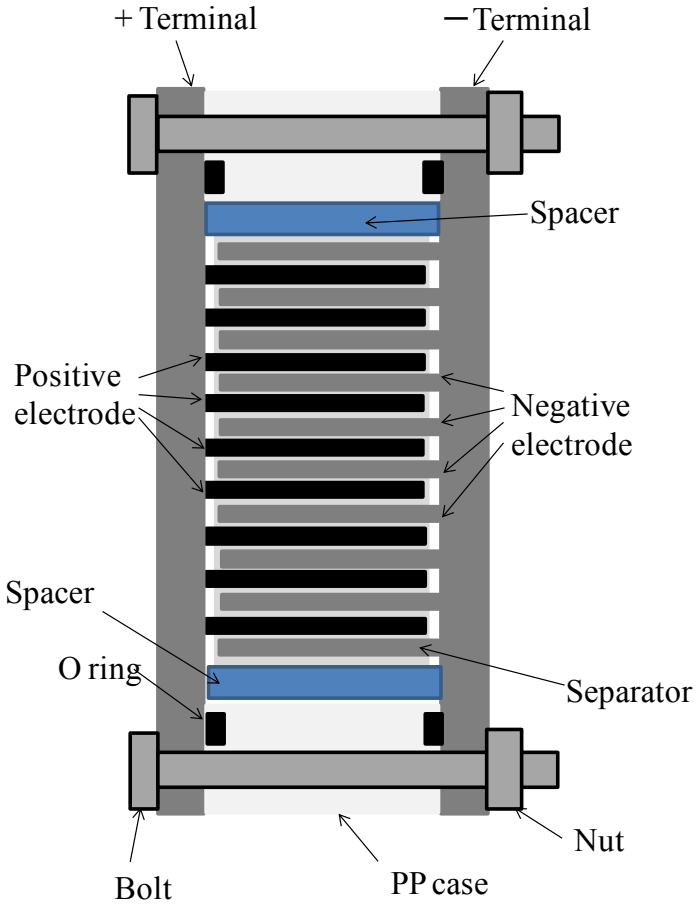

Figure 3: Schematic view of GIGACELL®-type test battery.

Figure 4 shows the cycle-dependent battery performances, namely, the Ah-efficiency, average discharge voltage and voltage at the end of charging. The initial performances were maintained to the 100th cycle. After 130 cycles, the Ah efficiency decreased, and a discharge-voltage reduction and charge-voltage increase were also observed.

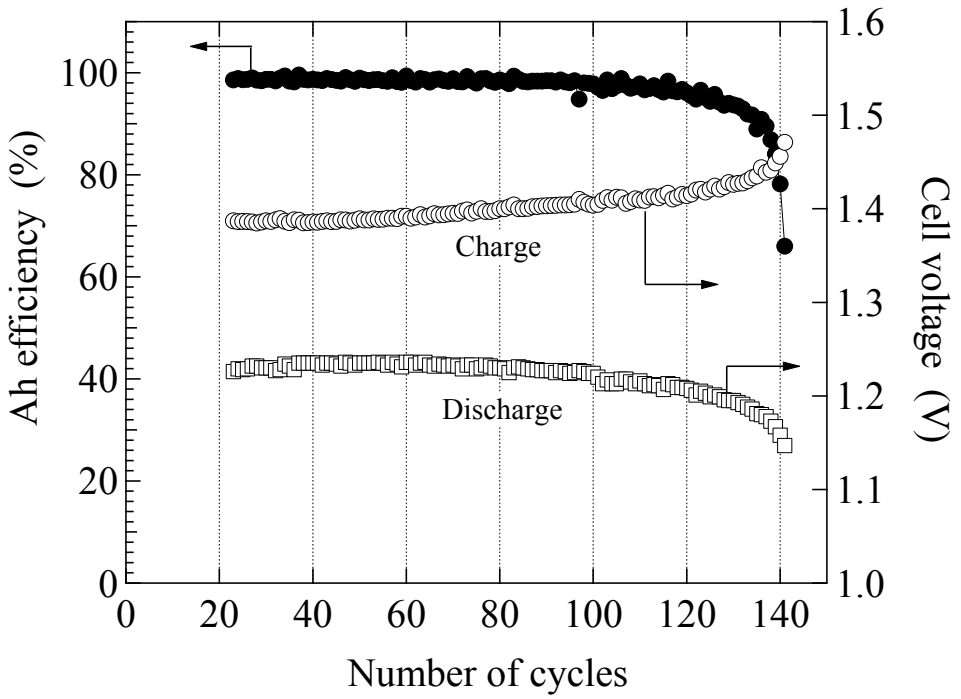

Figure 4: Cycle-life performance of the test battery without separator compression.

Figure 5 shows the pressure variation during the charge and discharge processes at the 41th and 130th cycles. At the 41th cycle, the pressure decreased during the initial step of the charging process, and increased with the increasing charging. At the beginning of the discharge process, the pressure decreased, then increased from the middle of the discharge again. The pressure variation exhibited a similar behavior at the 130th cycle, but the pressure level rose in comparison to the value at the 41th cycle. The pressure value at the 130th cycle was in the range of 1.5 ~ 2.4 kgf/cm^2. This value drastically increased to 10kgf/cm^2 after the 130th cycle. It is considered that the electrode, which absorbs the electrolyte, expands, and therefore, the pressure rose. Electrolyte absorption would cause the separator to dry out, which led to the deterioration of the battery performance.

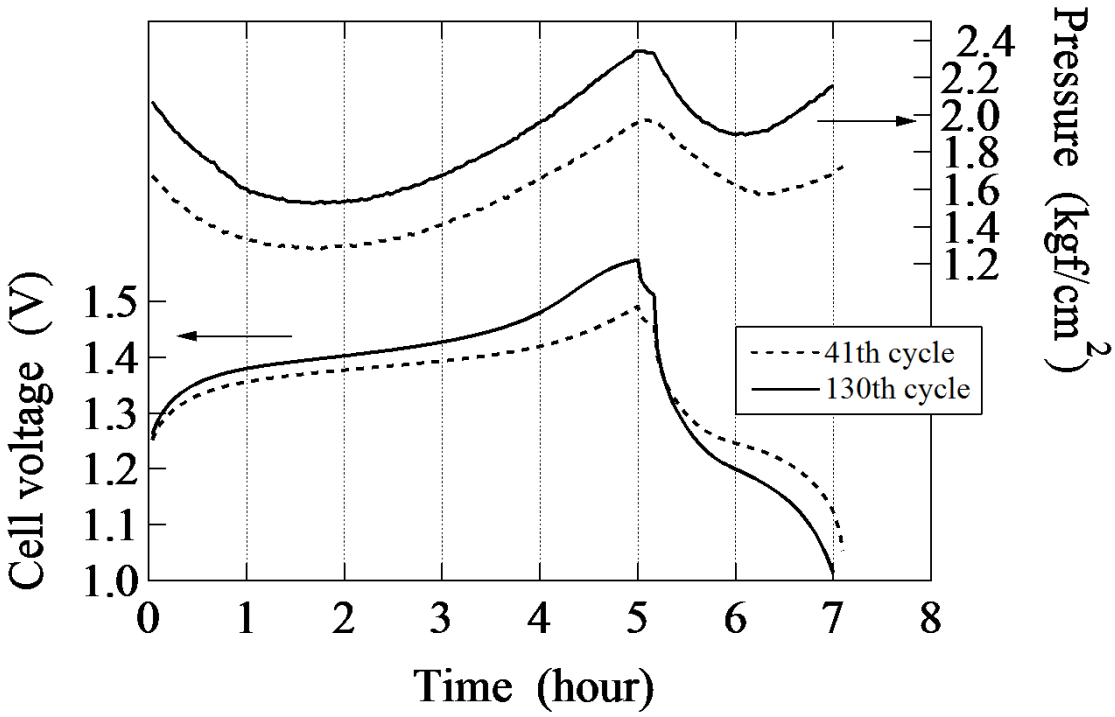

Figure 5: Voltage and pressure observations during charge-discharge process.

2.1.3.3. Cycle-life performance

Because the polypropylene (PP) nonwoven fabric, which is used as the separator, includes a space between the fibers, the separator thickness can be controlled if it is compressed. Spacers were added as shown in Fig. 3 and the separator was compressed so that the design thickness of the separator became 0.2mmt or 0.3mmt when the electrode bundle was placed in the cell frame.

Figure 6 shows the cycle-life performances of the test cell with the design thickness of the separator of 0.2mmt and 0.3mmt. These cells exhibited longer cycle-life than that of the cell in Fig. 4. The cycle-life performance of the cell with the 0.2mmt separator was doubled in comparison to that of the cell with the 0.3mmt separator.

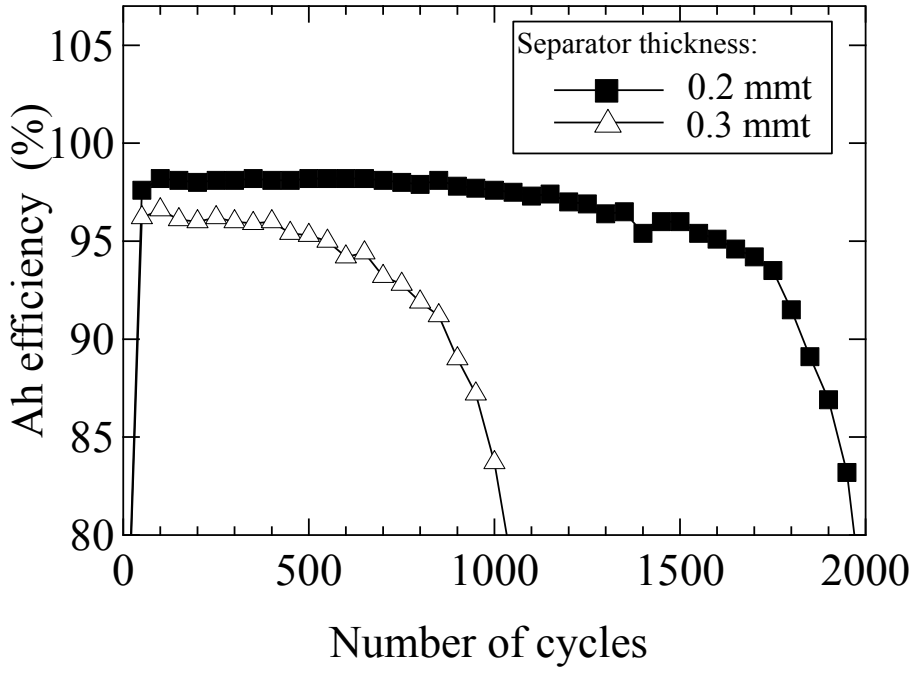

Figure 6: Cycle-life performance with the separator compression (a) 0.2mmt as the designed thickness, (b) 0.3mmt.

The results in Figs 4 and 6 indicate that thinner design thickness gives the longer cycle-life. It is considered that repulsive force from the compressed separator increases pressure to the electrodes, and therefore, the electrolyte absorption by the electrode would be reduced, which maintained the battery performance. Table 3 summarizes the battery performances, such as the discharge voltage and Ah-efficiency. These values were improved with decreasing the separator thickness. Meanwhile, there was a concern that the space decrease due to the separator compression would decrease the electrolyte which could be held in the separator. In order to understand these results, the porosity of the compressed separator was estimated as shown in Fig. 7(a). The porosity was equivalent to the ratio of the cavity between the fibers, and it was defined as the shade density of the separator divided by the truth density. The porosity decreased with the increasing compression and became approximately 0 by compressing to 0.1mmt. In addition, the porosity decreased by 10% when the separator thickness decreased to 0.2mmt from 0.3mmt.

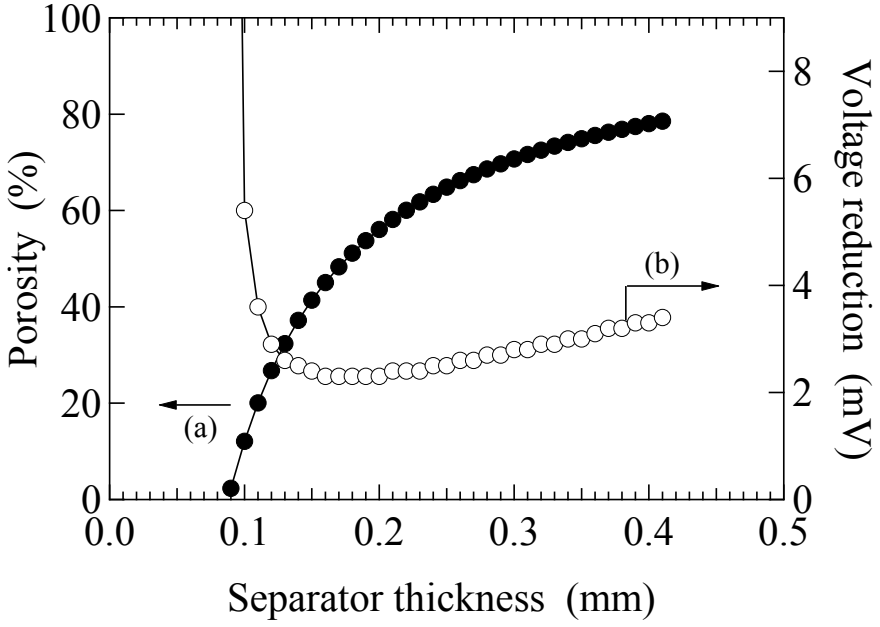

Figure 7: Calculated values of (a) the porosity and (b) voltage drop dependent on the designed separator thickness.

Table 3: Sepecification and peformance of the test batteries

Granulated particle electrode		Separator		Battery performance	
thickness	density	thickness	replusive force	Average discharge voltage	Ah efficiency
mm	g/cm3	mm	kgf/cm^2	V	%
1.2	1.9	0.3	<0.01	1.199	95.3
1.2	1.9	0.2	1.2	1.223	98.2

For the measured electrolyte resistance (R_e = 2 Ω·cm), porosity and separator thickness, the voltage drops were calculated from the following relational expressions.

$$\text{Resistance between the electrodes} = (R_e / \text{porosity}) \times \text{separator thickness} \quad \text{(I)}$$

$$\text{Voltage drop during the discharge process} = \text{(I)} \times \text{discharge current} \quad \text{(II)}$$

Figure 7(b) shows the relationship between the separator thickness and discharge-voltage decrease at the 1C-rate discharge, suggesting that the voltage reduction is slightly decreased when the separator was compressed from 0.3mmt to 0.2mmt. Namely, the porosity decrease in this range does not remove electrolyte from the separator, and there would be little influence on the ionic diffusion during the electrochemical reaction. Meanwhile, the separator compression would increase the adhesion between the active material particle and substrate, and improve the electrical conductivity of the active material. Therefore, at a 0.2mmt separator thickness, the battery performance was improved. This consideration is consistent to the observed voltage value in Table 3. Meanwhile, a high voltage decrease would occur if the electrolyte in the separator could not remain as the porosity approached 0%. The aim of the compressed separator thickness such that the electrolyte, which does not affect the charge-discharge reaction, would be an approximate 0.15mmt.

Factors affecting the cycle-life improvement for the 0.2mmt separator compression include electrode expansion restraint by the repulsive force from a compressed separator, preventing the electrolyte absorption of the electrode and drying of the separator.

Figure 8 shows the repulsive force of the separator, which was measured by an autograph instrument. The repulsive force was gradually increased when the separator thickness is less than 0.28mmt. A 1.6kgf/cm^2 repulsive force was observed for the 0.2mmt compressed thickness, while it was approximately 3kgf/cm^2 at the 0.18mmt. The former value is comparable or higher than that of the observed pressure of the electrode expansion in Fig. 5. These results suggest that a moderate repulsive force suppresses the electrode expansion, and contributes to improving the cycle-life performance. A further improvement in the cycle-life performance would be expected by raising the compression to 0.15 ~ 0.18mmt.

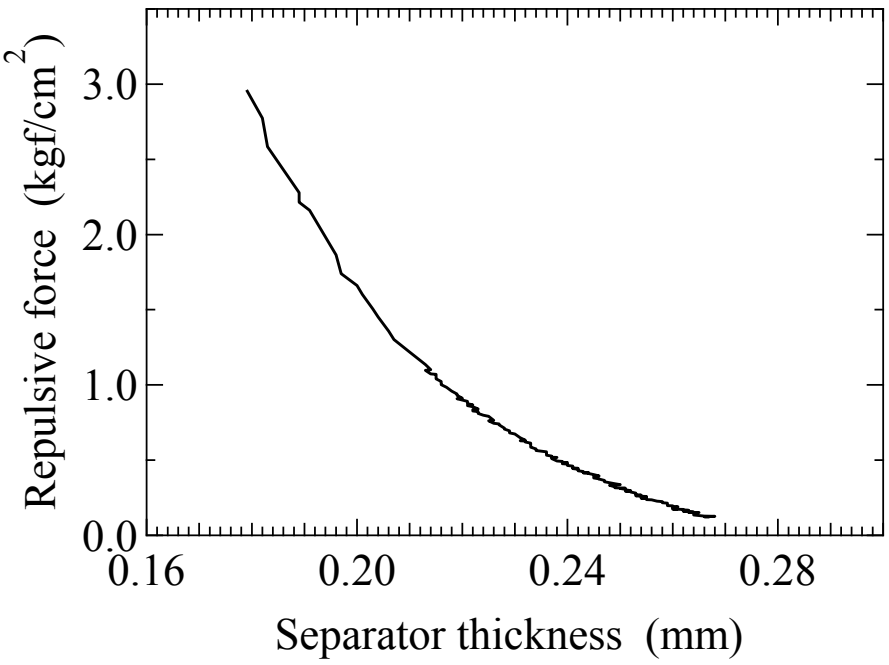

Figure 8: Repulsive force dependent on the compressed separator thickness observed by an autograph instrument.

2.1.4. Conclusion

The active material powder was granulated with CB, PAN and EVA, and the granulated particles were sandwiched between two nickel-foam pieces to form plate-like electrodes for the Ni-MH battery. The positive electrode with the 5wt% of CB, PAN and EVA as additives exhibited the highest discharge capacity. The battery test using the GIGACELL®-type single cells showed that the cycle-life performance was influenced by the separator compression. At a 0.2mmt separator thickness, no remarkable capacity loss was observed for 2000 cycles. The repulsive force dependent on the separator compression would suppress the electrolyte absorption of the electrode and dry out the separator, contributing to an improved cycle-life performance

References

Sakai, T. (2010). The role of battery technologies for reducing carbon dioxide emission, Funtai Gijutsu, Vol.2, 17 - 24.

Sakai, T., and Sato, N. (2003). Development of large scale rechargeable batteries for vehicles. CMC Publishing, Tokyo.

Nishimura, K., and Tsutsumi. K. (2007). A wet synthesis sealing up battery, Powder Science and Engineering, Vol.39(7) 1 - 6.

Tsutsumi, K (2008). The latest energy saving technology development on railway system, Journal of the Japan Institute of Energy, Vol.87(7) 506 - 509.

Tsutsumi, K., and Matsumura, T. (2009). Revolution in storage battery technology and adoption by electric railways, Science & Technology in Japan, Vol. 26, 21 - 24.

Yamazaki, H., Akiyama, S., Hirashima, T., Kataoka, M., and Matsuo, K. (2010). Urban Transportation that is friendly for people and the environment –SWIMO-X Low-floor battery-driven light rail vehicle-, Kawasaki Technical Review. Vol.170, 16 - 19.

Ogura, K., Matsumura, T., Tonda, C., Nishimura, and K., Kataoka, M. (2010). Effective Utilization of Energy from Train Regenerative Braking –Battery Power System for Railways-, Kawasaki Technical Review. Vol.170, 24 - 27.

Takasaki, T., and Nishimura, K., Saito, M., Iwaki, T., and Sakai, T. (2013). Cobalt-free materials for nickel-metal hydride battery: self-discharge suppression and overdischarge -resistance improvement, Electrochemistry, in press.

Fleischer, A. (1948). Sintered plates for nickel-cadmium batteries, Journal of the Electrochemical Society, Vol. 94(6), 289 - 299.

Falk, S.U., and Salkind, A.J. (1969). Alkaline Storage Batteries, John Wiley & Sons, New York.

Ng, P.K., and Schneider, W. (1986). Distribution of nickel hydroxide in sintered nickel

plaques measured by radiotracer method during electroimpregnation, Journal of the Electrochemical Society, Vol.133, 17 - 21.

Oshitani, M., Yufu, H., Takashima, K., Tsuji, S., and Matsumaru, Y. (1989). Development of a pasted nickel electrode with high active material utilization, Journal of the Electrochemical Society, Vol.136, 1590 - 1593.

Yao, M., Okuno, K., Iwaki, T., Kato, M., and Harada, K.. Park, J-J., Tanase, S., and Sakai, T. (2007). Influence of nickel foam pore structure on the high-rate capability of nickel/metal-hydride batteries, Journal of the Electrochemical Society, Vol.154(7), A709 – A714.

2.2 Development of Ni-MH battery with a new structure suitable for scaling-up and verification test

2.2.1. Introduction

After the Industrial Revolution human beings invented methods for obtaining electric energy from fossil fuels. The consumption of electrical energy has been increasing at an accelerated pace as modern industrialization permits mass production and mass consumption, and as the development of IT technology shifts society towards being information-oriented. These changes have caused dwindling reserves of fossil fuels, pollution of the atmosphere, global warming and other environment-related problems.

Since the Green New Deal was launched globally, a great deal of interest has arisen in Japan in alternative energy saving and other new technologies (Sakai, 2010). An increase in the proportion of renewable energy electric-generation, including solar and wind power energy, is expected in the future. Saving energy by using electric storage devices is being actively promoted not only for automobiles but also for trains and other vehicles in the mass transportation system (Nishimura and Tsutsumi, 2007; Tsutsumi, 2008; Tsutsumi and Matsumura, 2009; Yamazaki et al., 2010; Ogura et al., 2010).

Electric storage devices are one of the key technologies for popularizing alternatives to oil and promoting the saving of energy. In particular, high-power storage batteries with a high capacity are essential for generating electric power and absorbing the load changes of the mass transportation system. In response to such demand it is necessary to secure the further durability of high-safety, high-power and high-energy-density storage batteries like the Ni-MH battery.

For industrial use, cell capacity should be increased further and multiple cells stacked in series in order to manage a high voltage. When charge/discharge is conducted with a large current of around 1,000 A, a great amount of Joule heat will be generated and, as a

result, battery temperature will increase and the battery life will be shortened unless the heat is effectively removed. This is a major challenge when batteries are used in industry, where batteries are required to have 10 to 15 years of durability.

The conventional battery-structure employs a general method of welding metal tabs to electrodes and extracting electricity from collecting terminals. This method increases resistance while polarization increases at a distant section from the tabs when the sizes of the electrodes are enlarged. On the other hand, when the number of electrodes is increased, flow control and cost increase while the number of welding places increases.

We have proposed a new high-capacity, high-power and low-cost battery structure with a method that enables current collecting at multiple electrodes through the use of large-area metal plates, and with conduction retained as the electrodes and current collectors are not welded together but make contact. In order to affirm the utility of this battery structure, the sizes of the batteries were increased from 1-cell (1 Wh) with a capacity of 0.77 Ah, 30-cell (5 kWh) with a capacity of 141 Ah, to 10-cell (14 kWh) with a capacity of 1,200 Ah, and battery performances were verified.

2.2.2. Experimental

Figure 1 shows a conceptual diagram of a single cell of the newly structured battery. Strip positive-electrodes and strip negative-electrodes are loaded alternately on a pleated separator, and the plates with the same polar character are placed on the same side in order to build an electrode body. The electrode body is first embedded in a polypropylene celluloid-rim and then a nickel-plating steel-plate is located on each positive electrode and negative electrode in order to build a current collector. To secure contact between the electrode and the current collector, fix-plates were placed outside of the current collector and they were fixed in a direction so as to compress against the

electrode body. With this structure, the electrodes and the steel-plates are not welded but current is collected by force of pressure, and thus this is easy to manufacture even if the scale is expanded. This new method of collecting current without using welding on the cell cases but by force of pressure is called a GIGACELL structure and a battery produced from this method is called a GIGACELL-type battery.

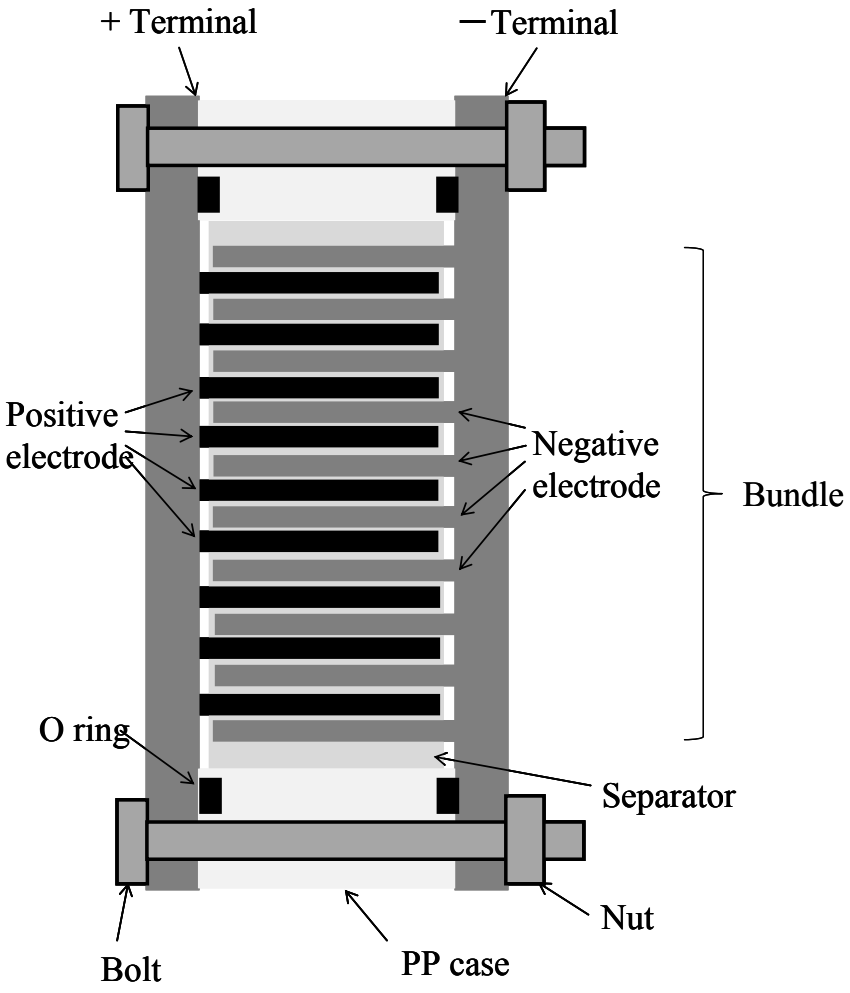

Figure 1: Conceptual diagram of a GIGACELL-structured cell

The positive electrode was prepared by adding slurry, which is made by mixing nickel hydroxide powder, conductive aid material and binder material, to foaming nickel. The slurry was first made by mixing carbon powder (5 wt%) (CB), equine viral arteritis (5 wt%) (EVA) and xylene (20 %) with nickel hydroxide (100 wt%), and then the slurry was impregnated with foaming nickel, dried and pressed in order to produce a 0.35 mmT sheet-shape electrode. The sheet-shape electrodes obtained were cut to a size of 130 mm-length and 29 mm-width, and they were used as strip electrodes.

The negative electrode was prepared by applying slurry, which was made by mixing alloy powder with conductive aid material and binder material, to punching metal. The aqueous slurry was first made by using carboxymethyl cellulose (0.2 wt%) as a bodying agent and styrene-butadiene rubber (0.5 wt%) as a binder for quinary alloys ($MmNi_{3.7}Co_{0.7}Mn_{0.3}Al_{0.3}$) hydrogen occlusion alloy (100 wt%), and then the aqueous slurry was applied to the punching metal, dried and pressed to produce a 0.35 mmT sheet-shape electrode. The sheet-shape electrodes obtained were cut in the size of 130 mm-length and 29 mm-width, and they were used as strip electrodes.

The content ratio of the negative electrode and positive electrode was 3.7 (3.7 times of the positive electrode when the alloy content was 300 mAh/g). The electrolytic solution contained binary alloys of 4.8N-KOH and 1.2N-NaOH, and the separator was a pleated separator made of hydrophilic-treated polypropylene unwoven-cloth.

Table 1 shows the specifications of each battery.

Table 1: The capacity, sizes of electrodes and the number of electrodes loaded of each battery.

	Battery capacity	Electrode size	Number of Electrode		Number of Stacking	energy
	Ah	mm	Positive	Negative		kWh
a	1.3	29 × 60	6	7	1	0.0016
b	141	29 × 230	150	151	30	5.1
c	1200	29 × 230	1200	1208	10	14.4

Figure 2 shows an enlarged conceptual diagram of a GIGACELL-structured battery. Both the 30-cell module and the 10-cell module batteries were designed with a bipolar structure. Aluminum perforated pipes were located between cells as heat sinks, and a cooling fan sends air through the structure.

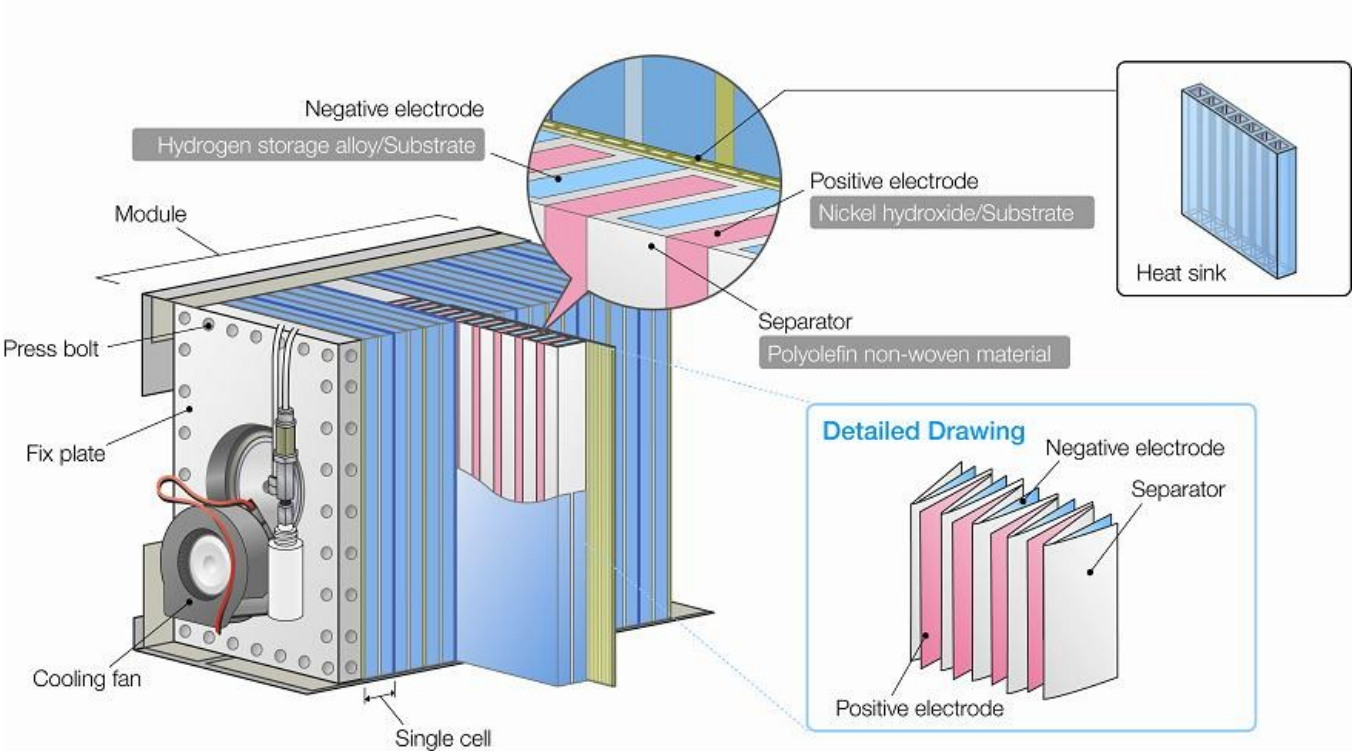

Figure 2: Conceptual diagram of a GIGACELL structure

Figure 3 shows the exterior of each battery.

a)

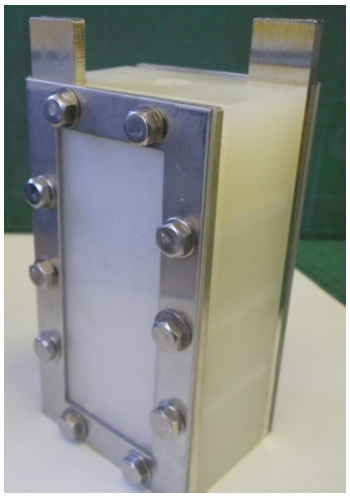

b)

c)

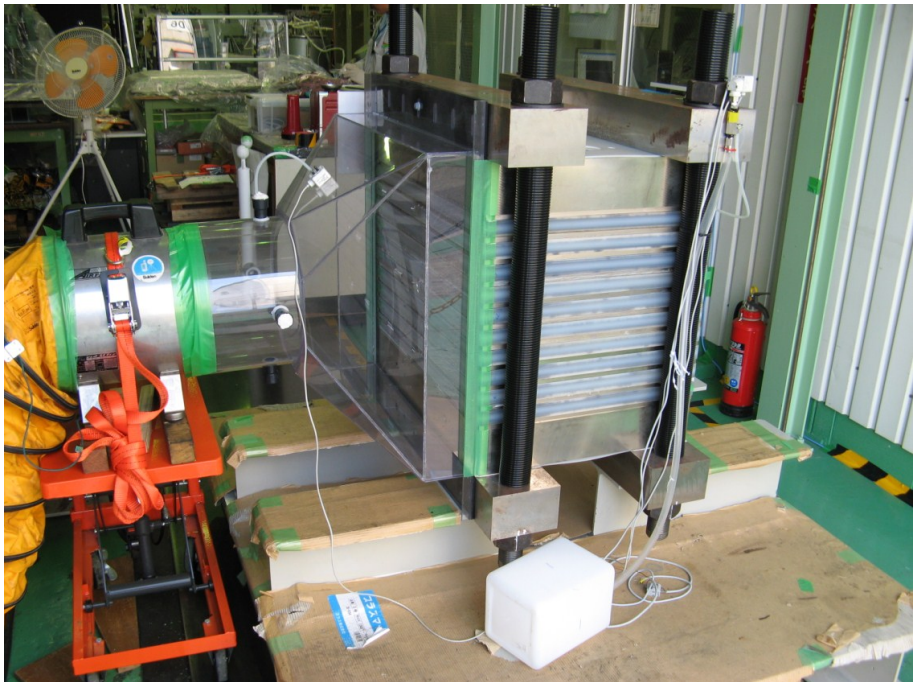

Figure 3: Exterior of each battery

a) 0.77 Ah－single cell　　b) 141 Ah－30-cell　　c) 1,200 Ah－10-cell

2.2.3. Results and discussion

2.2.3.1. Evaluation of a single-cell battery with a capacity of 0.77Ah

Figure 4 shows the discharge curve of a single-cell battery with a capacity of 0.77 Ah at a current rate of 0.5 C~1.5 C. After the battery was charged at a current rate of 1 C (0.77 A) so that the capacity reached 0.77 Ah of rating capacity, discharges were conducted at each rate. Approximately 1.2 V discharge voltage and a discharge capacity of 0.7 Ah and over were observed at the time of discharge at the current rate of 1.5 C (= 1.155 A).

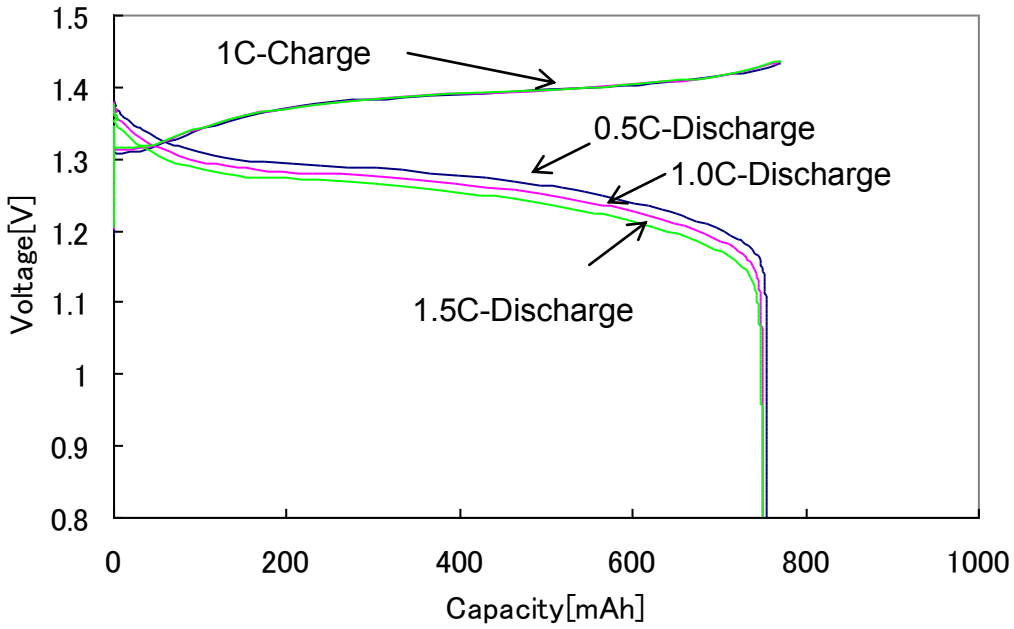

Figure 4: Charge/discharge characteristics of a single-cell with a capacity of 0.77Ah

Figure 5 shows a graph of current values and voltage values at 10 seconds after discharge initiation. The internal resistance of the battery can be calculated as 31.6 mΩ from the gradient.

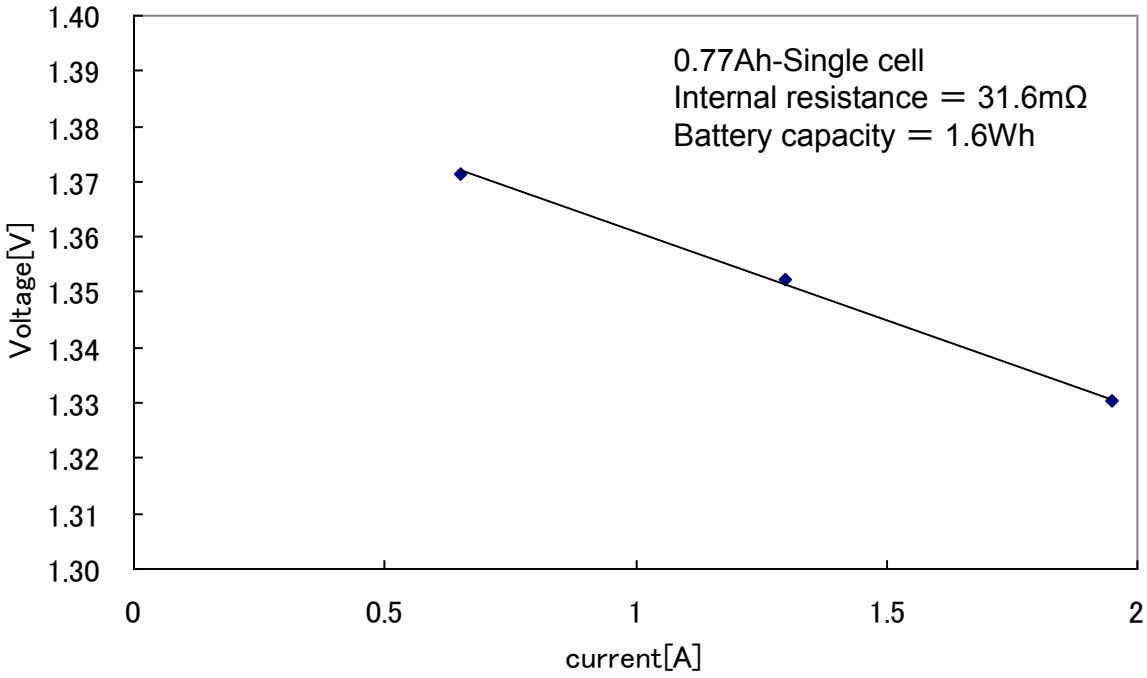

Figure 5: Relation between current and voltage of a single-cell with a capacity of 0.77 Ah at 10 seconds after discharge initiation

Figure 6 shows the result of a cycle test for a single-cell with a capacity of 1.3 Ah when the battery capacity was almost doubled. After the battery was charged at a current rate of 2 C so that the capacity reached 1.3 Ah, the battery was discharged at the current rate of 2 C until it reached 0.8 V. The Ah-efficiency (discharge capacity/charge capacity) was 99 % and over from the early period on the cycle, and efficiency was sustained up to around a 1,000-cycle. Efficiency began declining gradually after the 1,000-cycle, and it declined to approximately 85 % at 1,900 cycles.

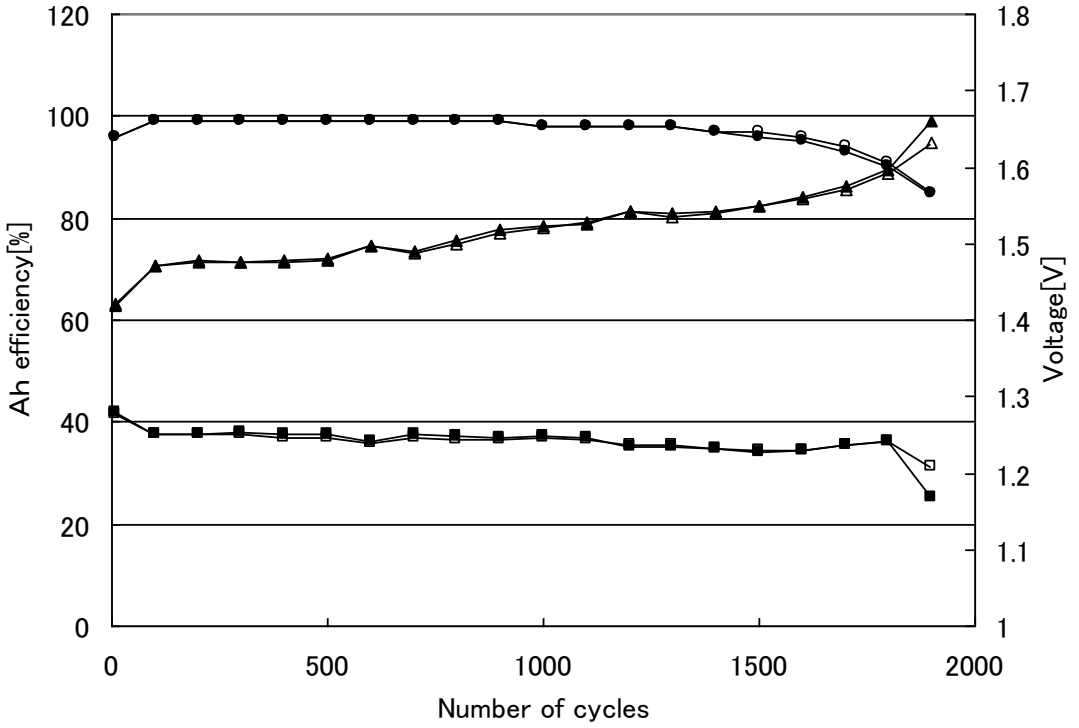

Figure 6: Results of cycle test for a single-cell with a capacity of 1.3 Ah

2.2.3.2. Evaluation of a 30-cell module with a capacity of 141 Ah

Figure 7 shows a charge/discharge graph of a 30-cell module with a capacity of 141 Ah. After the battery was charged with a current rate of 0.2 C (= 28.2 A) so that the capacity reached 141 Ah of rating capacity, discharges were conducted at each rate. Approximately 1.2 V discharge voltage and a discharge capacity of 130Ah and over were observed at the time of discharge at 1.5 C (= 211.5 A). The temperature increase was approximately 8 °C.

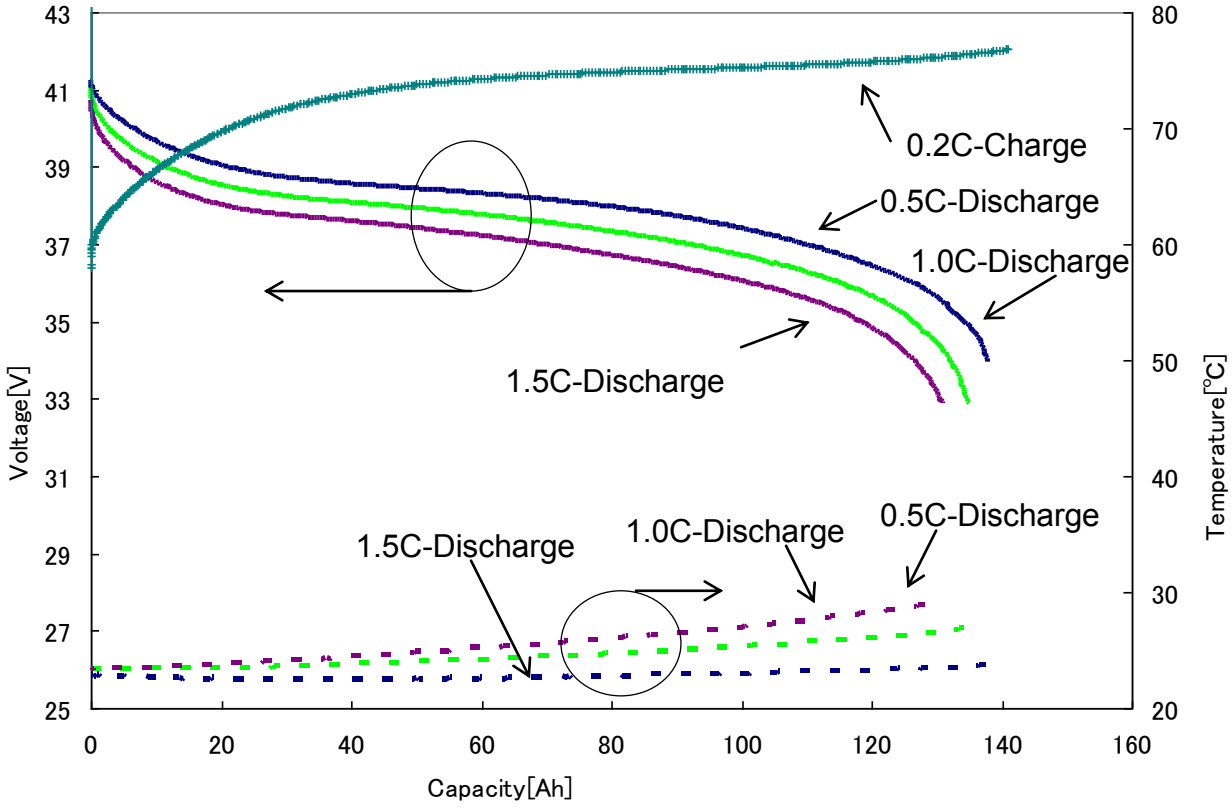

Figure 7: Charge/discharge characteristics of a 30-module with a capacity of 141 Ah

Figure 8 shows a graph of voltage values and current values at 10 seconds after discharge initiation. The internal resistance of the battery can be calculated as 6.1 mΩ from the gradient of the straight line.

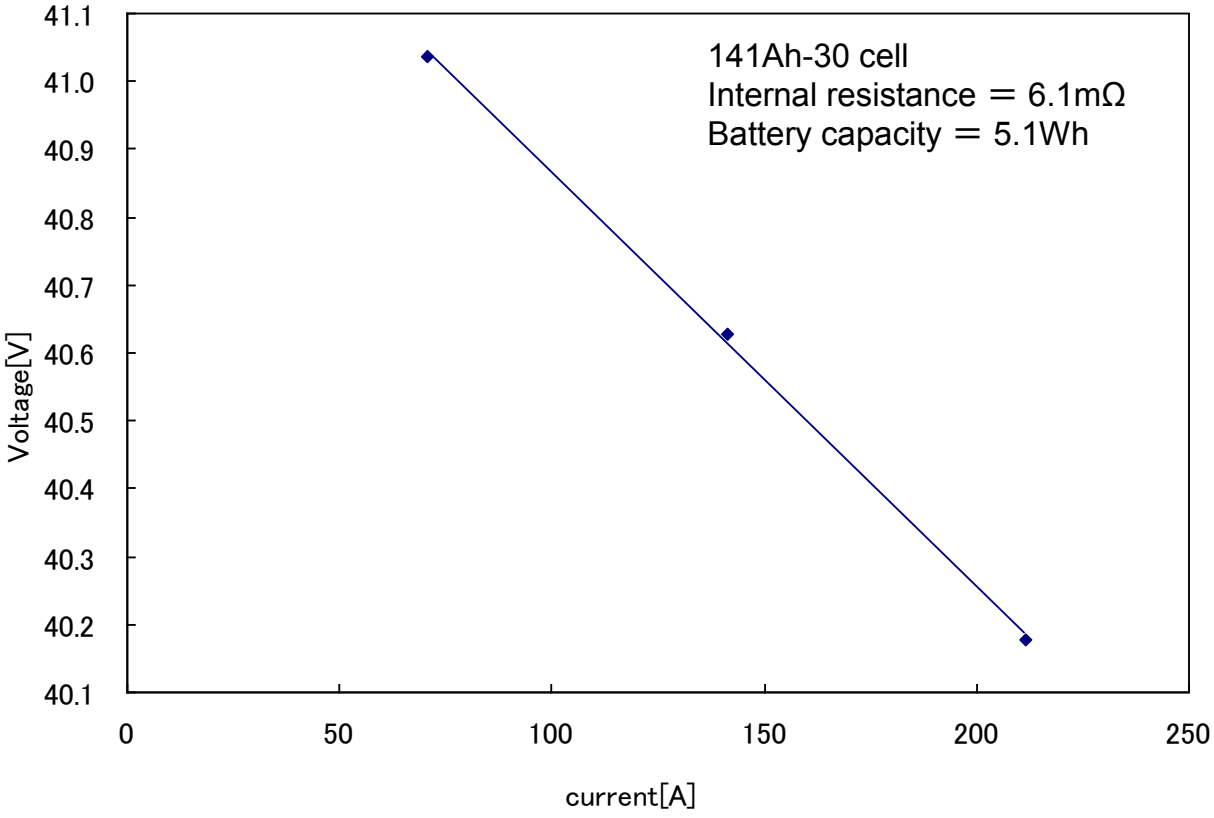

Figure 8: Relation between current and voltage of a 30-module with a capacity of 141 Ah at 10 seconds after discharge initiation

2.2.3.3. Evaluation of a 10-cell module with a capacity of 1,200 Ah

Figure 9 shows the discharge curve of the battery at current rates of 0.5 C~1.5 C. After the battery was charged with a current rate of 0.2 C (= 240 A) so that the capacity reached 1,200Ah of rating capacity, discharges were conducted at each rate. Approximately 1.24 V discharge voltage and a discharge capacity of 1,100 Ah and over were observed at the time of discharge at 1.5 C (= 1,800 A), and the temperature increase was approximately 5 °C.

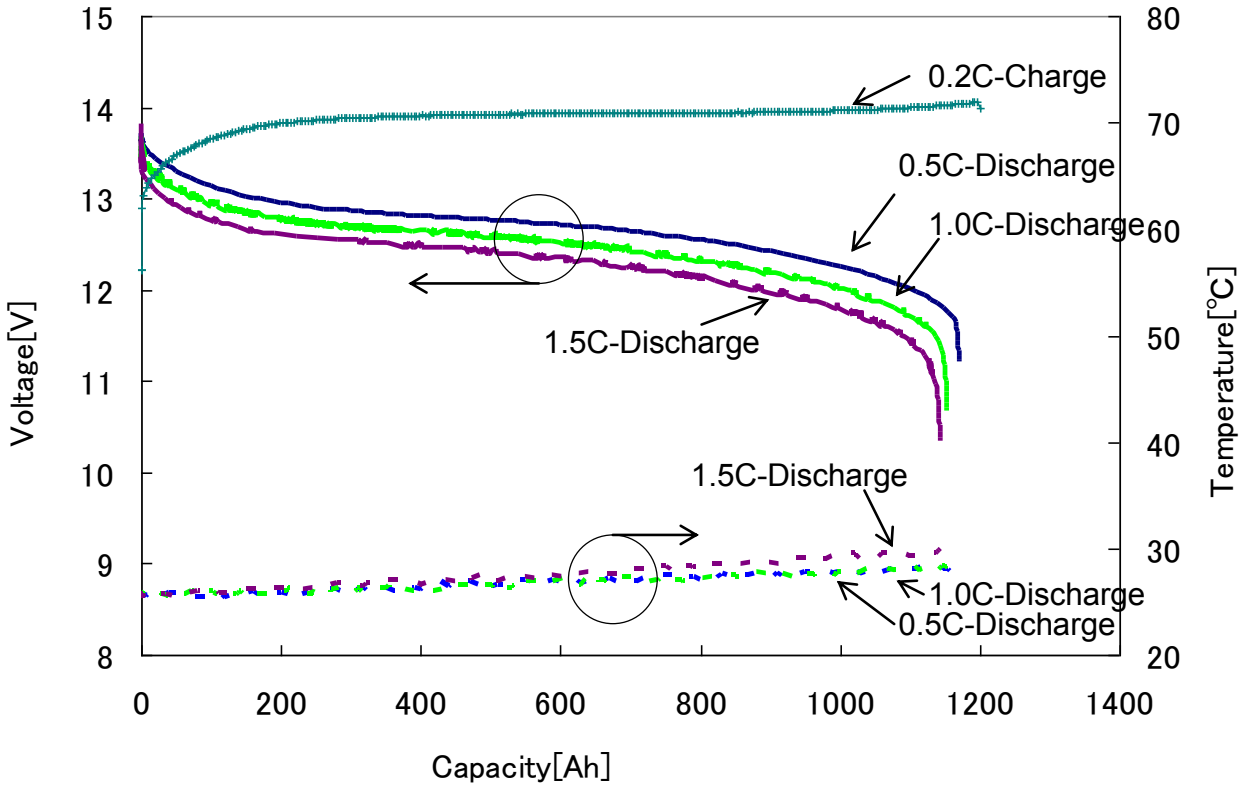

Figure 9: Charge/discharge characteristics of a 10-module with a capacity of 1,200 Ah

Figure 10 shows a graph of voltage values and current values at 10 seconds after discharge initiation. The internal resistance of the battery can be calculated as 0.25 mΩ from the gradient.

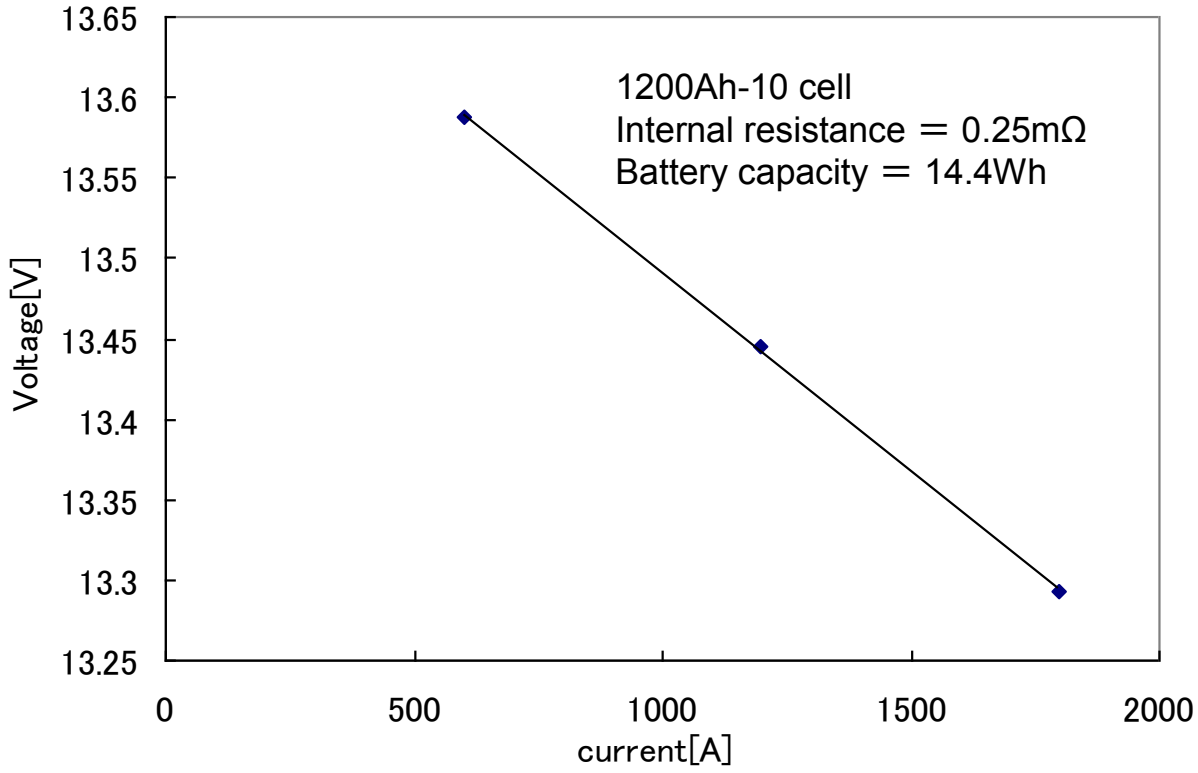

Figure 10: Relation between current and voltage of a 10-module with a capacity of 1,200 Ah at 10 seconds after discharge initiation

2.2.3.4. Comparisons among batteries

To make comparisons of the values of the internal resistance of batteries with a different number of stacks and various capacities, internal resistance value was standardized and set as mΩ･Ah/cell.

Figure 11 shows the capacity and internal resistance of each battery. It was found that even when the capacity of a battery increases, the internal resistance is sustained at a similar value, and when the size of battery is increased, the internal resistance shows no increase.

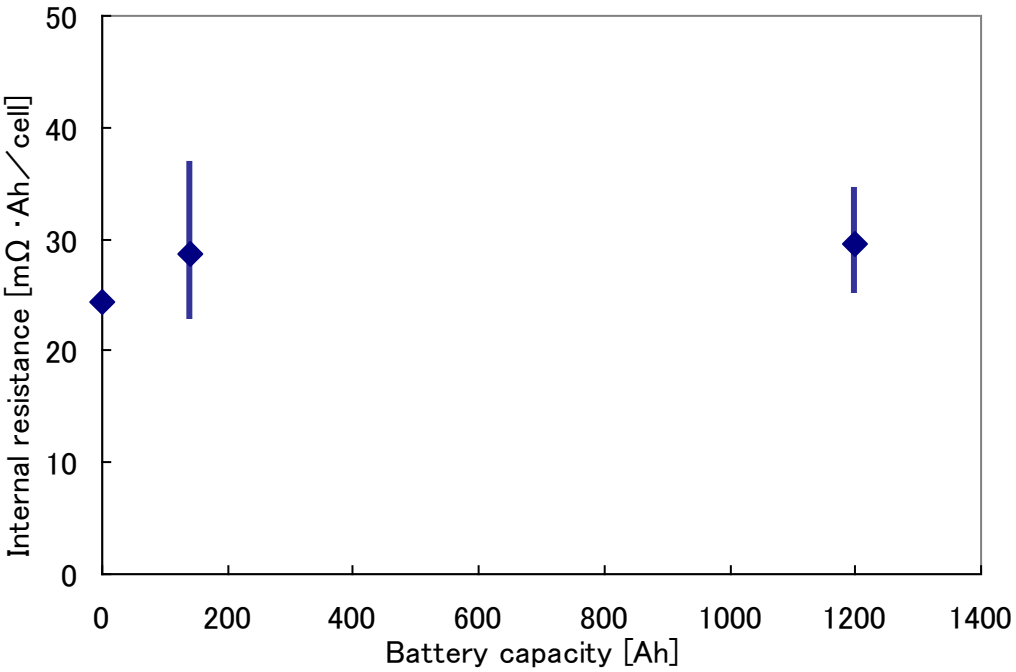

Figure 11: The capacity and internal resistance of each battery

Figure 12 shows the dispersion of internal resistance of each cell when modules have capacities of 141 Ah and 1,200 Ah. The internal resistance values were 30 mΩAh ± 7 mΩAh for a 30-cell module with a capacity of 141 Ah and 30 mΩAh ± 5 mΩAh for a 10-cell module with a capacity of 1,200 Ah. This shows that even when the size of the battery is increased, it is possible to keep the dispersion among cells small.

These results verified that, though a GIGACELL battery is structured with merely the contact of electrodes and current collectors rather than having them welded, the battery does not exhibit an increase of internal resistance even if its scale is expanded, nor a large increase of temperature.

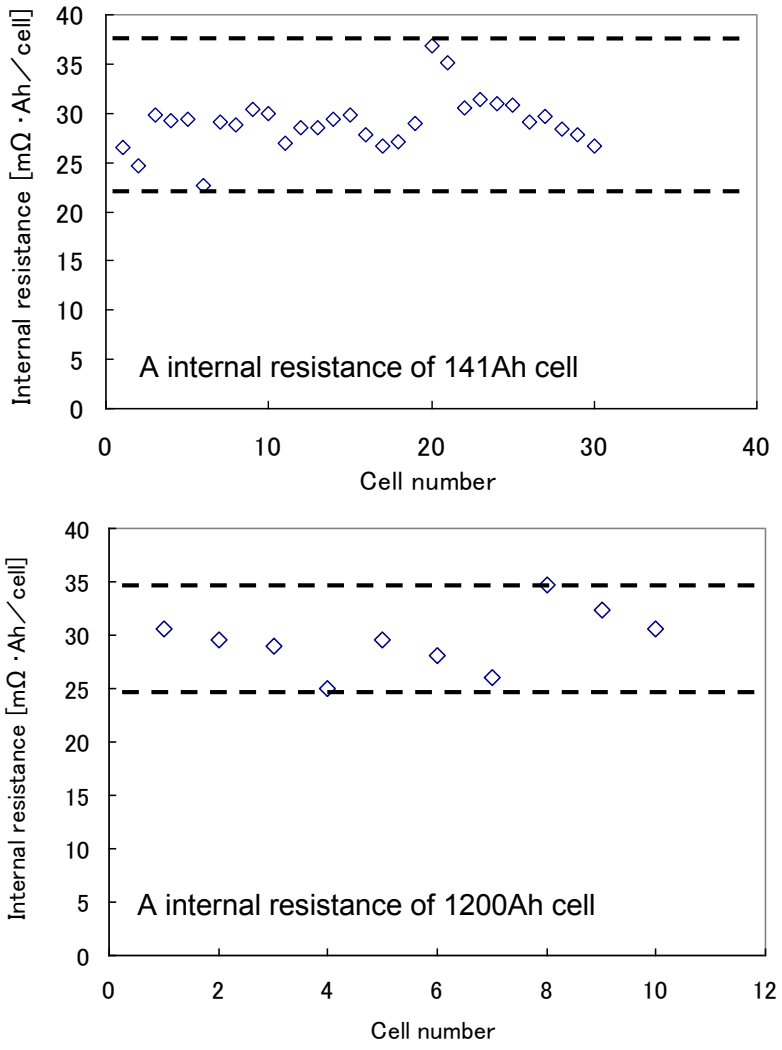

Figure 12: Verification of repeatability at different capacities of each battery

2.2.4. Conclusion

Heat generation must be minimized when the scale of a battery is expanded. A new method was found for reducing the internal resistance of an Ni-MH battery.

The structure of collecting current only by the contact of electrodes rather than having them welded was called GIGACELL, and it was verified that even if the scale of the battery is expanded, the internal resistance is sustained at a certain value.

The temperature increase of the battery was kept small by sending air through the structure with a cooling fan.

Performance tests verified that this GIGACELL structure is a battery structure which is suitable for large cells.

A lot of improvements were made to resolve the dispersion in the internal resistance of cells, and there is no dispersion in the commercialized GIGACELL of today.

References

Sakai, T. (2010). The role of battery technologies for reducing carbon dioxide emission. Funtai Gijutsu, Vol. 2, 17-24.

Nishimura, K., and Tsutsumi. K. (2007). A wet synthesis sealing up battery. Powder Science and Engineering, Vol. 39 (7), 1-6.

Tsutsumi, K (2008). The latest energy saving technology development on railway system. Journal of the Japan Institute of Energy, Vol. 87 (7), 506-509.

Tsutsumi, K., and Matsumura, T. (2009). Revolution in storage battery technology and adoption by electric railways. Science & Technology in Japan, Vol. 26, 21-24.

Yamazaki, H., Akiyama, S., Hirashima, T., Kataoka, M., and Matsuo, K. (2010). Urban transportation that is friendly for people and the environment: SWIMO-X low-floor battery-driven light rail vehicle. Kawasaki Technical Review, Vol. 170, 16-19.

Ogura, K., Matsumura, T., Tonda, C., Nishimura, K., and Kataoka, M. (2010). Effective utilization of energy from train regenerative braking: Battery power system for railways. Kawasaki Technical Review, Vol. 170, 24-27.

2.3 Introduction of large-sized nickel-metal hydride battery GIGACELL® for industrial applications

2.3.1. Introduction

Hydrogen storage material is a good medium to store gaseous hydrogen at a normal pressure and ambient temperature, which provides a possible new way to design various energy storage systems [1-3]. A nickel-metal hydride (Ni-MH) battery has been developed using a combination of hydrogen storage alloys and battery technologies [4-6]. This battery has two times a higher energy density and fewer environmental problems than the Ni-Cd battery. Ni-MH batteries have been commercialized in Japan since 1990. The Ni-MH batteries are widely used as the power sources of hybrid electric vehicles (HEVs) as well as consumer electronic devices [7-9]. The demand for the Ni-MH batteries is increasing due to the increasing focus on the environment and its sustainability.

A new fiscal policy, “Green New Deal”, was deployed on a global scale in order to realize a low carbon society and improve the self-sufficiency energy supply ratio. In Japan, targets are reducing the amount of greenhouse-gas emissions by 25% in 2020 compared to 1990, and increasing the rate of renewable energy, such as solar and wind, from the present 1% to 10%. A smart grid, which is a method of controlling the renewable energies with large load-fluctuations by secondary batteries and IT technology, is being actively developed on a global scale [10]. The development of large-sized high-performance batteries will promote the widespread use of a new power generation, transmission and distribution system in the social-infrastructure.

Kawasaki Heavy Industries (KHI) has recently developed a large-sized high-power Ni-MH battery, GIGACELL®, as shown in Figure 1. Verification tests have been conducted for several industrial applications, such as SWIMO®, a battery-driven light

rail vehicle (LRV), Battery Power System (BPS) for railways and power generation and stabilization of the Power Grid [11-17]. In this paper, the innovative design of the GIGACELL® and the results of the verification tests are described.

Figure 1 GIGACELL® battery

2.3.2. Design and Performance of GIGACELL®

Figure 2 is a schematic view showing the structure of the GIGACELL®. The GIGACELL® is composed of individual cells that are connected in series at their cell walls, with the front and rear surfaces becoming the positive and negative terminals, thus forming the bipolar structure. The cell walls provide a large cross-sectional area that minimizes energy loss that usually occurs when the cells are connected. The high voltage of the battery is accomplished by increasing the number of cells arranged in the bipolar structure. Inside each cell, pre-formed stripes of positive and negative electrodes are inserted into the respective sides of the pleat-folded separator. Increasing the three-dimensional elements of the pre-formed strips (height, width and quantity)

expands the capacity of the battery. The bipolar design of the GIGACELL® prevents overheating of the battery, with a cooling fan sending cooling air through the heat-sink. It also reduces the energy loss between cells allowing a greater capacity. In addition, no welding is used on the cell cases, therefore, the GIGACELL® can be easily disassembled for recycling.

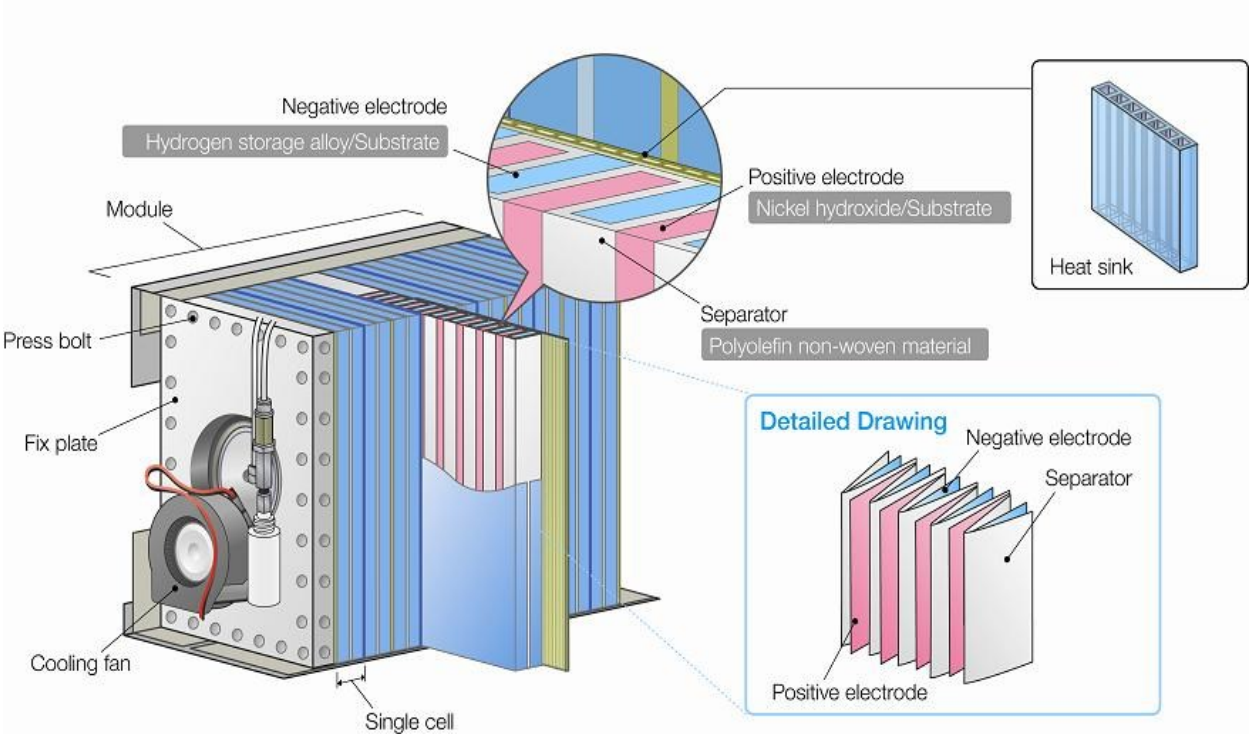

Figure 2 Schematic view showing the structure of the GIGACELL®.

Figure 3(a) shows the discharge curves of a 30-cell module with a 150Ah rating. An approximate 38V discharge voltage (1.27V/cell) and 97% discharge capacity was observed at the 1C rate (= 150A). Even at the 5C-rate (= 750A), an approximate 35V discharge voltage (= 1.17V/cell) and 90% discharge capacity are maintained.

Figure 3(b) shows a cycle-life performance of a single 3.5Ah cell of the GIGACELL®. An approximate 98% efficiency was observed after charging to 2.8Ah

(80% of the rated cell capacity). No capacity decay is observed after 11,000 cycles. The average voltage was 1.24V during the cycling. As just described, the structure of the GIGACELL® is suitable for use in a high-power, large-sized battery with a long cycle-life.

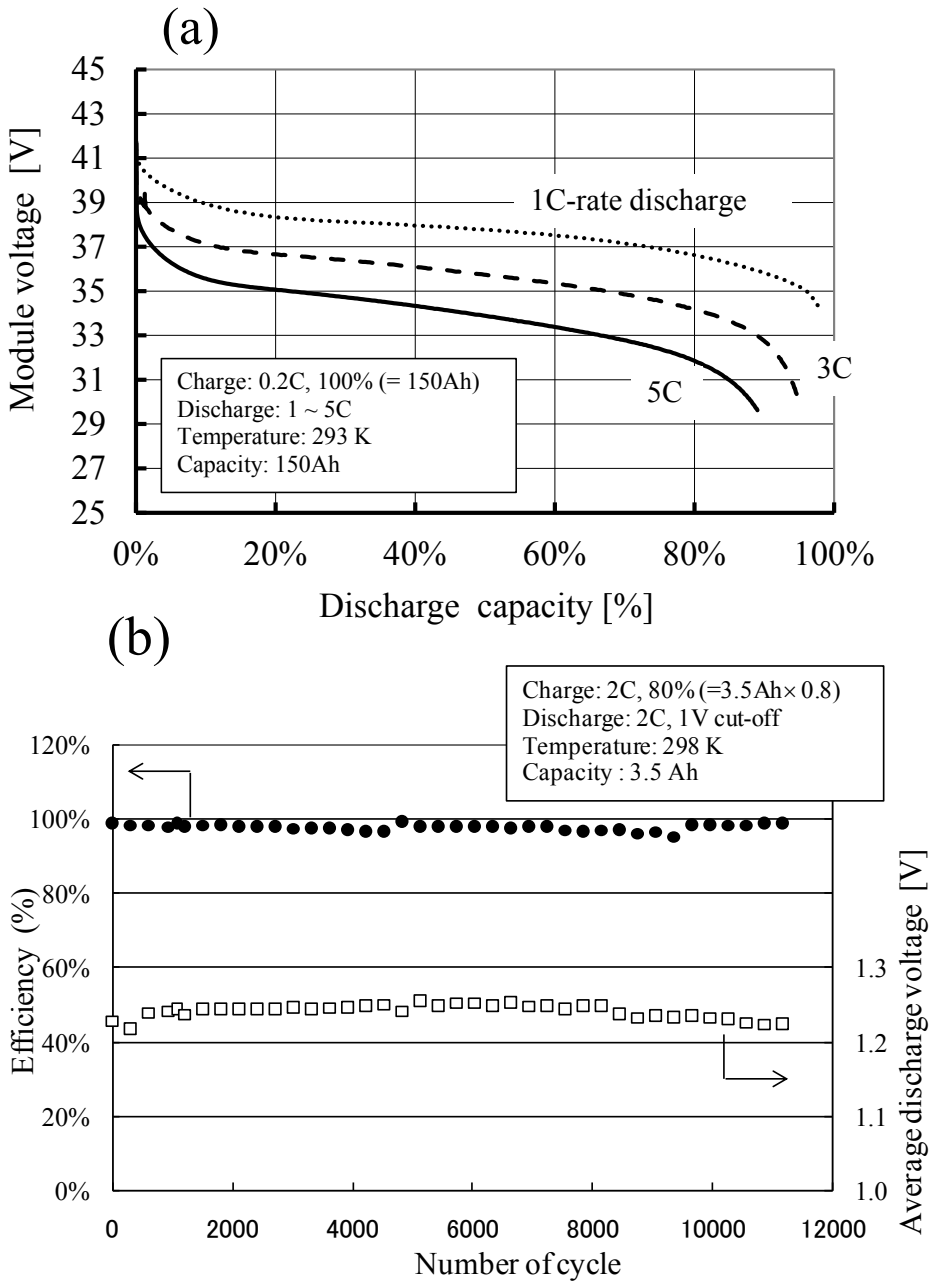

Figure 3(a) Discharge curves of 150Ah module(30-cells) at 298K and various currents. 3(b)Cycle-life performance of 3.5Ah single cell at 298K.

2.3.3. Verification tests of GIGACELL®

2.3.3.1 Battery-driven light rail vehicle, SWIMO®

KHI developed a battery-driven light rail vehicle (LRV) SWIMO® that is equipped with the GIGACELL®. Figure 4(a) shows the experimental vehicle called SWIMO-X. The structure and specifications of the SWIMO-X were reported in a previous study [11, 13, 14]. A wide and low floor was realized by storing the compact GIGACELL® under the seats. A total of 16 modules (115kWh) were installed in the SWIMO-X. In 2007, a running test of the SWIMO-X was performed by the Sapporo City Transportation Bureau during the winter [13]. The LRV was able to operate for over 10 km using the onboard GIGACELL® without recharging.

Figure 4(b) shows an outline of the battery-driven system for the LRV. In the electrified sections, the power-supply line mainly provides power to the LRV. The batteries can provide power when there is a voltage drop from the power supply line. In the non-electrified sections, the onboard batteries provide power to the LRV. The batteries can also capture and store regenerated energy. Moreover, the energy stored in the battery can be used for power when starting as well as for operating the auxiliary equipment. The railway operator can reduce the number of substations by spacing them farther apart. Moreover, it is now possible to entirely eliminate power lines for some sections of the track and operate the SWIMO® solely by using its onboard GIGACELL®.

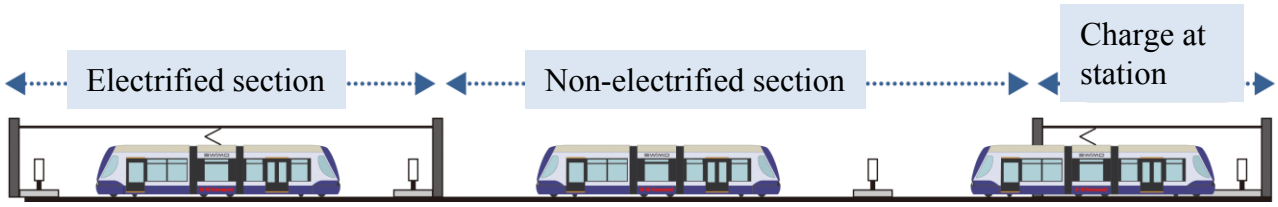

Figure 4(a) Experimental vehicle called SWIMO-X.

(b) An outline of the battery-driven system for the LRV.

2.3.3.2. Battery power system (BPS) for railways

With today's rail system, regenerative braking is a significant achievement. An electric train generates electricity using regenerative braking when decelerating, and the electricity will be supplied to another train during acceleration. However, trains cannot generate the maximum amount of regenerative braking energy when there are no nearby trains needing electricity, or when the line voltage is too high. The surplus energy surges down toward the catenary wire and is dissipated as heat. This termination of regenerative braking is known as "regenerative failure". In this case, trains will have to rely on its mechanical brake for stopping, which will increase brake wear and maintenance costs.

Figure 5 shows a schematic illustration of the wayside energy storage system for railways, which KHI calls the Battery Power System or (BPS) for railways. The BPS is electricity storage equipment that is installed near a substation. Generally, 20 or 40 GIGACELL® batteries are connected in series in one BPS unit.

The BPS accumulates any excessive electricity when the power supply line voltage rises, thus stabilizing the line voltage. With the BPS, the surplus energy can be stored in the GIGACELL®, and discharged when needed, thus ensuring efficient use of the regenerative braking energy at all times. Heavy train traffic, such as during rush hour, can cause the voltage supplied to the trains to drop. At such times, the BPS discharges to provide supplemental power to the trains that will help to the train operator to avoid costly peak energy surcharges. In addition, the GIGACELL® equipped BPS is directly connected to the power line, eliminating the need for any type of expensive controllers that can cause electromagnetic interference (EMI)-related problems.

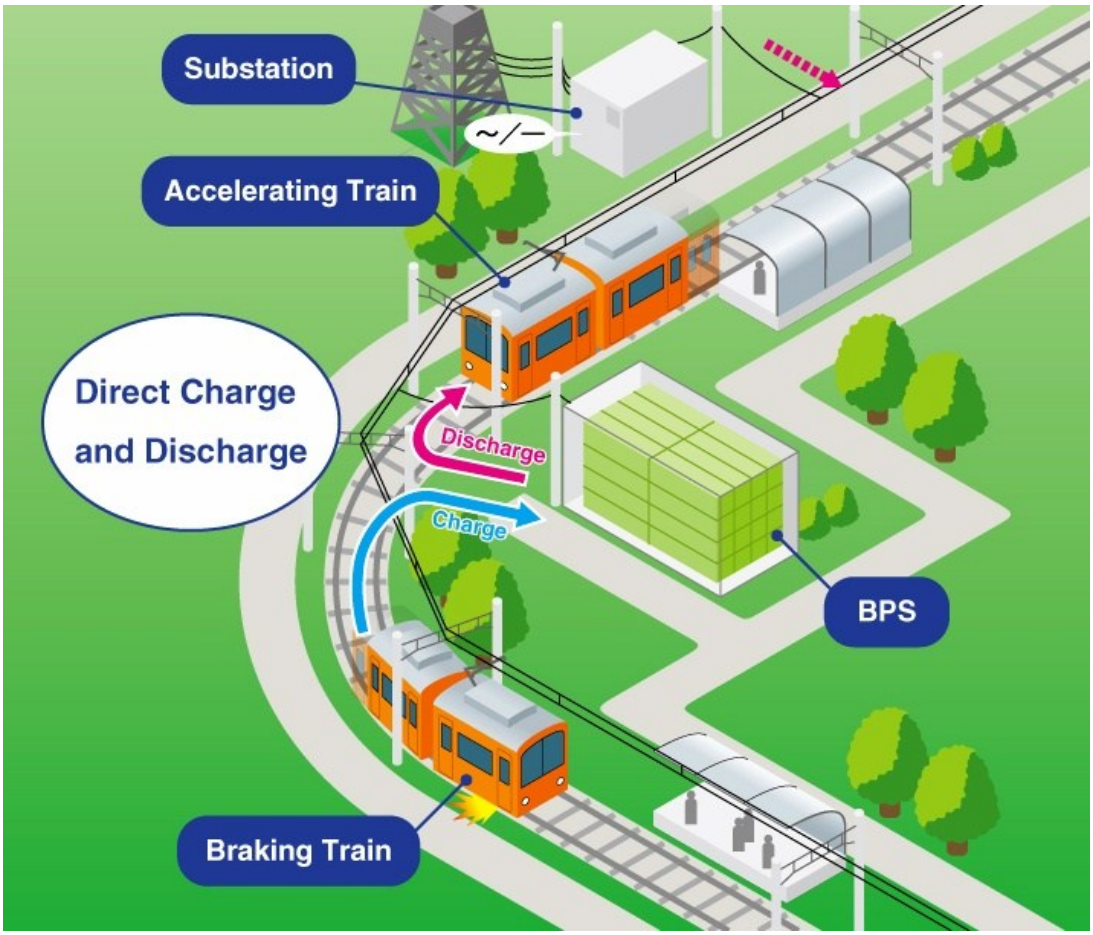

Figure 5 Schematic illustration of the wayside energy storage system for railways.

Kawasaki's long experience in the railway industry has enabled the BPS to be successful in numerous verification tests. Several of Japan's top operators, such as the Osaka Municipal Transportation Bureau (Osaka subway) and Tokyu Corporation, have started commercial use of the BPS. The Tokyo monorail has also determined to introduce the GIGACELL® equipped BPS into their systems.

The first BPS verification test was conducted in November 2007 in the Osaka subway, which is the second largest subway network in Japan [17]. The current commercial BPS at the Komagawa substation consists of two banks (19 GIGACELLs/bank; 205kWh). This system has saved 449MWh/year. This value corresponds to 5% of the total energy consumption of the substation.

Figure 6 shows the transitions of charge/discharge power during operation of the BPS at the Komagawa substation in 2011. This is a 750V DC system. Performance without BPS is shown by the gray line. The train's propulsion system cancelled the regenerative braking when the voltage at the pantograph reached 900V. After the BPS was installed, which is shown by the black line, the maximum voltage during regenerative braking was kept at 854V, preventing the cancellation of regenerative braking. With the introduction of BPS, the range of voltage fluctuations decreased from 236V to 136V. The tests resulted in 1136kWh battery charges per day.

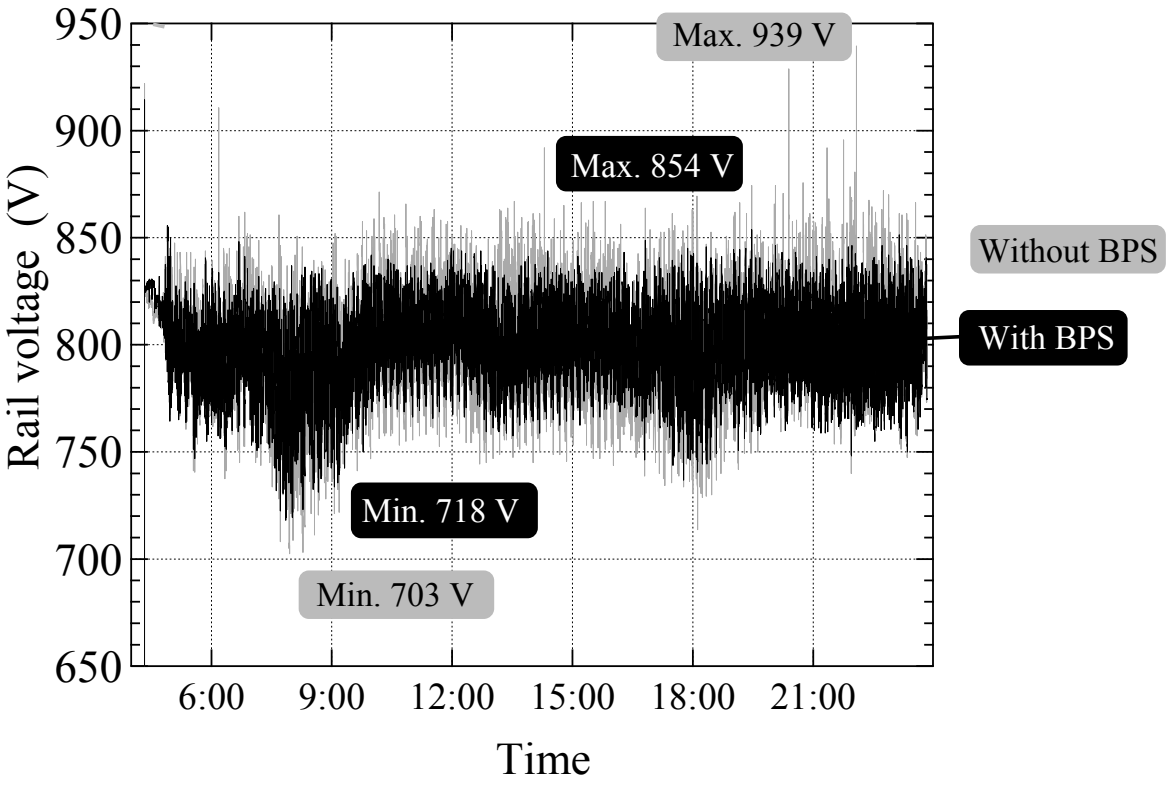

Figure 6 The transitions of charge/discharge power during operation of the BPS at the Komagawa substation in 2011.

The Tokyu Corporation is the largest privately-owned operator in Japan. Their verification test of the BPS was conducted from August, 2010 to September, 2011. Commercial use at the Tsukimino substation was started in November, 2011. The current commercial BPS consists of 4 banks (Four banks of 20 GIGACELL modules per bank give a total of 420kWh). Figure 7 shows the BPS operation data for the Tsukimino substation on the Tokyu line. On the 1500V line where the testing was done, an approximate 4000 charge/discharge cycles were recorded on the BPS system in one day. Currently, the total charged and discharged amounts are 4229 and 3914 kWh per day respectively. This system has saved 1600MWh of energy per year. This value corresponds to 4.8% of the total energy consumption for the substation.

The verification test of the Tokyo monorail has already been conducted in 2010. The monorail line, which goes to the Haneda airport, travels through a harbor area. In case of an emergency, electrical power to propel the trains to the nearest station is indispensable for ensuring the passenger safety. In the emergency running test, the BPS system enabled a monorail to power as far as 10.2 km away. The emergency power supply function of the BPS has proven to be valuable for the operator. The Tokyo monorail has also decided to introduce the GIGACELL® equipped BPS into their systems.

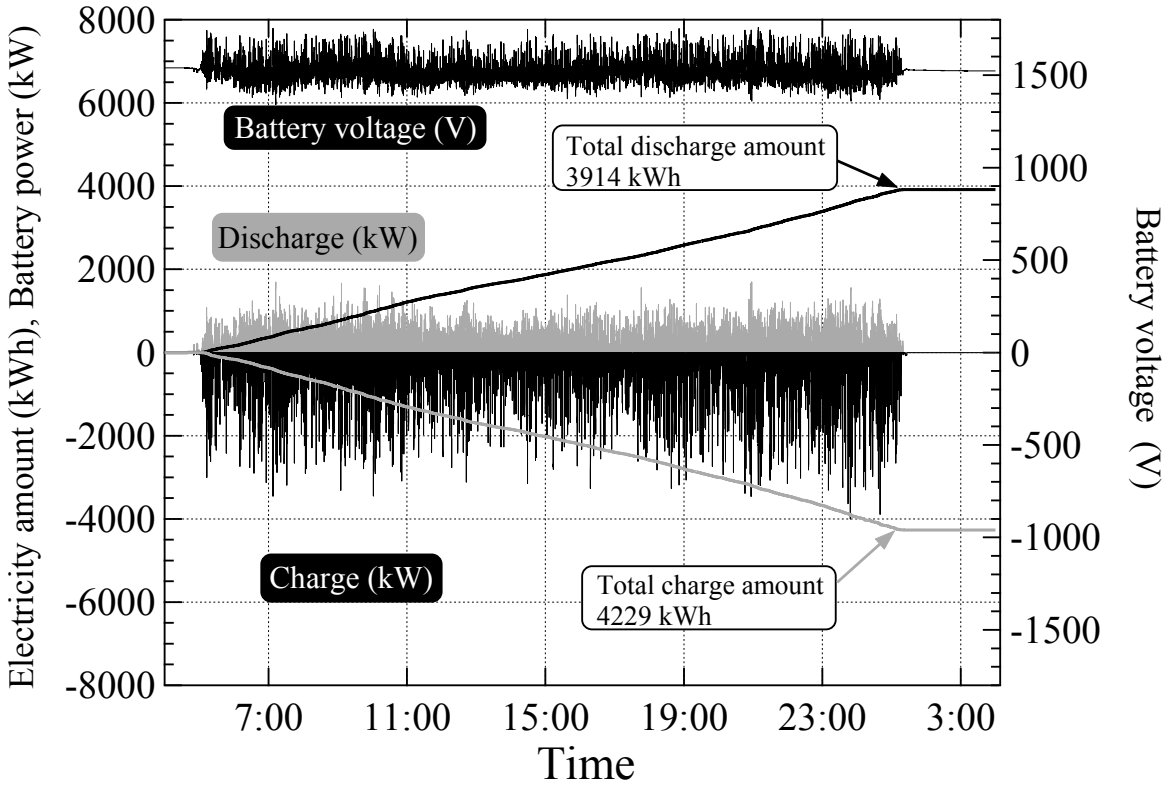

Figure 7 The BPS operation data for the Tsukimino substation on the Tokyu line.

2.3.3.3. Stabilization of Power Grid

In this section, the verification tests of GIGACELL® in a power grid that incorporates solar and wind power will be introduced. With the natural power sources such as these, there is a concern that daily weather changes could cause sharp and large fluctuations in the electrical output. This will become a barrier when high numbers of such natural power sources are connected to the power grids. Therefore, in order to enable the wide use of these renewable energy sources, it is essential that the output of wind- and solar-power sources is stabilized through the use of energy storage systems.

The use of GIGACELL batteries in conjunction with solar power plants is being undertaken on a commercial basis at the Yachiyo-shoin High School in the northern part of Japan's main island and at Kawasaki's west-Kobe plant. Furthermore, a verification test is in progress at the Nissin Electric Corporation. In these applications, the solar panels generate between 100 and 300 kW, and the GIGACELL capacities are from 150 to 270 kWh. The GIGACELLs are being used for peak shaving to reduce the large fluctuations in the electrical output and for power supply to operate auxiliary equipment in the case of emergency.

The use of GIGACELL batteries as part of a wind power plant is being commercially performed at the Nishime wind farm (Win Power Co., Ltd.) in Akita prefecture in northern Japan. Figure 8 shows the wind-power, GIGACELL® and smoothed outputs during the tests. Wind power also exhibits large fluctuations in the electrical output due to the daily changes in the weather. With wind-power output, short-cycle fluctuations caused by the unstable characteristics of the wind are common. The GIGACELL® is charged and discharged in response to the wind conditions, greatly reducing fluctuations in the power supplied to the grid. If the wind power is higher than the smoothing target value, the GIGACELL® is charged with the extra energy and then

discharges it when the output is below the target value.

Furthermore, Kawasaki has started a verification test of the stabilization of power frequency from solar panels connected to a commercial infrastructure. In 2010, 10MW solar panels and a 102 kWh GIGACELL array were installed at the Ishizugawa substation. This extensive test is being carried out with the cooperation of the Kansai Electric Co. Inc. and the Nissin Electric Corporation.

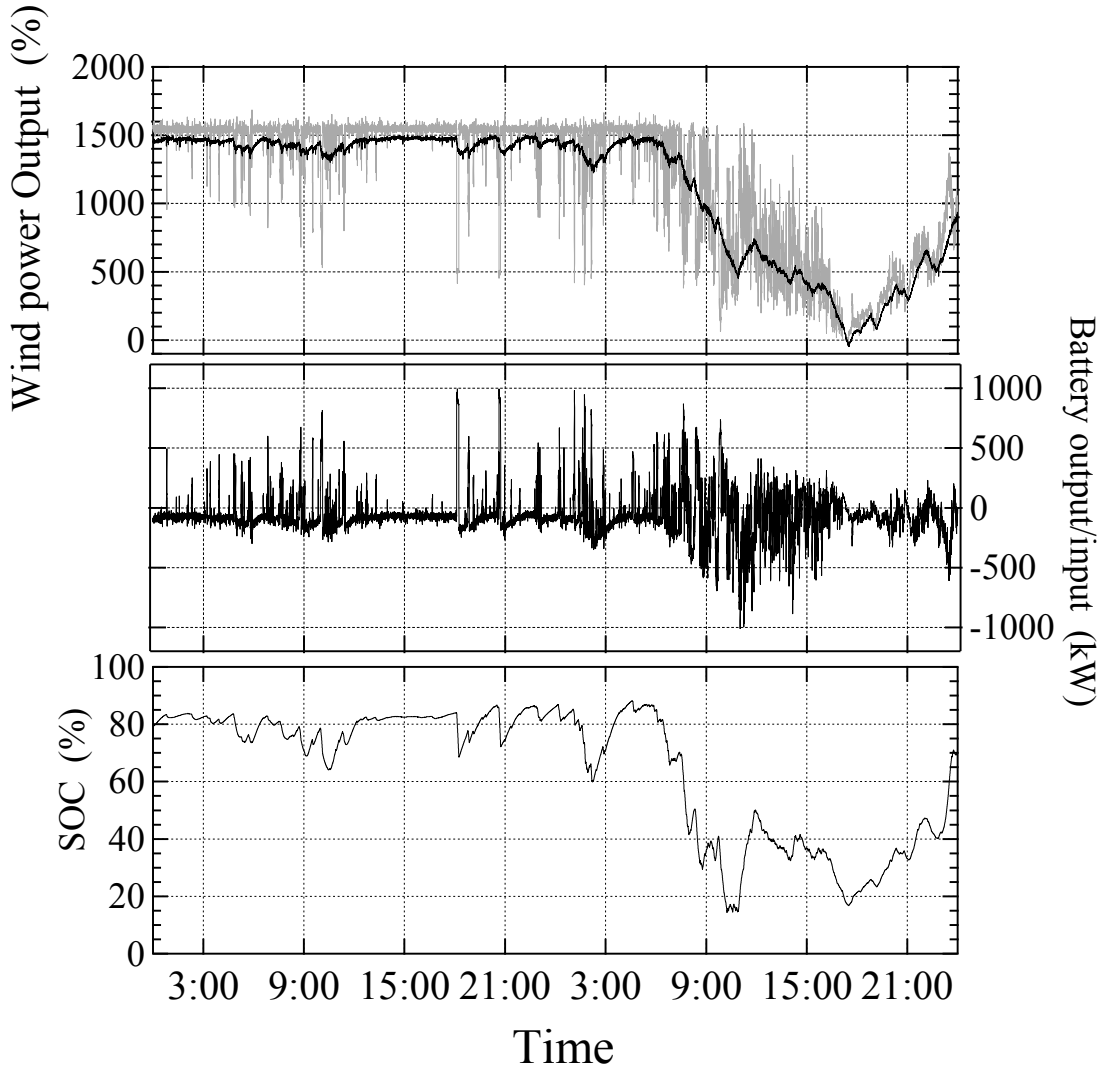

Figure 8 The wind-power, GIGACELL® and smoothed outputs during the tests.

Figure 9 shows the frequency of the AC power, inverter output, SOC and bias state for one day during the test at the Ishizugawa substation. The battery is charged when the frequency exceeds 60Hz, while the battery is discharged when the frequency is less than 60Hz. For example, between 15:07 and 15:36, the frequency showed a tendency towards being less than 60Hz. At times like these, the inverter output continues increasing and the SOC of the battery was reduced. As shown by the arrows and circles, the charge-bias was turned on when the SOC was less than 40% to protect the battery from being overdischarged. Meanwhile, the charge-bias was turned off when the SOC reached 45%. A 50kW reduction in invertor output was observed during the charge-bias activated process as shown by the square frame. If the charge-bias as had not been activated, the inverter output would behave like the black line.

If the high amount of renewable energy source were incorporated into the today's power grid, the use of the energy storage system such as GIGACELL would be indispensable to stabilize the AC frequency. Destabilization in the AC frequency may cause various troubles such as electric-power failure and generator breakdown.

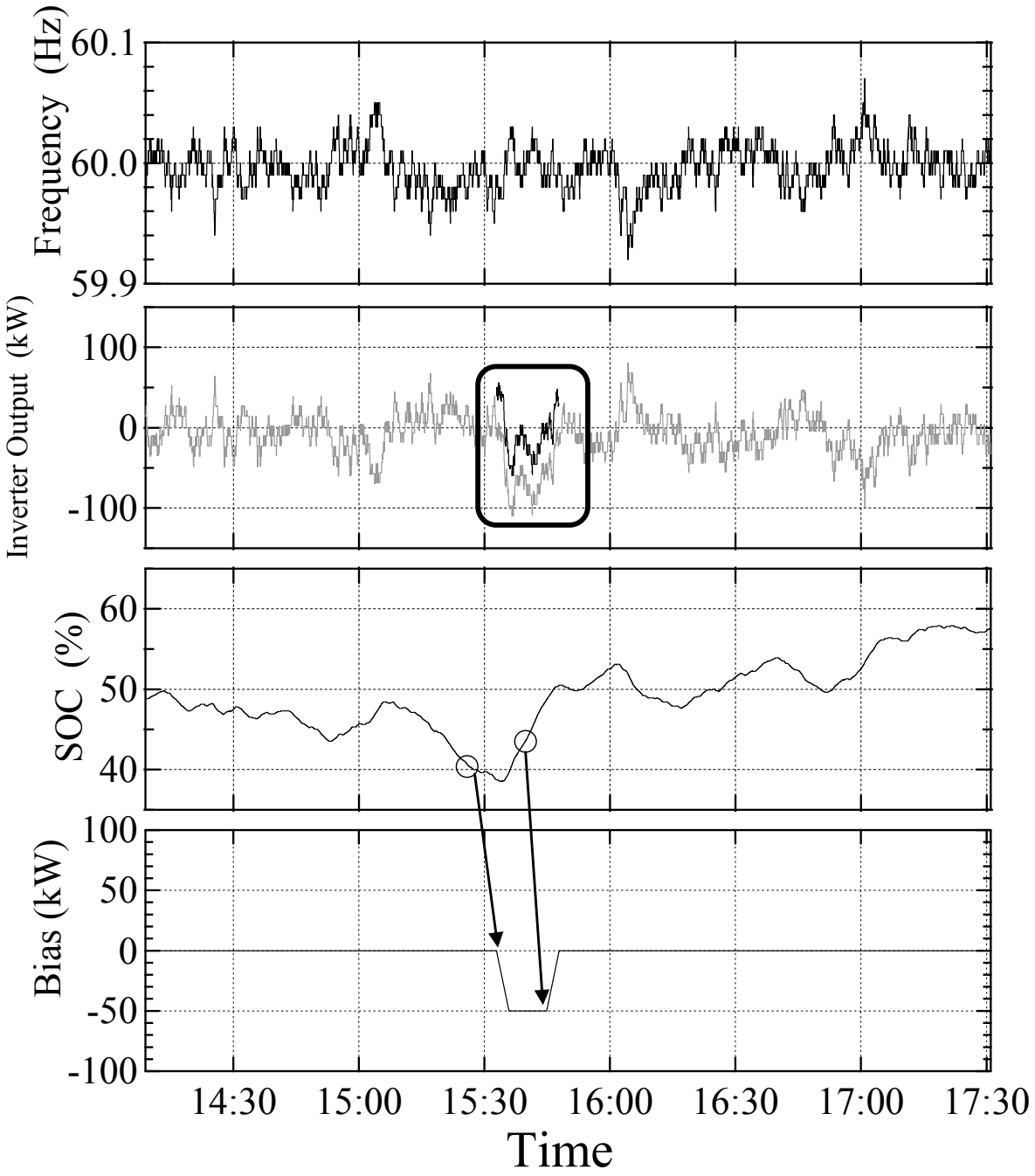

Figure 9 The frequency of the AC power, inverter output, SOC and bias state for one day during the test at the Ishizugawa substation.

In the future, the demand of large-scale high-power energy storage system will be increased for stabilization of large-scale power grids. As stated above, the bipolar structure of the GIGACELL® allows for the increase in both the number and capacity of the cells. Figure 10 shows the extremely large-sized battery stack with 40 cells and 1500Ah (75kWh). Despite the large capacity, this battery exhibited an approximately equivalent discharge curve compared with the normal sized GIGACELL as shown in Figure 11. In the future, KHI will continue to improve the development of innovative battery technology for the social-infrastructure.

Figure 10 the extremely large-sized battery stack with 40 cells and 1500Ah (75kWh).

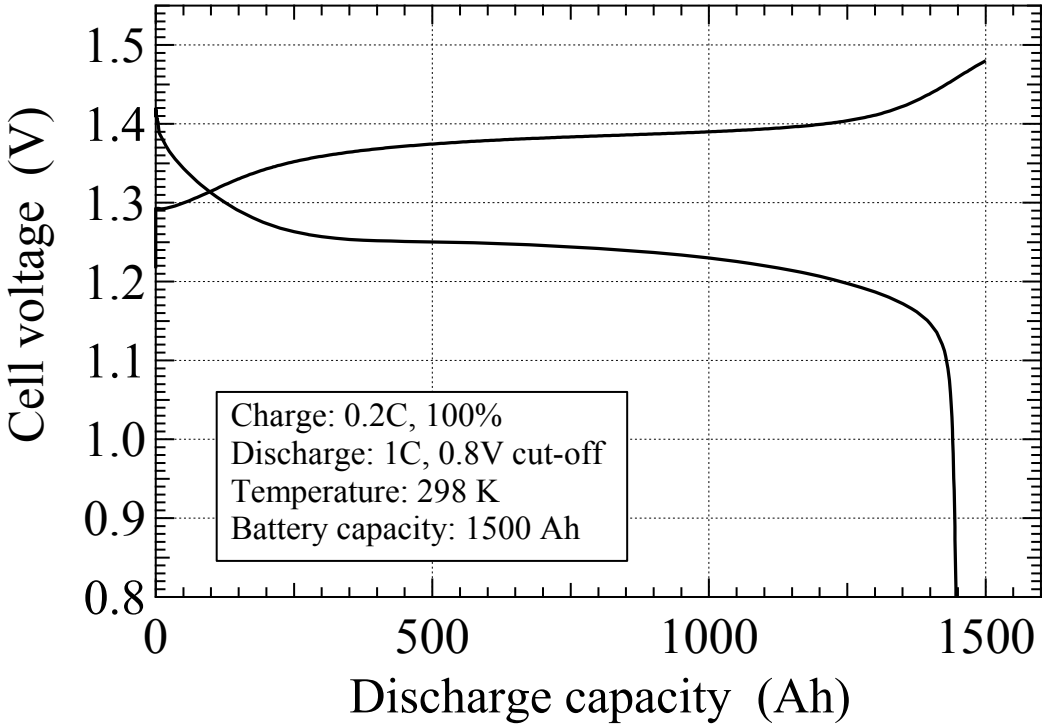

Figure 11 Charge/discharge characteristics of 40 cells with 1500Ah

2.3.4. Conclusion

The high-performance battery has become one of the key components for environmental protection and its sustainability. KHI has developed a large-sized high-power Ni-MH battery, called the GIGACELL®. This battery shows a great potential for various industrial applications, such as LRV, BPS for railways and stabilization of the power grid. The GIGACELL® will significantly contribute to energy savings and reduction CO_2 emissions in future social-infrastructures. The GIGACELL® is viewed as a competitive candidate for next generation energy storage system.

Acknowlegements

The running test of SWIMO® was performed with the cooperation and support of the Sapporo Municipal Transportation Bureau. Examination of the BPS was performed with the cooperation and support of the Osaka Municipal Transportation Bureau, Tokyu Corporation and Tokyo monorail. Examinations of the power-grid and wind-power generations were supported by the New Energy and Industrial Technology Development Organization (NEDO), “Development of an Electric Energy Storage System for Grid-connection with New Energy Resources: Development of Practical Applications: Development of an Advanced Nickel-Metal Hydride Battery”. Examinations of the power-grid and solar-powered generations were performed with the cooperation and support of Kansai Electric Power Co., Inc., and Nissin Electric Co., Ltd.

References

[1] J.J. Reilly, R.H. Wiswall Jr, *Inorg. Chem.* 7 (1968) 2254.

[2] H. Zijlstra, F.F. Westendorp, *Solid St. Commun.* 7 (1969) 857.

[3] G. Sandrock, *J. Alloys Compd.* **293-295** (1999) 877.

[4] Y. Osumi, H. Suzuki, A. Kato, M. Nakane, Y. Miyake, *Nippon Kagaku Kaishi,* 11 (1978) 1472.

[5] Y. Osumi, A. Kato, H. Suzuki, M. Nakane, Y. Miyake, *J. Less-Common Met.* 66 (1979) 67.

[6] I. Uehara, T. Sakai, H. Ishikawa, *J. Alloys Compd.* 253-254 (1997) 635.

[7] T. Sakai, I. Uehara, H. Ishikawa, *J. Alloys. Compd*. **293-295** (1999) 762.

[8] A. Taniguchi, N. Fujioka, M. Ikoma, A. Ohta, *J. Power Sources.* **100** (2001) 117.

[9] K. Shinyama, Y. Magari, K. Kumagae, H. Nakamura, T. Nohma, M. Takee, K. Ishiwa, *J. Power Sources*. **141** (2005) 193.

[10] T. Sakai, *J. Jpn. Inst. Energy.* **89** (2010) 420.

[11] K. Nishimura, K. Tsutsumi, *Powder Science and Engineering.* **39(7)** (2007) 1.

[12] K. Tsutsumi, *J. Jpn. Inst. Energy.* **87(7)** (2008) 506.

[13] Y. Oku, *Kawasaki Technical Review.* **169** (2009) 12.

[14] K. Tsutsumi, T. Matsumura, *Science & Technology in Japan.* **26** (2009) 22.

[15] *High-capacity Fully-Sealed Nickel-Metal Hydride Battery [GIGACELL®]*, Kawasaki Heavy Industries, Ltd.

[16] H. Yamazaki, S. Akiyama, T. Hirashima, M. Kataoka, K. Matsuo, *Kawasaki Technical Review.* **170** (2010) 26.

[17] K. Ogura, T. Matsumura, C. Tonda, K. Nishimura, M. Kataoka, *Kawasaki Technical Review.* **170** (2010) 24.

Chapter 3

Development of cobalt-free nickel-metal hydride battery for industrial applications

3.1 Cobalt-free materials for nickel-metal hydride battery: self-discharge suppression and overdischarge-resistance improvement

3.1.1 Introduction

Applications of nickel-metal hydride (Ni-MH) batteries have been extended from consumer-use electric devices to the hybrid electric vehicle (HEV) [1]. Research and development of this battery is now focused on application to large-sized industrial equipment such as a battery-driven train, wayside energy storage system for railways and a power-grid as a renewable energy source [2-4].

For industrial applications, a number of single cells are stacked in series to assemble a high-voltage battery module. Each of the cells are equally charged and discharged during the initial cycles. However, the increasing self-discharge in some cells causes a difference in the state-of-charge (SOC) among the cells, and these cells would be degraded by overdischarge. In order to modify the Ni-MH battery for social-infrastructure use, it is important to improve its self-discharge suppression and overdischarge resistance as well as its high-power and long cycle-life performances.

For the negative electrode, the AB_5 type $Mm(Ni,Co,Mn,Al)_5$ (Mm: misch-metal, A: Mm, B: transition metals and Al) alloys have been generally used [5,6]. In these types alloys, its cobalt (Co) was added to improve the cycle-life performance of the alloy electrode. However, the Co and manganese (Mn) cause an increasing self-discharge [7, 8]. Discovery of the $REMg_2Ni_9$ with the high discharge capacity of 370mAh/g [9-15] has led to the development of various RE-Mg-Ni based alloys ($AB_{3.0\text{-}3.7}$; A = rare earth and Mg, B = transition metals and Al) [16-20]. In these crystal structures, the AB_5 lattice and AB_2 one are alternately stacked in the c-axis direction. The stacked structure would maintain a good cycle-life performance in spite of the Co-less or Co-free composition.

For the positive electrode, the $Ni(OH)_2$ particles are generally coated with CoOOH in order to increase the active material utilization [21, 22]. However, the CoOOH conductive network is easily reduced by an overdischarge and thus disruption of the conductive network is a concern. Recently, Morishita *et al*. reported that CeO_2 improves the overdischarge resistance of the CoOOH network [23]. Meanwhile, the development of an oxidation-resistant carbon has provided a possible way to design a Co-free positive electrode for the Ni-MH battery [24].

Moreover, the cost of Co has exhibited a noticeable fluctuation and has often increased over the past three decades. In 2008, the highest price (> 110 US$/t) in history was recorded for some unexplained reason. After 2010, its price has had a stable transition due to an excess supply. However, concern about a stable supply in the future still remains. The development of Co-free materials is an important subject for reducing the cost of the Ni-MH battery.

In this study, Co-free materials, which improve the self-discharge suppression and overdischarge resistance, were developed for the large-sized Ni-MH battery for use in the social-infrastructure. As the negative materials, $RE_{0.9}Mg_{0.1}Ni_xAl_{0.2}$ (x = 3.9 ~ 4.3, $AB_{4.1\text{-}4.5}$) alloys are prepared for producing a low self-discharge negative electrode. These alloys have a higher B/A ratio than those of the conventional RE-Mg-Ni alloys [16-20] and contain a substantial AB_5-type phase with the stacking structured one. The content of the AB_5-type phase dependence on the B/A ratio was investigated by synchrotron X-ray diffraction (XRD) and transmission electron microscopy (TEM). The correlation between the AB_5 content and battery characteristics was discussed. Meanwhile, as the positive conductive material, an oxidation-resistant carbon[24] was used as a substitute for the conventional CoOOH. In order to develop a conductive network among the $Ni(OH)_2$ particles, the carbon-coated $Ni(OH)_2$ was prepared by

spraying a carbon dispersion onto the $Ni(OH)_2$ particles using a fluid-bed coating technique.

3.1.2 Experimental

3.1.2.1 Electrode and battery preparation

As the negative electrode materials, the $RE_{0.9}Mg_{0.1}Ni_xAl_{0.2}$ (x = 3.9 ~ 4.3) alloys were synthesized using an induction furnace with an argon atmosphere [19]. The RE portion consists of La, Pr and Nd. Table 3.1.1 summarizes the alloy compositions used in this study.

Table 3.1.1 Nominal compositions of the $RE_{0.9}Mg_{0.1}Ni_xAl_{0.2}$ alloys.

	A-site		B-site		B/A ratio
	La/Pr/Nd	Mg	Ni(x)	Al	
Alloy#1	0.50/0.15/0.35	0.1	3.9	0.2	4.1
Alloy#2	0.60/0.12/0.28	0.1	4.1	0.2	4.3
Alloy#3	0.70/0.09/0.21	0.1	4.3	0.2	4.5

A-site: RE (=La, Pr and Nd) and Mg, B-site: Ni and Al

An oxidation-resistant carbon (CB) and ethylene-vinyl-acetate (EVA) were dispersed in a xylene solvent at the molar ratio of 1 : 1. The prepared carbon dispersion was sprayed onto spherical $Ni(OH)_2$ particles (diameter: ca. 10μm) using a fluid-bed coating apparatus (Powrex Co., Ltd., Japan) to obtain the carbon(CB)-coated $Ni(OH)_2$ powder as the active material of the positive electrode. The CB-coated $Ni(OH)_2$ consists of $Ni(OH)_2$, CB and EVA with the weight ratio of 100 : 5 : 5. The oxidation-resistant carbon was prepared by annealing the carbon black at approximately 2500K in an inert-gas atmosphere.

The negative and positive electrodes were prepared by a paste method, namely, the material powder, binder and thickening agents were thoroughly mixed with water. The paste was then loaded on a nickel-foam substrate and pressed to form a plate with a thickness of 0.4 mm. The negative paste consists of the alloy powder, styrene butadiene rubber (SBR) as the binder, carboxyl-methyl-cellulose (CMC) as the thickening agent and water. On the other hand, the positive one contains the CB-coated $Ni(OH)_2$ powder, CMC and water.

For the cylindrical battery construction, the negative and positive electrodes were spirally wound together with a sulfonated polypropylene separator, and this bundle was then inserted into a cylindrical case. After the electrolyte (30wt. % KOH with $30gL^{-1}$LiOH) was added, the cell was sealed. The negative electrode capacity is 4 times that of the positive one (N/P = 4). The battery capacities were 760mAh. For the open-type battery, the positive electrode was held between two negative electrodes using a non-woven polypropylene separator. The N/P ratio and battery capacities were 10 and 120mAh, respectively. The charge/discharge curves were recorded using a computer-controlled charge/discharge system (BLS series, Keisokuki Center Co., Japan) equipped with a thermostatic chamber at 298 K. Table 3.1.2 summarizes the battery specifications used in this study.

Table 3.1.2 List of the test batteries used in this study

	Battery name	Rated capacity	Subject (Fig number)	Battery type	Positive conductive agent	Negative alloy	N/P ratio*
(I)	Battery(1A) Battery(1B)	760 mAh	Self-discharge (Fig.6)	Cylindrical	$Co(OH)_2$	Alloy#1 $MmNi_{4.0}Co_{0.6}Mn_{0.3}Al_{0.3}$	4
(II)	Battery(2A) Battery(2B)	600 mAh	Overcharge (Fig.9)	Cylindrical	Carbon $Co(OH)_2$	Alloy#1	4
(III)	Battery(3A) Battery(3B)	120 mAh	Overdischarge (Fig.10)	Open-type	Carbon $Co(OH)_2$	Alloy#1	10

*N/P = (Negative electrode capacity) / (positive electrode capacity)

3.1.2.2 Analyses

Synchrotron X-ray diffraction (XRD) patterns of the alloys were obtained from the beam line BL19B2 at the synchrotron radiation facility, SPring-8, Japan. The wavelengths were calibrated to λ = 0.412 Å using CeO_2 as the standard. The XRD samples were prepared by adding the powder to a Lindeman glass capillary with a 0.2-μm inner diameter. The structural analysis was carried out using the Rietveld program, RIETAN-2000.[25]

Thin-film alloy samples for the scanning transmission electron microscopy (STEM) measurements were prepared using an ion-polishing instrument. High-angle annular dark field (HAADF) images, which correspond to the high-resolution atomic arrangement, were observed using a JEM-ARM200F equipped with a Cs-corrector for the STEM (JEOL, Ltd., Japan).

The morphologies of the carbon-coated $Ni(OH)_2$ were observed using a scanning electron microscope (SEM, JSM-6390, JEOL, Ltd., Japan).

The electrochemical impedance spectra (EIS) of the $Ni(OH)_2$ samples were measured by a frequency response analyzer (SI 1280B, Solartron, UK).

The X-ray photoemission spectra (XPS) of the $Ni(OH)_2$ samples were observed using an X-ray photoemission spectrometer (XPS, JPS-9010MX, JEOL, Ltd., Japan).

3.1.3. Results and discussion

3.1.3.1 Characterization and electrochemical performances of the alloy electrodes

Figure 3.1.1 shows the discharge capacity of the alloy electrodes in the KOH electrolyte. The electrodes were discharged after a 400mAh/g charging at a 100mA/g current. These alloys were easily activated, and the maximum 340 mAh/g discharge capacity (= C_{max}) was observed during the 2nd cycle. The alloy#1 exhibited a better

capacity retention than alloys#2 and #3. The capacity retention of each alloy in the 48th cycle (= C_{48}/C_{max}) became high in the order of alloy#3 (82%) < alloy#2 (86%) < alloy#1 (91%).

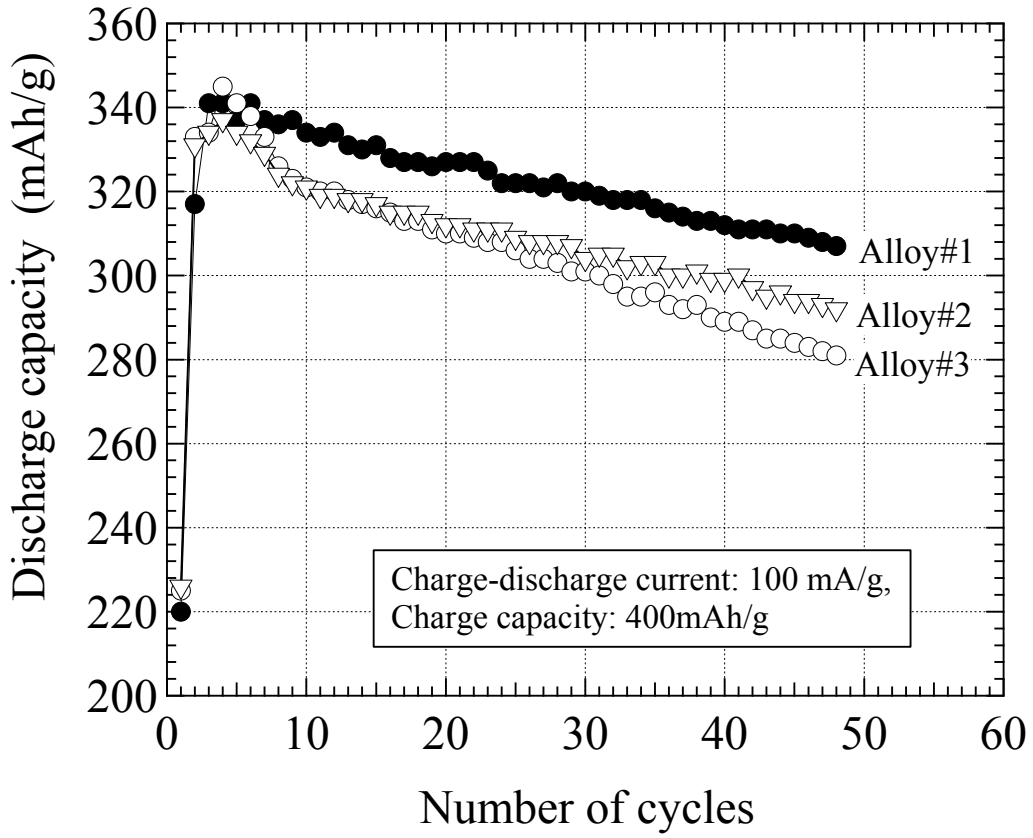

Figure 3.1.1 Capacity retention of the alloy electrodes in 8N KOH solution.

Figure 3.1.2 shows the XRD pattern and Rietveld refinements for alloy#1. In this refinement, the rare-earth and transition-metal sites were replaced by vertical species, i.e., $La_{0.50}Pr_{0.15}Nd_{0.35}$ and $Ni_{0.95}Al_{0.05}$, respectively. A four-phase model with the $CaCu_5$-type (1:5H), Ce_2Ni_7-type (2:7H), Ce_5Co_{19}-type (5:19H) and Pr_5Co_{19}-type (5:19R) ones reasonably reproduced the observed pattern. For alloy#2, the equivalent four-phase model was used to refine the XRD pattern. For alloy#3, three phase with

1:5H, 5:19H and 5:19R ones was the reasonable model. Table 3.1.3 summarizes the phase components and refinement parameters of alloys#1 - #3.

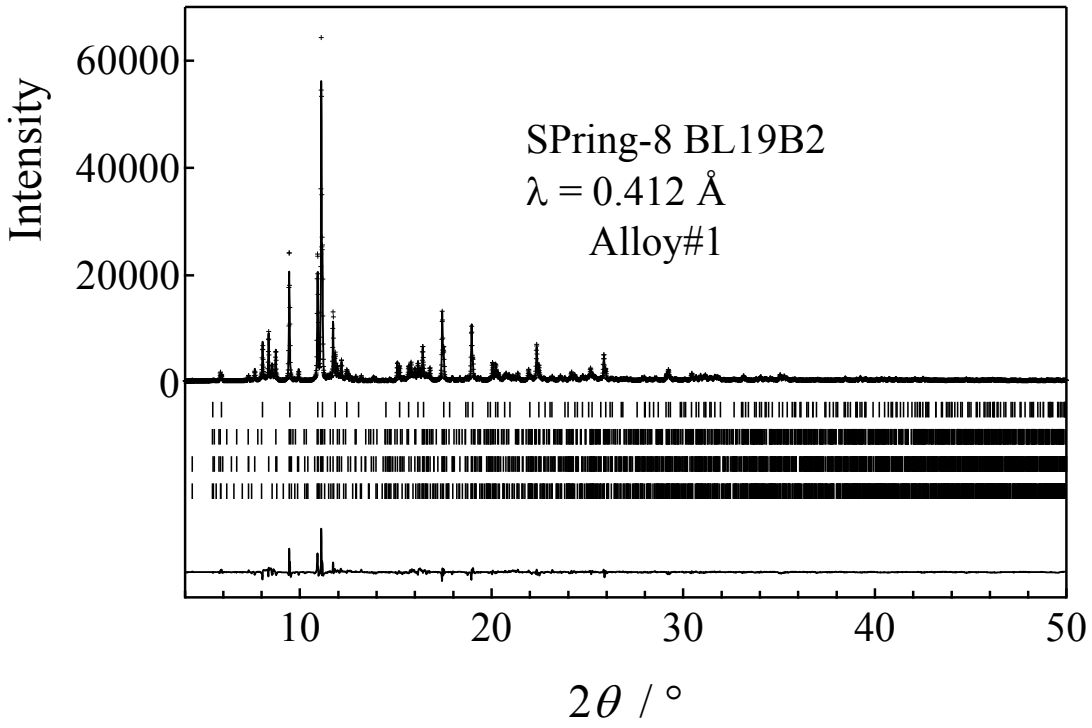

Figure 3.1.2 Synchrotron X-ray diffraction pattern and Rietveld refinement for alloy#1.

Figure 3.1.3 shows the phase abundance of alloys#1 - #3 determined by the Rietveld refinements. For alloy#1, two 5:19 phases occupy approximately 70wt.%. Meanwhile, for alloy#3, the 1:5H phase occupies approximately 70wt.%. The abundance of the 1:5H phase increased with the increasing B/A ratio. The observed faster capacity fading in alloys#2 and #3 is probably related to the greater abundance of the 1:5H phase. In the conventional $MmNi_5$-based alloys with the 1:5H structure, cobalt addition is indispensable as it suppresses the pulverization of the alloy and maintains the cycle-life performance. In alloys #1-#3, there is no cobalt addition. The greater abundance of the 1:5H phase could cause pulverization of the alloy and subsequent capacity fading.

Table 3.1.3 Phase components, R values, mass fractions and cell parameters obtained from the Rietveld refinements using the synchrotron XRD data of alloys#1 - #3

Alloy#1 R_{wp} = 11.89%, R_p = 8.99%, R_e = 3.23%

Phase	R_B	R_F	Space group	Abundance (wt.%)	Cell parameters (Å)
$CaCu_5$-type	3.98	1.47	P6/mmm	24	a = 4.9968(2) c = 3.9975(2)
Ce_2Ni_7-type	4.42	1.51	P63/mmc	9	a = 5.015(2) c = 24.23(1)
Ce_5Co_{19}-type	4.02	1.44	R3-m	51	a = 5.0126(2) c = 48.441(2)
Pr_5Co_{19}-type	4.08	1.48	P63/mmc	16	a = 5.0136(4) c = 32.304(3)

Alloy#2 R_{wp} = 11.90%, R_p = 8.77%, R_e = 3.57%

Phase	R_B	R_F	Space group	Abundance (wt.%)	Cell parameter (Å)
$CaCu_5$-type	3.47	1.55	P6/mmm	46	a = 4.9948(1) c = 3.9948(1)
Ce_2Ni_7-type	4.59	2.05	R3-m	4	a = 5.0158(9) c = 24.221(5)
Ce_5Co_{19}-type	4.32	1.68	R3-m	37	a = 5.0072(1) c = 48.325(2)
Pr_5Co_{19}-type	4.44	1.81	P63/mmc	13	a = 5.0021(5) c = 32.090(4)

Alloy#3 R_{wp} = 14.33%, R_p =10.6%, R_e = 3.22%

Phase	R_B	R_F	Space group	Abundance (wt.%)	Cell parameter (Å)
$CaCu_5$-type	5.71	3.41	P6/mmm	70	a = 5.0174(2) c = 4.0022(1)
Ce_5Co_{19}-type	6.19	3.67	R3-m	19	a = 5.0208(4) c = 48.318(3)
Pr_5Co_{19}-type	6.65	3.77	P6/mmm	11	a = 5.0214(8) c = 32.213(3)

Figure 3.1.4 shows the electron diffraction (ED) pattern of the alloys. The diffraction spots are arrayed along a line perpendicular to the c* direction. Patterns (a) and (b) were observed in different regions of an alloy#1 grain. Each of the patterns was indexed on the basis of the hexagonal 5:19H and rhombohedral 5:19R structures[26], respectively. Alloy#1 contained multiple stacking-structured phases. For alloy#3, the pattern like (c), which was indexed to a hexagonal 1:5H structure, was mainly observed.

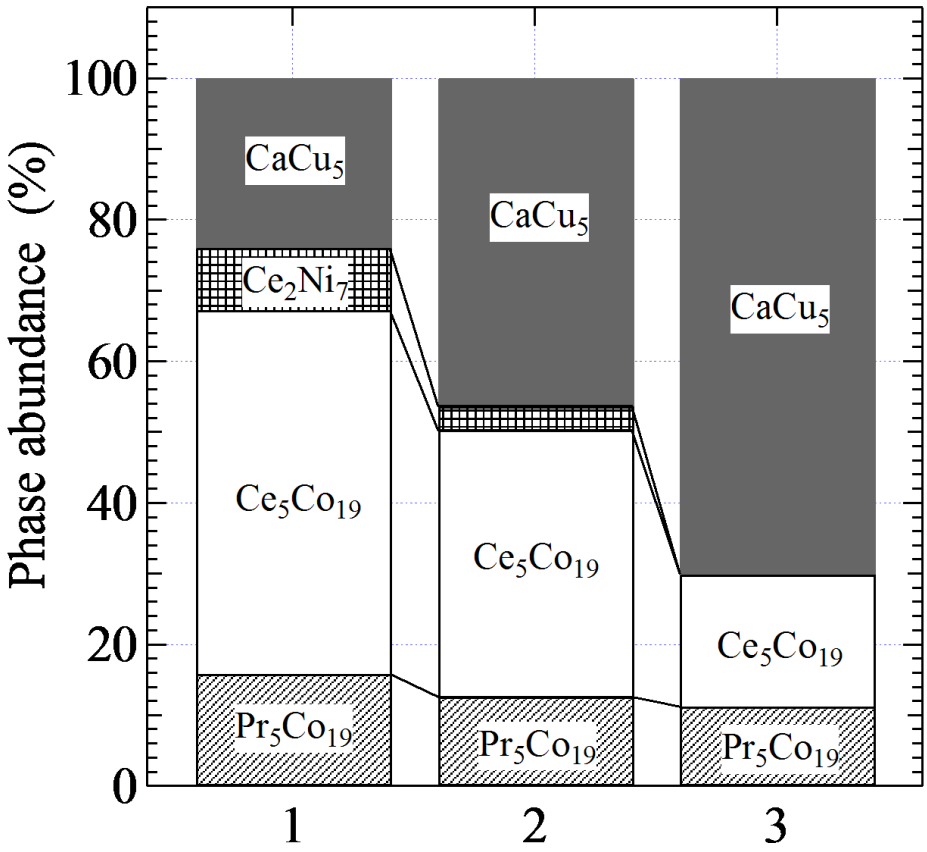

Figure.3.1.3 Phase abundances of alloys#1 - #3 obtained by Rietveld refinement.

In addition, streaks in the c* direction were often observed as shown in (d). This feature suggests that alloy#3 mainly consists of the 1:5H phase, and pieces of the stacking-structured phases, such as the 5:19-types, are contained in the 1:5H phase. These results are consistent with the XRD measurements.

Figure 3.1.5 shows an HAADF image of alloy#1 observed by scanning transmission electron microscopy (STEM). A high-resolution atomic arrangement was observed. The white contrasts are the atom positions. The perpendicular direction of the image is the *c*-axis direction corresponding to the direction in which the blocks composed of fundamental units are stacked. The square frames are placed on the position of a single $CaCu_5$-type lattice. This atomic arrangement corresponds to the 5:19R phase.

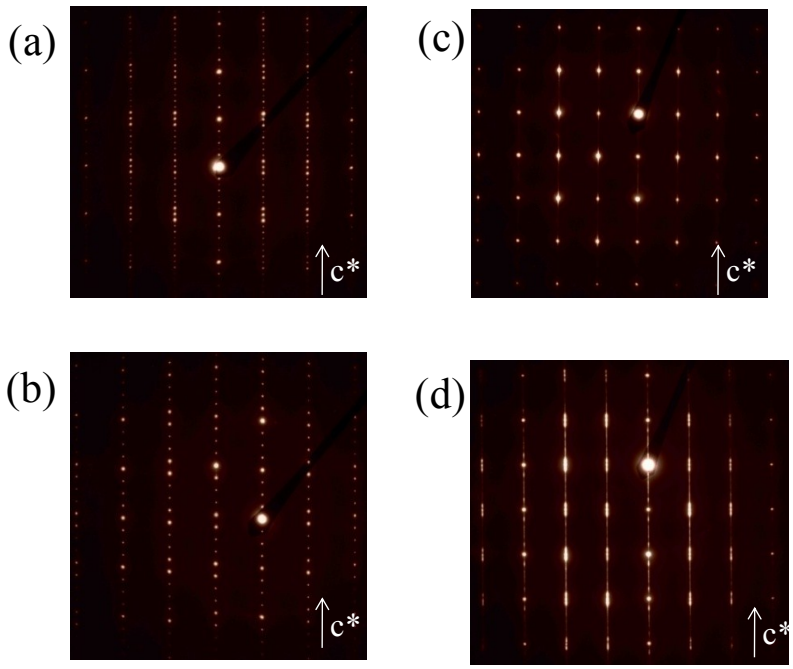

Figure 3.1.4 Electron diffraction (ED) patterns for (a), (b) alloy#1 and for (c), (d) alloy#3.

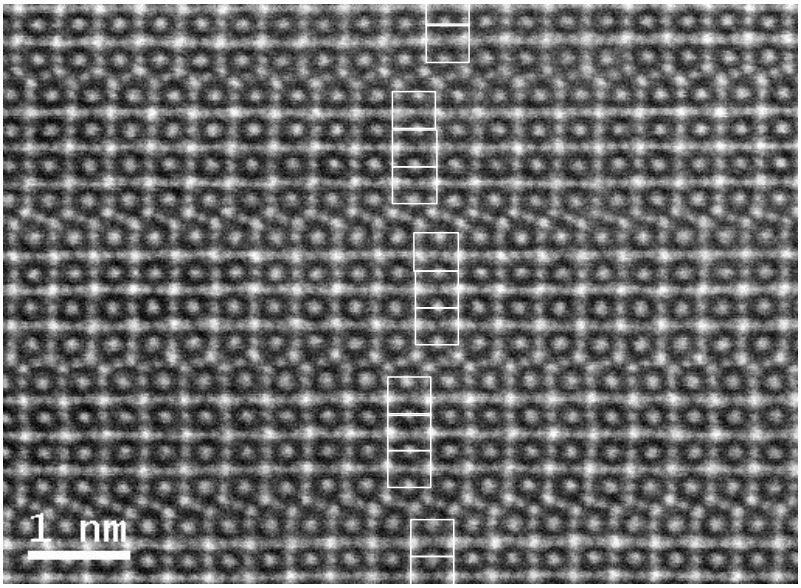

Figure 3.1.5 HAADF image of alloy#1

3.1.3.2 Battery performances of the developed alloys

The self-discharge characteristics of batteries(1A) and (1B) were observed during the charge/discharge cycles. The battery specifications are shown in Table 2(I). Before constructing battery(1B), the $MmNi_{4.0}Co_{0.6}Mn_{0.3}Al_{0.3}$ alloy was immersed in a 353K alkaline-solution to remove the Co, Mn and Al on the surface of the alloy particles. The charged batteries were held on open circuit in a 318K thermostatic chamber for 1 week, and then discharged in a 298K chamber.

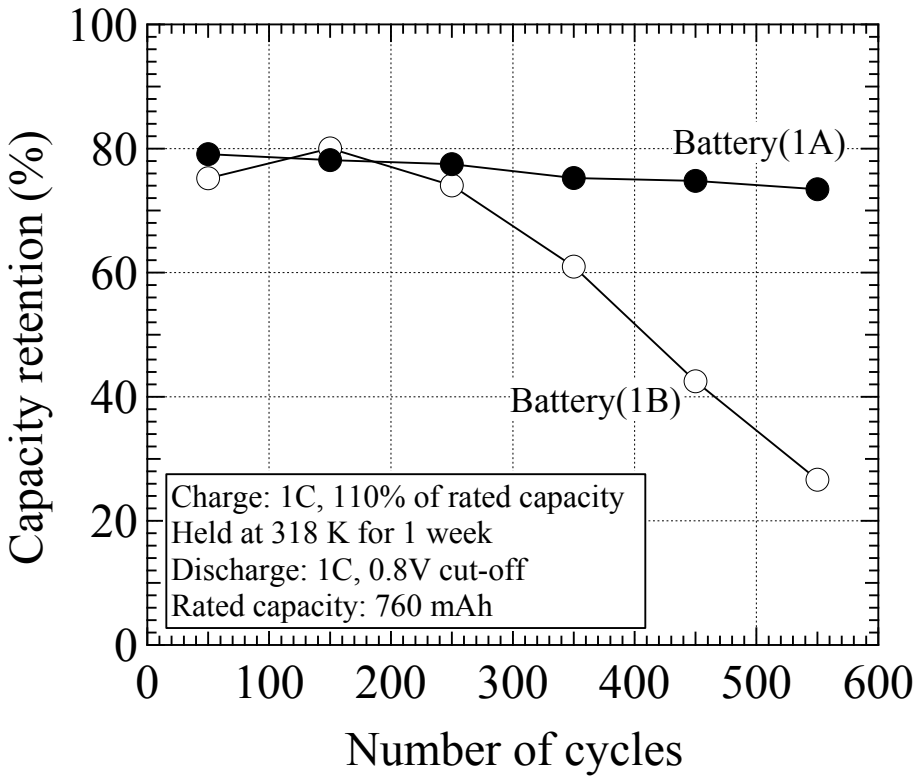

Figure 3.1.6 Plots of remaining capacity after storage at 318 K for 1 week for batteries(1A) and (1B).

Figure 3.1.6 shows the plots of the discharge capacity after this treatment. This measurement was carried out at the 40th, 150th, 250th, 350th, 450th and 550th cycles.

Battery(1A) exhibited an approximate 80% of the rated capacity at the 40th cycle and maintained this initial value even after 550 cycles. Meanwhile, the capacity of battery(1B) significantly decreased with the increasing number of cycles. The difference in the self-discharge characteristics would be ascribed to the composition of the negative alloys.

When the conventional $MmNi_5$-based alloys are immersed in alkaline solution, the elution of Co, Mn and Al was observed based on ICP spectroscopy measurements. These elements were removed from the surface of the alloy particles. The alkaline immersion treatment before battery construction would be effective in suppressing the self-discharge increasing, especially during the initial 150 cycles. However, deterioration of the capacity retention was observed after 250 cycles. Charge and discharge cycling produces pulverization of the alloy. The elution of Co, Mn and Al, which causes increasing self-discharge, would be increased on the new pulverized surface.

For battery(1B), the positive electrode side of the separator, which was removed from the battery after cycling, changed to a black color. Meanwhile, for battery(1A) using alloy#1, no separator color change was observed. The SEM and EDS measurements of the separators showed that deposits containing Co and Mn were observed in the AB_5 alloy battery as shown in Fig. 3.1.7. The eluted Co and Mn could be oxidized and deposited on the positive side of the separator. For example, the cobalt metal (Co) in the alloy is oxidized and eluted in electrolyte as Co^{2+}.[27, 28] Then, the eluted Co^{2+} is possibly oxidized in Co^{3+} by a reaction with NiOOH and deposited on the positive side of the separator. This reaction could be one of the origins of self-discharge increasing. Furthermore, the CoOOH with Co^{3+} is reported to have high electrical conductivity[22], and could form micro-short-circuits between both electrodes becoming

the origin of the increasing self-discharge[8]. Meanwhile, for alloy#1, no deposits were observed on the separator after cycling. These results suggest that alloy#1 has an improved effect on the self-discharge suppression of the Ni-MH battery.

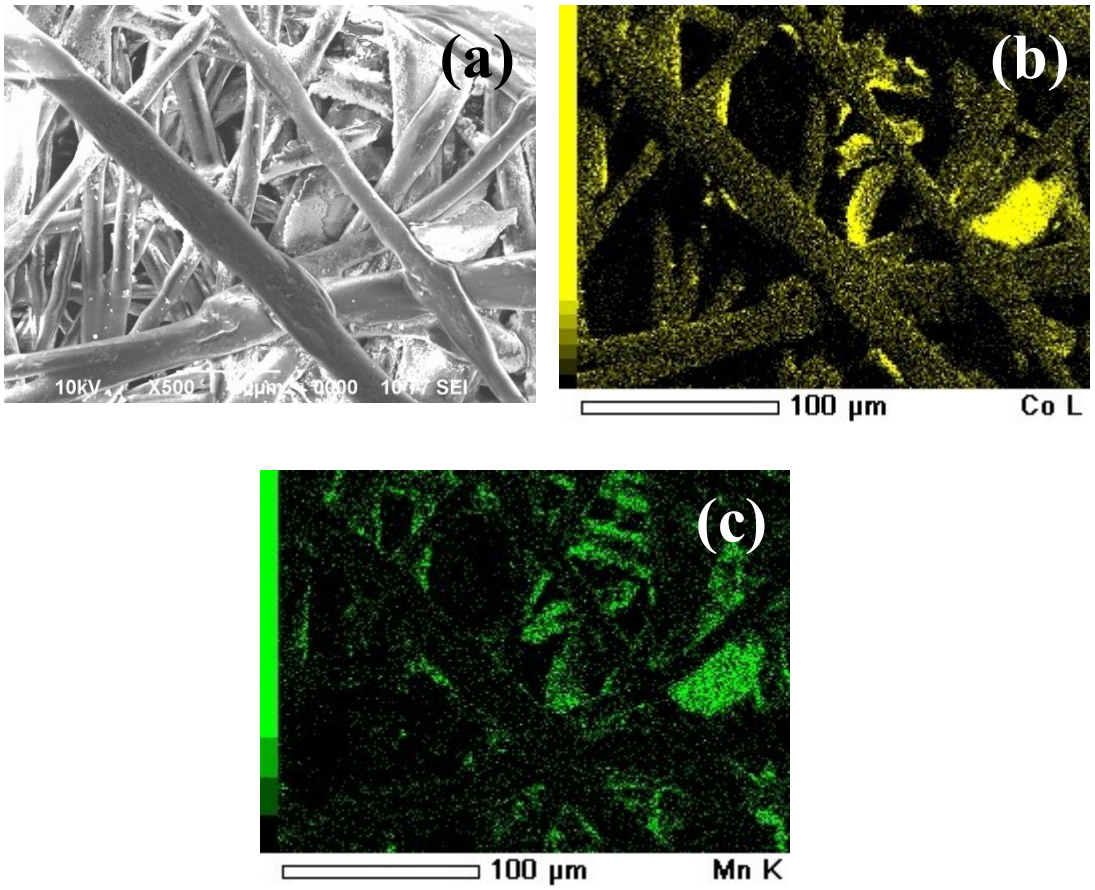

Figure 3.1.7 (a) SEM image of the separator after cycling, and EDS mapping for (b) Co-L and (c) Mn-K lines.

3.1.3.3 Preparation of CB-coated $Ni(OH)_2$ and battery performances

Figure 3.1.8 shows an SEM image of the carbon-coated $Ni(OH)_2$. The surface of the $Ni(OH)_2$ particles was coated with a carbon layer by spraying the carbon dispersion using a fluid-bed coating apparatus. The electrical conductance of the 5 wt% CB-coated

$Ni(OH)_2$ was 5×10^{-3} $S \cdot cm^{-1}$. The conductance of the CoOOH-coated $Ni(OH)_2$ was of the same order.

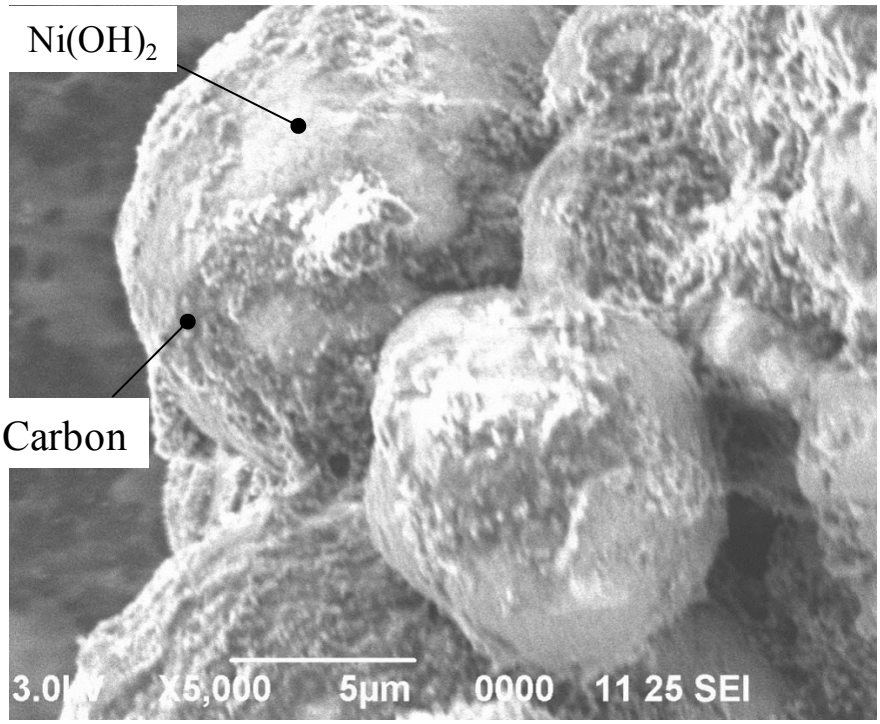

Figure 3.1.8 SEM photograph of the carbon-coated $Ni(OH)_2$.

Figure 3.1.9 shows the overcharge characteristics of cylindrical batteries(2A) and (2B). The battery specifications are shown in Table 2(II). As positive electrode materials, the carbon-coated and $Co(OH)_2$-coated $Ni(OH)_2$ were used for batteries (2A) and (2B), respectively. Alloy#1 was used as the negative electrode material. The charge capacity was 150% of the rated capacity. Although the discharge capacity of the CB-coated one was lower than that of the CoOOH coated one, no noticeable decrease in the discharge capacity was observed after 150 cycles of the overcharging treatment. These results suggest that the carbon used in this study exhibits an adequate oxidation-resistance for at least several hundred cycles.

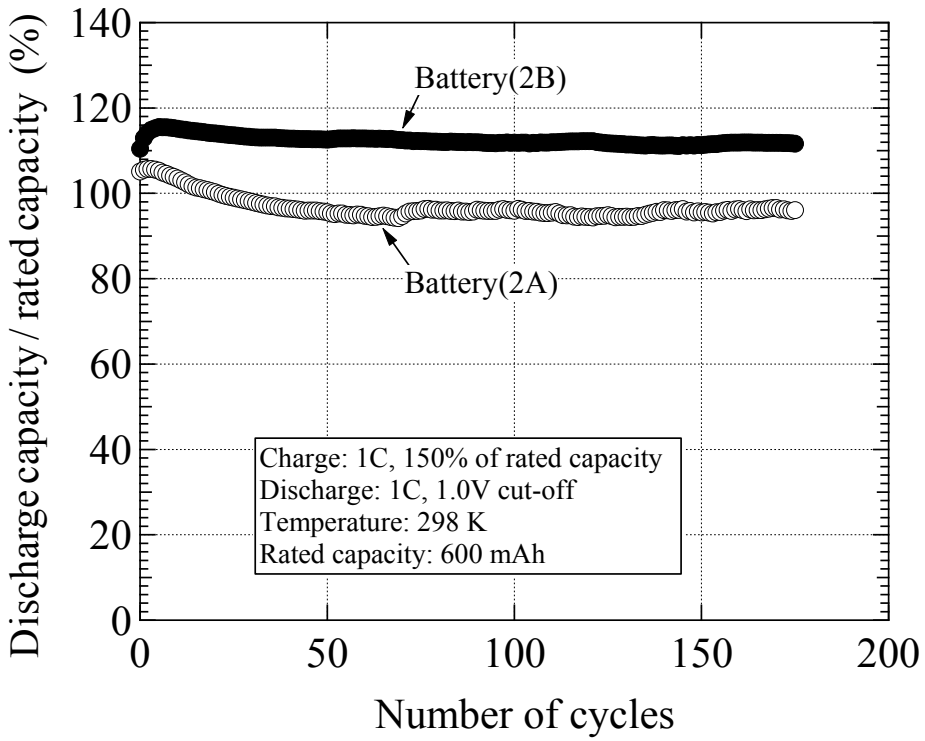

Figure 3.1.9 Cycle life performances of batteries (2A) and (2B) after 150% overcharging of the rated capacity.

Open-type batteries (3A) and (3B) were overdischarged to investigate the influence. The battery specifications are shown in Table 2(III). As positive electrode materials, the carbon-coated and $Co(OH)_2$-coated $Ni(OH)_2$ were used for batteries (3A) and (3B), respectively. Alloy#1 was used as the negative electrode material. The cells were charged and discharged at the 0.2C rate during the first 10 cycles for activation. After a 200% overdischarge of the rated capacity, a 0.25C-rate charge/discharge cycle was carried out as shown in Fig. 3.1.10. Battery(3A) containing the CB-coated electrode exhibited an 82% rated capacity, while the battery(3B) containing the CoOOH-coated one exhibited a 39% capacity. The carbon-coated electrode exhibited a higher discharge capacity indicating a better overdischarge resistance.

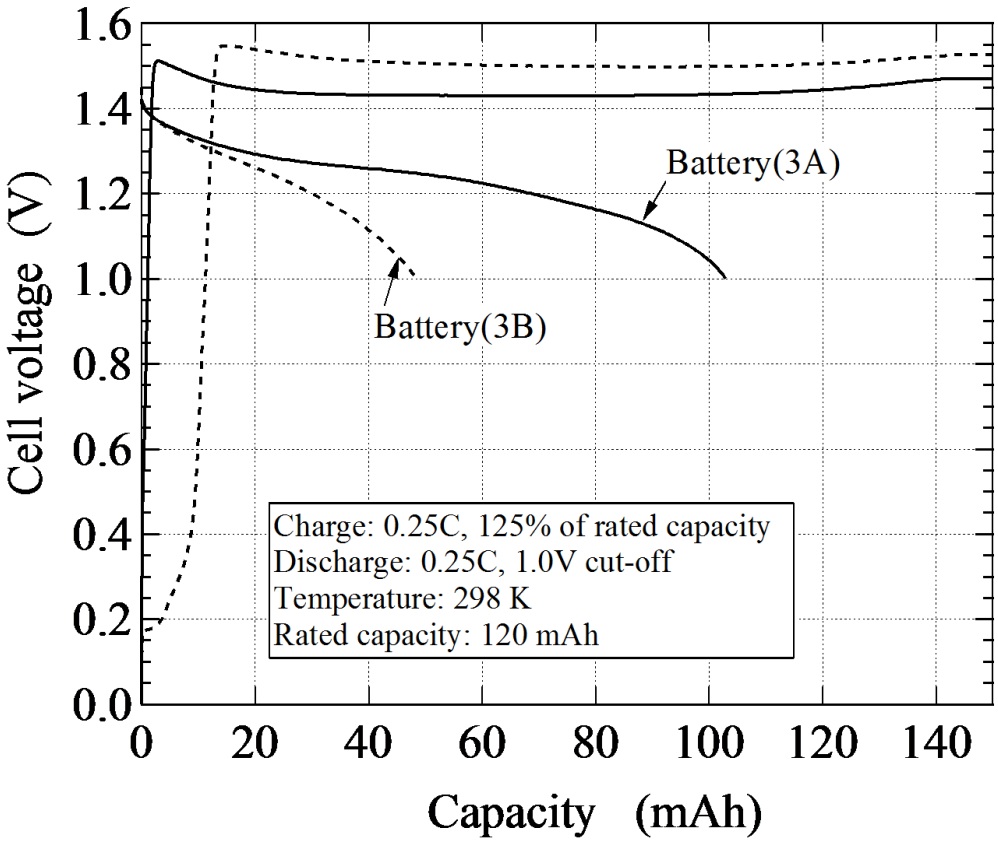

Figure 3.1.10 Charge and discharge curves of batteries(3A) and (3B) after 200% overdischarge of the rated capacity.

Figure 3.1.11 shows the electrochemical impedance spectra (EIS) of the positive electrode before and after the overdischarge process. These spectra show a semicircle resulting from the charge transfer resistance (R_{ct}) and a slope resulting from the Warburg impedance (Z_W). For the CB-coated $Ni(OH)_2$ electrode, the R_{ct} is equivalent before and after the overdischarge process, while that for the cobalt-coated one significantly increased. These results suggest that the CoOOH conductive network is damaged by the overdischarge process. Figure 3.1.12 shows the X-ray photoemission spectra (XPS) of the Co on the $Ni(OH)_2$. The Co-2p peaks were observed at 780eV and 795eV. These peaks shifted to the lower energy side after the overdischarge treatment.

The Co valence was changed from Co^{3+} to Co^{2+}, indicating that the CoOOH was reduced to the $Co(OH)_2$ by the overdischarge treatment. Furthermore, the reduced $Co(OH)_2$ would be retransformed to the CoOOH during the charging process. In Fig. 3.1.10, an approximate 10mAh at the beginning of the charge process of battery (3B) probably corresponds to the $Co(OH)_2$ oxidation. One of the reasons for the lower discharge capacity of battery (3B) would be related to the fact that not only $Ni(OH)_2$ but also the $Co(OH)_2$ is oxidized during the charging.

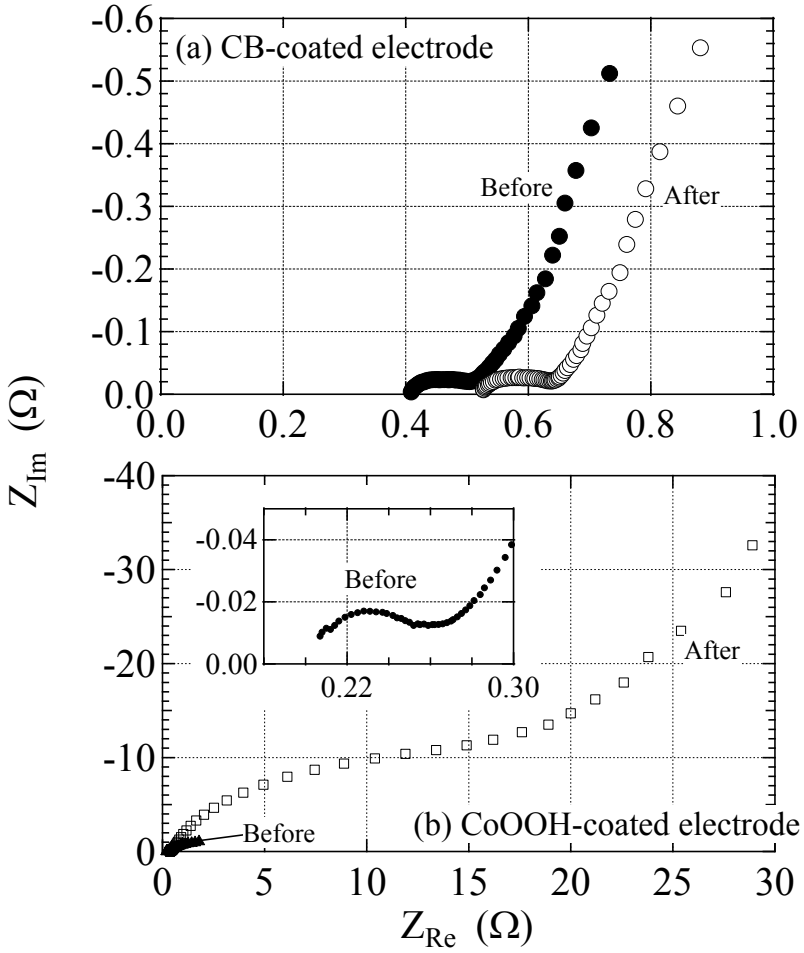

Figure 3.1.11 Electrochemical impedance spectra (EIS) of positive electrodes before and after the overdischarge process: (a)battery(3A) and (b) battery(3B).

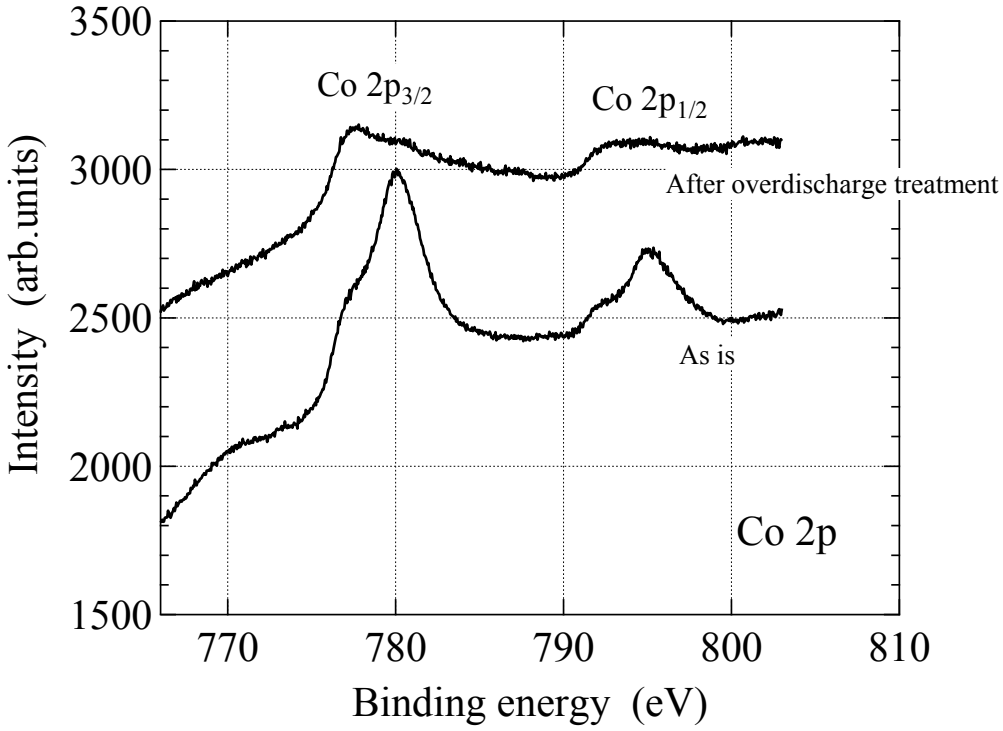

Figure 3.1.12 X-ray photoemission spectra (XPS) of Co-2p state for the CoOOH-coated nickel electrode (a) as-prepared and (b) after the overdischarge treatment.

The Co-free electrodes were used in a Kawasaki-developed industrial battery, called the GIGACELL[2-4], in order to realize a Co-free Ni-MH battery.[29] A single-type cell containing the Co-free electrodes exhibited approximately 2000 charge/discharge cycles. Furthermore, for the GIGACELL-type structure, scale-up was easily accomplished. A large-sized Co-free battery with a 205Ah rating was constructed. At the 2C-rate, the Co-free cell exhibited a better high-rate performance than the cell containing the conventional electrodes. The voltage and Ah efficiency of the former one are higher by 100mV and 7%, respectively, than those of the latter one. The development of the Co-free electrode materials would provide an advanced Ni-MH battery having a self-discharge suppression and overdischarge resistance as well as the high-power and long cycle-life performances for use in future large scale operations.

3.1.4 Conclusion

$RE_{0.9}Mg_{0.1}Ni_xAl_{0.2}$ alloys (RE: rare earth, x = 3.9 ~ 4.3) were prepared for producing a low self-discharge nickel-metal hydride (Ni-MH) battery. The alloys contains 4 phases, such as $CaCu_5$-type (1:5H), Ce_2Ni_7-type (2:7H), Ce_5Co_{19}-type (5:19R) and Pr_5Co_{19}-type (5:19H) ones. The phase abundance of the 1:5H one increased with the increasing x value. The capacity retention during the electrochemical test has a correlation to the abundance of the 1:5H phase. Based on the battery test using a cylinder-type sealed cell, the cell using alloy#1 as the negative material exhibited better self-discharge characteristics than that using the conventional $Mm(Ni,Co,Mn,Al)_5$-type alloy.

A carbon-coated $Ni(OH)_2$ was prepared by spraying a carbon dispersion onto $Ni(OH)_2$ particles using a fluid-bed coating apparatus. The overcharge and overdischarge performances of the CB-coated $Ni(OH)_2$ are comparable or better than those of the conventional CoOOH-coated one. The CoOOH conductive network is easily damaged by any overdischarge treatment. A Co-free Ni-MH battery consisting of these Co-free electrodes would combine several good battery characteristics, such as a low self-discharge and overdischarge resistance.

References

[1] T. Sakai, *J. Jpn. Inst. Energy (Review),* 89 420-426 (2010).

[2] K. Tsutsumi, *J. Jpn. Inst. Energy*, 87(7), 506 (2008).

[3] Y. Oku, *Kawasaki Technical Review,* 169, 10 (2009).

[4] K. Ishikawa, *Daikibo denryoku-chozo you chikudenchi* (Ed. Denki kagakukai energy kaigi), chapter 4, p. 113, Nikkan Kogyo Shinbun, Ltd., Tokyo, Japan (2011).

[5] T. Sakai, H. Miyamura, N. Kuriyama, A. Kato, K. Oguro, H. Ishikawa, *J. Electrochem. Soc.,* 137(3), 795 (1990).

[6] T. Sakai, H. Yoshinaga, H. Miyamura, N. Kuriyama, H. Ishikawa, *J. Alloys. Compd.,* 180, 37 (1992).

[7] K. Shinyama, Y. Magari, H. Akita, K. Kumagae, H. Nakamura, S. Matsuta, T. Nohma, M. Takee, K. Ishiwa, *J. Power Sources,* 143, 265 (2005).

[8] M. Kanemoto, T. Ozaki, T. Kakeya, D. Okuda, M. Kodama, R. Okuyama, *GS-Yuasa Technical Report,* 8, 22 (2011).

[9] K. Kadir, T. Sakai, I. Uehara, *J. Alloys. Compd.,* 257, 115 (1997).

[10] K. Kadir, N. Kuriyama, T. Sakai, I. Uehara, *J. Alloys. Compd.,* 284, 145 (1999).

[11] K. Kadir, T. Sakai, I. Uehara, *J. Alloys. Compd.,* 287, 264 (1999).

[12] K. Kadir, H. Tanaka, T. Sakai, I. Uehara, *J. Alloys. Compd.,* 289, 66 (1999).

[13] K. Kadir, T. Sakai, I. Uehara, *J. Alloys. Compd.,* 302, 112 (2000).

[14] T. Sakai, K. Kadir, M. Nagatani, H. Takeshita, H. Tanaka, N. Kuriyama, I. Uehara, *40th Battery Symposium, Kyoto, Japan, Abstr*., p. 133 (1999) [in Japanese].

[15] J. Chen, N. Kuriyama, H. Takeshita, H. Tanaka, T. Sakai, M. Haruta, *Electrochem. Solid State Lett.* 3(6), 304 (2000).

[16] T. Kohno, H. Yoshida, F. Kawashima, T. Inaba, I. Sakai, M. Yamamoto, M. Kanda, *J. Alloys. Compd.,* 311, L5, (2000).

[17] H. Pan, Y. Liu, M. Gao, Y. Lei, Q. Wang., *J. Electrochem. Soc,* 150(5), A565, (2003).

[18] S. Yasuoka, Y. Magari, T. Murata, T. Tanaka, J. Ishida, H. Nakamura, T. Nohma, M. Kihara, Y. Baba, H. Teraoka, *J. Power Sources,* 156, 662, (2006).

[19] T. Ozaki, M. Kanemoto, T. Kakeya, Y. Kitano, M. Kuzuhara, M. Watada, S. Tanase, T. Sakai, *J. Alloys. Compd,* 446-447, 620 (2007).

[20] T. Ozaki, M. Kanemoto, T. Kakeya, Y. Kitano, M. Kuzuhara, M. Watada, S. Tanase, T. Sakai, *ITE Letters on Batteries, New Technologies & Medicine,* 8(4), 394 (2007).

[21] I. Matsumoto, M. Ikeyama, T. Iwaki and H. Ogawa, *Denki Kagaku* (*presently Electrochemistry*), 54, 159 (1986).

[22] M. Oshitani, H. Yufu, K. Takashima, S. Tsuji and Y. Matsumaru, *J. Electrochem. Soc.*, 136, 1590 (1989).

[23] M. Morishita, T. Kakeya, M. Kanemoto, M. Kodama, T. Sakai, *J. Electrochem. Soc.,* 159(12), A2069 (2012).

[24] H. Kakegawa, K. Higaki, K. Nishimura, and S. Kasimura, JP Patent/ 4641329.

[25] F. Izumi, T. Ikeda, *Mater. Sci. Forum,* 321-324, 198 (2000).

[26] Y. Kitano, T. Ozaki, M. Kanemoto, M. Komatsu, S. Tanase, T. Sakai, *Mater. Trans.* 48, 2123 (2007).

[27] T. Sakai, M. Muta, H. Miyamura, N. Kuriyama and H. Ishikawa, *Electrochem. Soc. Proc.,* 93-8, 240 (1993).

[28] F. Meli, T. Sakai, A. Züttel, L. Schlapbach, *J. Alloys. Compd.,* 221, 284 (1995).

[29] T. Takasaki, K. Nishimura, M. Saito, H. Fukunaga, T. Iwaki and T. Sakai, *J. Alloys. Compd.,* (2013) in press.

3.2 Cobalt-free nickel-metal hydride battery for industrial applications

3.2.1 Introduction

The nickel-metal hydride (Ni-MH) battery has been widely used for hybrid electric vehicles (HEVs) as well as consumer electronic devices [1]. Recently, its application has been extended to large-scale industrial equipment such as the battery power system (BPS) for railways and power-grids as a renewable energy source [2, 3]. In order to promote the widespread-use of the Ni-MH batteries, further high-power output, long cycle-life and low costs are required.

For industrial applications, a number of single cells are stacked to assemble a high-voltage battery module. Each of the cells are equally charged and discharged. However, a difference in the state of charge (SOC) gradually increases with the increasing self-discharge in some cells, and these cells would be overdischarged. The positive electrode material, $Ni(OH)_2$, is coated with CoOOH to increase the active material utilization [4]. The overdischarge causes not only disruption of the CoOOH conductive network, but also degradation of the cell and module performances. The self-discharge suppression and overdischarge-resistance improvement are important requirements to maintain the battery-module performance over the long term.

In the conventional Ni-MH batteries, AB_5 type $Mm(Ni, Co, Mn, Al)_5$ alloys [5] and CoOOH-coated $Ni(OH)_2$ [4] have been used as the negative and positive electrode materials, respectively. In these materials, the Co is the essential to improve the battery performances. However, the increasing Co price has often been observed in the past three decades and only about 10% Co in the alloys accounted for half of the total alloy cost [6]. Noticeable fluctuations in Co pricing would be a serious concern for the battery material costs in the future. Therefore, the development of Co-free materials is an important subject for the Ni-MH battery.

The discovery of $REMg_2Ni_9$ with the high discharge capacity of 370mAh/g provided a alternative way to design new negative electrode alloys [7-13]. A series of RE-Mg-Ni based alloys ($AB_{3.0\text{-}4.0}$; A = rare earth, Ca and Mg, B = transition metals and Al), which contains less cobalt or no cobalt, has been developed by many groups [14-19]. These high-capacity alloys have contributed to increasing the capacity of the consumer-based batteries.

In this study, for the Co-free negative electrode with a high-power and low self-discharge, the $RE_{0.9}Mg_{0.1}Ni_{3.9}Al_{0.2}$ ($AB_{4.1}$) alloy was prepared. Moreover, a carbon-coated $Ni(OH)_2$ using an oxidation-resistant carbon material was developed to produce a Co-free Ni-MH battery. The battery performances of the Co-free materials were tested using a large-sized Ni-MH cell with a 205 Ah rating.

3.2.2 Experimental

The $RE_{0.9}Mg_{0.1}Ni_{3.9}Al_{0.2}$ alloy was synthesized using the previously reported method [17]. The RE consists of La, Pr and Nd with the molar ratio of 0.5 : 0.15 : 0.35. The phase compositions of the samples were characterized by X-ray diffraction (XRD) using the synchrotron radiation facility, SPring-8, Japan. The structural analysis was carried out using the Rietveld program, RIETAN-2000 [20]. The negative electrodes were prepared by the paste method. The alloy powder, styrene butadiene rubber (SBR) as the binder and carboxyl-methyl-cellulose (CMC) as the thickening agent were thoroughly mixed with water. The paste was loaded on a nickel-foam substrate and pressed to form a plate with a thickness of 0.4 mm.

An oxidation-resistant carbon and ethylene-vinyl-acetate were dispersed in xylene as the solvent. The prepared carbon dispersion was sprayed onto spherical $Ni(OH)_2$ particles using a fluid-bed coating apparatus (Powrex Co., Ltd., Japan) to obtain the

carbon-coated $Ni(OH)_2$ powder as the positive electrode material. The carbon-coated $Ni(OH)_2$ was formed into the positive electrode in the same manner as the negative electrode, namely, a paste consisting of the carbon-coated $Ni(OH)_2$ powder and CMC with water was loaded on a nickel foam substrate and pressed to form a plate with a thickness of 0.4 mm.

For the cylindrical battery construction, the negative and positive electrodes were spirally wound together with a sulfonated polypropylene separator and the bundle was then inserted into a cylindrical case. The negative alloy ($MmNi_{3.7}Co_{0.8}Mn_{0.4}Al_{0.3}$) was used as the reference for comparison. The composition is a typical one for consumer devices emphasizing the cycle-life as well as the capacity and power. The negative electrode capacity is 4 times that of the positive one (N/P = 4). The battery capacities were 400 ~ 800mAh. After the electrolyte (5.6mol/L- KOH with1.2mol/L-LiOH) was added, the battery was sealed.

Figure 3.2.1 is a schematic view showing the structure of a large-sized Ni-MH battery, called the GIGACELL® [2, 3]. The GIGACELL-type single cells with 750mAh ~ 205Ah ratings were constructed using the Co-free electrodes. Inside the cells, pre-formed stripes of positive and negative electrodes are inserted into the respective sides of the pleat-folded separator. The negative alloy ($MmNi_{3.7}Co_{0.7}Mn_{0.3}Al_{0.3}$) was used as the reference for the comparison. The composition was similar to that used for the conventional GIGACELL, mainly emphasizing the power performance. The capacity ratio was calculated to be N/P = 2.5. The electrolyte was 4.8mol/L-KOH + 1.2mol/L-NaOH.

The charge/discharge curves were recorded using a computer-controlled charge/discharge system (BLS series, Keisokuki Center Co., Japan, or SM8 series, Hokuto Denko Co., Japan) equipped with a thermostatic chamber at 298 K.

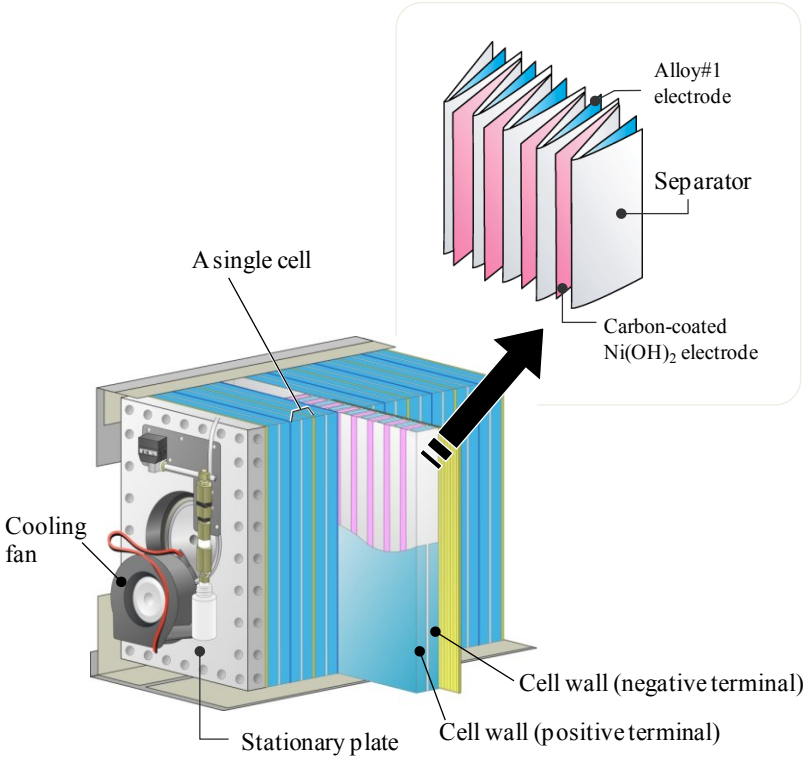

Figure3.2. 1 Schematic view of GIGACELL-type structure.

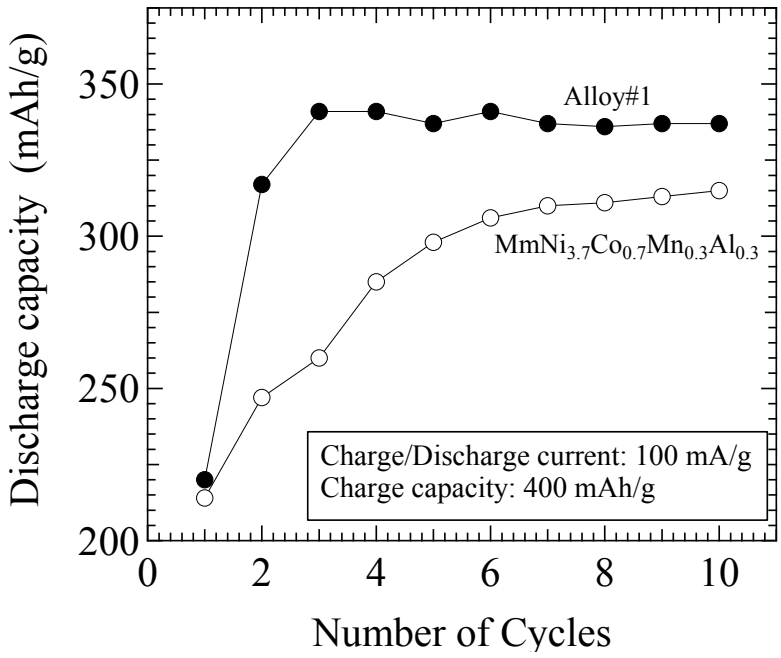

Figure 3.2.2 Capacity retention of the alloy electrodes in 8N-KOH solution.

3.2.3. Results and discussion

Figure 3.2.2 shows the discharge capacity of the alloy electrodes in a KOH electrolyte. The $RE_{0.9}Mg_{0.1}Ni_{3.9}Al_{0.2}$ alloy (alloy#1) was easily activated compared to the conventional AB_5 type $MmNi_{3.7}Co_{0.7}Mn_{0.3}Al_{0.3}$ one. Alloy#1 and AB_5 exhibited 340mAh/g and 315 mAh/g discharge capacities, respectively. A synchrotron XRD analysis indicated that the Rietveld refinement parameters, R_{wp}, R_p, R_e and S, were estimated to be 11.89%, 8.99%, 3.23% and 3.68, respectively. Alloy#1 contains multiple phases, namely, the $CaCu_5$-type (25wt. %), Ce_2Ni_7-type (10wt. %), Ce_5Co_{19}-type (50wt. %) and Pr_5Co_{19}-type (15wt. %) ones.

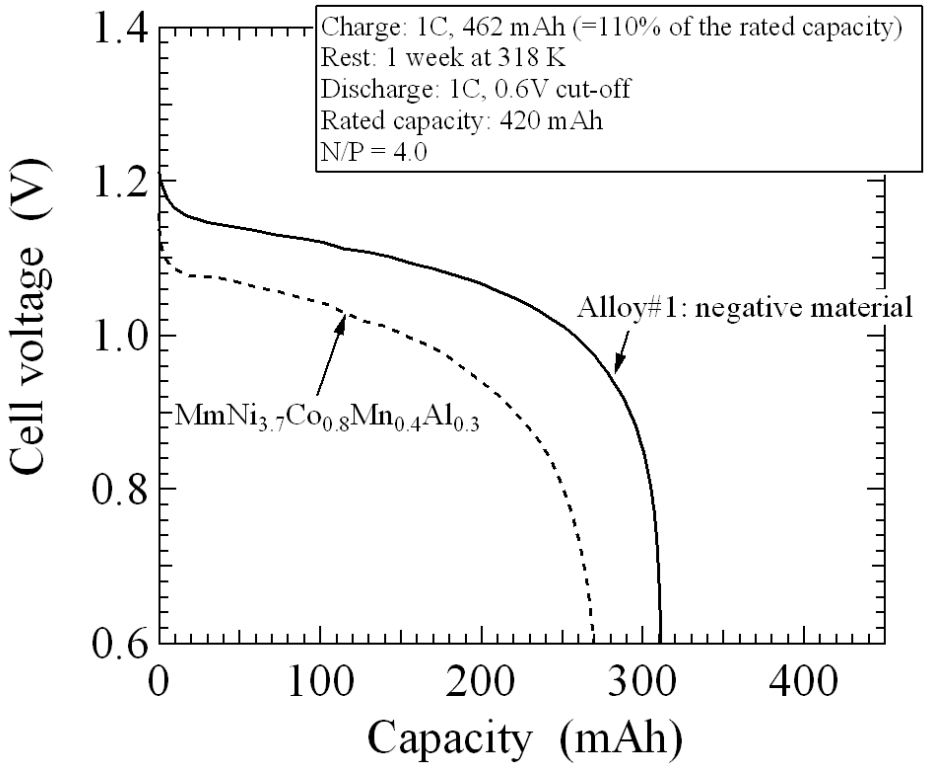

Figure 3.2.3 Discharge curves of the cylindrical batteries at various discharge currents. Solid and dashed lines correspond to alloy#1 and $MmNi_{3.7}Co_{0.8}Mn_{0.4}Al_{0.3}$ as negative alloy, respectively. The capacity ratio (N/P) between the negative electrode and positive one is 4.0.

Figure 3.2.3 shows the discharge curves of the cylindrical batteries at various currents. The battery specifications are equivalent except for the alloy used as the negative electrode. An approximate 1.2V discharge voltage and 99% of its rated capacity were observed for the battery containing alloy#1 at the 1C rate. The current value at the nC rate (n: positive number) was determined by multiplying the rated battery capacity and the n value. Even at the 10C rate, an approximate 1.0V voltage and 88% of its rated capacity was maintained. At the 10C rate, a 200mV difference was observed for the discharge voltage between both batteries. A comparatively good high-rate discharge performance was obtained using alloy#1.

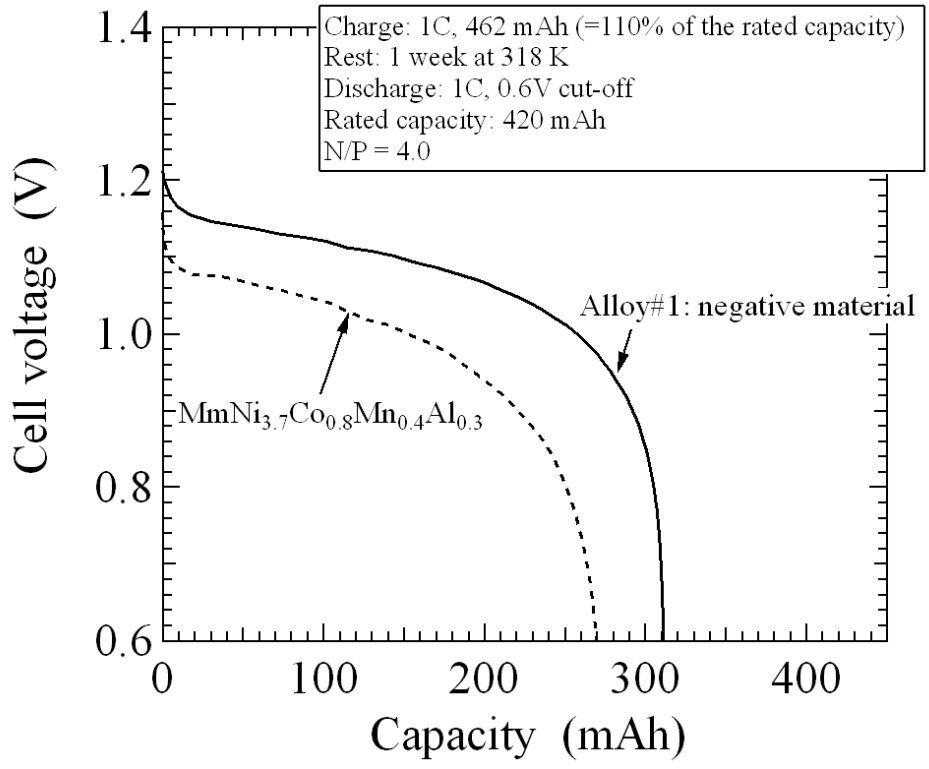

Figure 3.2.4 1C-rate discharge curves of the cylindrical batteries after storage at 318 K for 1 week. N/P = 4.0.

In order to investigate the self-discharge, the charged batteries were held at open circuit in a 318 K thermostatic chamber for 1 week. Figure 3.2.4 shows the discharge curves of the cylindrical batteries after this treatment. The battery containing alloy#1 maintained an approximate 74% of its rated capacity. Meanwhile, the one containing $MmNi_{3.7}Co_{0.8}Mn_{0.4}Al_{0.3}$ exhibited 64% of its rated capacity. For the latter battery, the Co and Mn released from the AB_5 alloy are deposited on the separator and positive electrode.

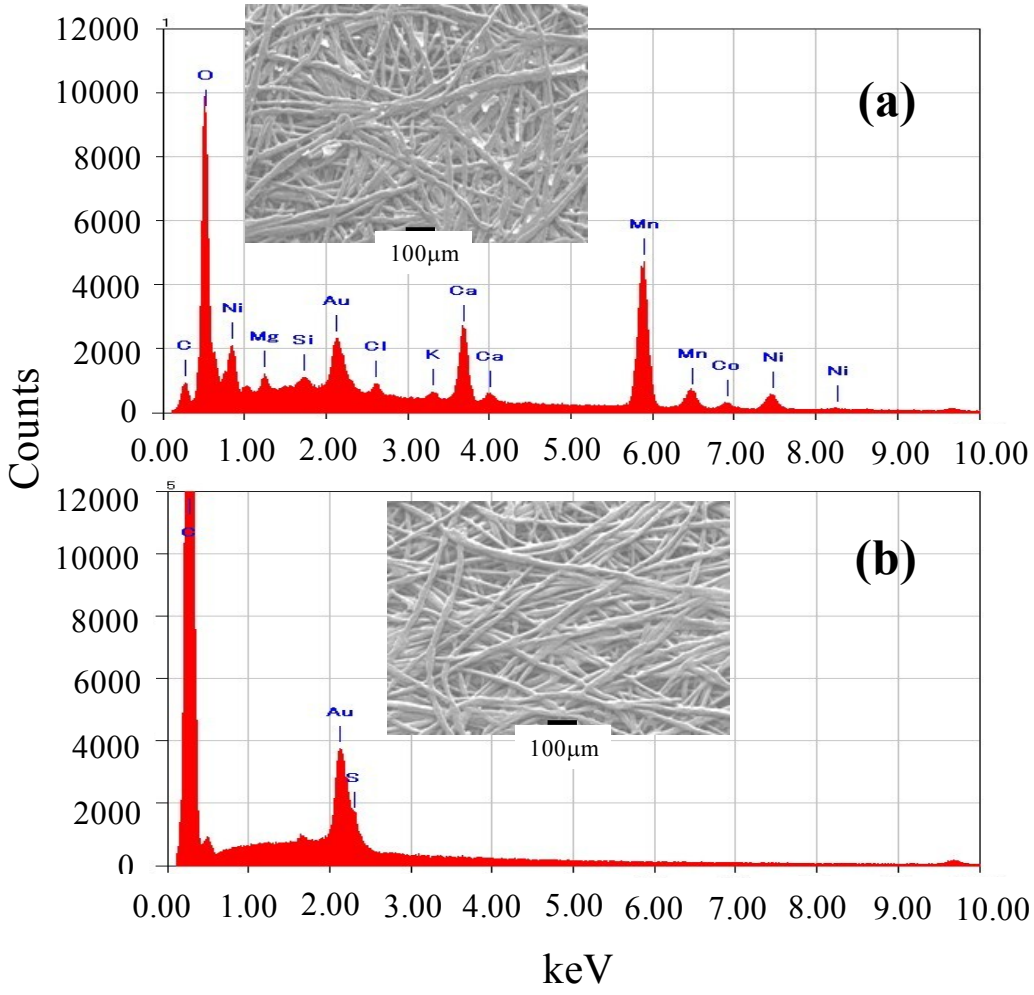

Figure 3.2.5 SEM image of the separators after cycling: (a) AB_5 ($MmNi_{3.7}Co_{0.7}Mn_{0.3}Al_{0.3}$) and (b) alloy#1 as negative alloys.

The deposits may accelerate the self-discharge of the positive electrode. As shown in Fig. 3.2.5(a), deposits containing Mn and Co were observed in the separator after cycling. Meanwhile, there was no deposit in the separator of the battery containing alloy#1 as shown in Fig. 3.2.5(b). These results suggest that the use of alloy#1 is effective for suppressing the self-discharge of the Ni-MH battery. In addition, Au was previously evaporated on the separator specimens in order to improve the low electrical conductivity. The sulfonated treatment of the separator would be the origin of the sulfur. The Ca was possibly contained in the mischmetal as an impurity.

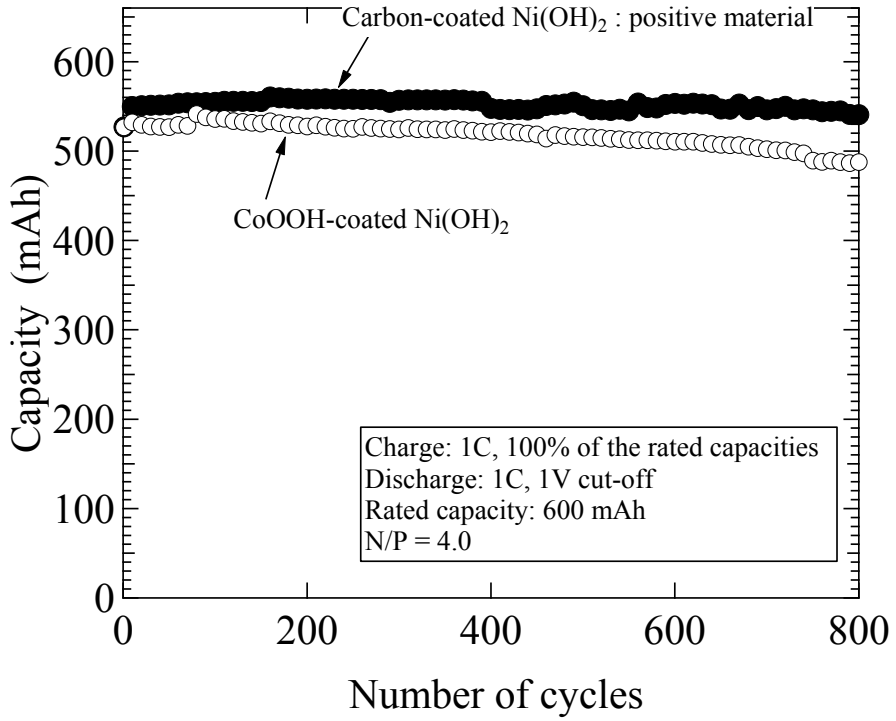

Figure 3.2.6 Cycle life performances of cylindrical batteries. N/P = 4.0.

Figure 3.2.6 shows the capacity retention of the cylindrical batteries. The battery specifications are equivalent except for the positive electrode materials. Both batteries

contain alloy#1 as the negative electrode material. For both batteries, no capacity decay was observed during 800 cycles. These results suggest that the carbon-coated $Ni(OH)_2$ exhibited an adequate charge/discharge cycling durability comparable to the conventional CoOOH coated one. Furthermore, the overdischarge resistance is expected to improve using carbon, which would exhibit a better resistance to reduction than the CoOOH.

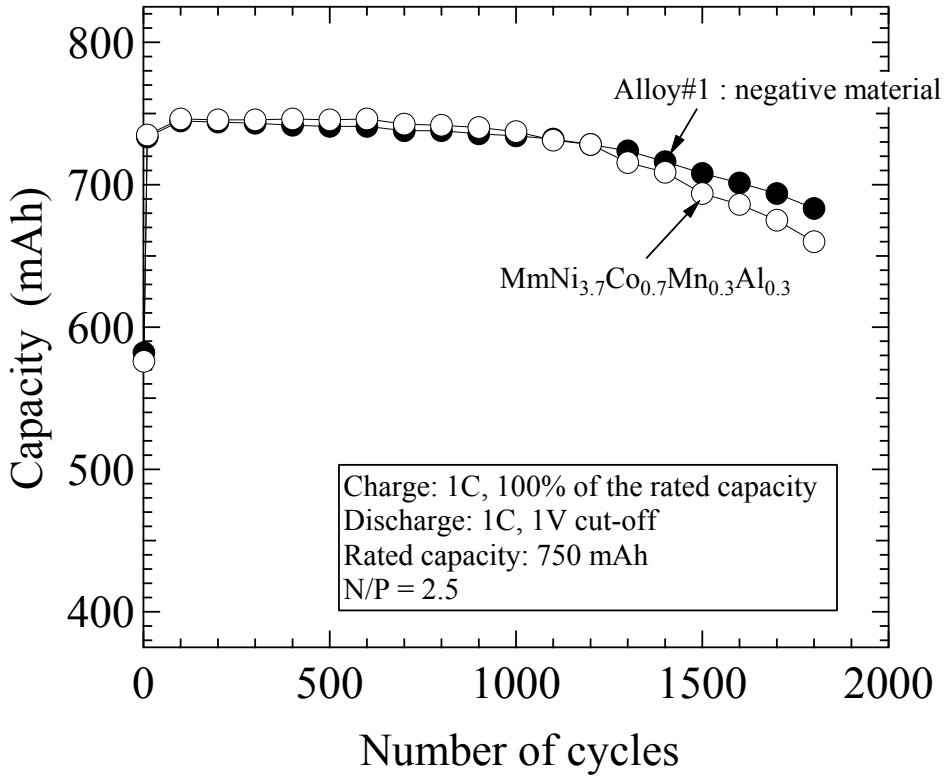

Figure 3.2.7 Cycle-life performance of single 750mAh GIGACELL-type cells. N/P = 2.5.

Figure 3.2.7 shows the cycle-life performance of a single 750mAh GIGACELL-type cell, containing the Co-free positive and negative materials. Another cell, which contained $MmNi_{3.7}Co_{0.7}Mn_{0.3}Al_{0.3}$ as the negative alloy, was also tested for comparison.

An approximate 99% Ah-efficiency was observed after charging to 750mAh. The initial discharge capacity was maintained after 1000 cycles. After 1800 cycles, both cells maintained an approximate 85% Ah-efficiency. The Co-free cell exhibits a capacity retention comparable to the cell containing $MmNi_{3.7}Co_{0.7}Mn_{0.3}Al_{0.3}$ alloy.

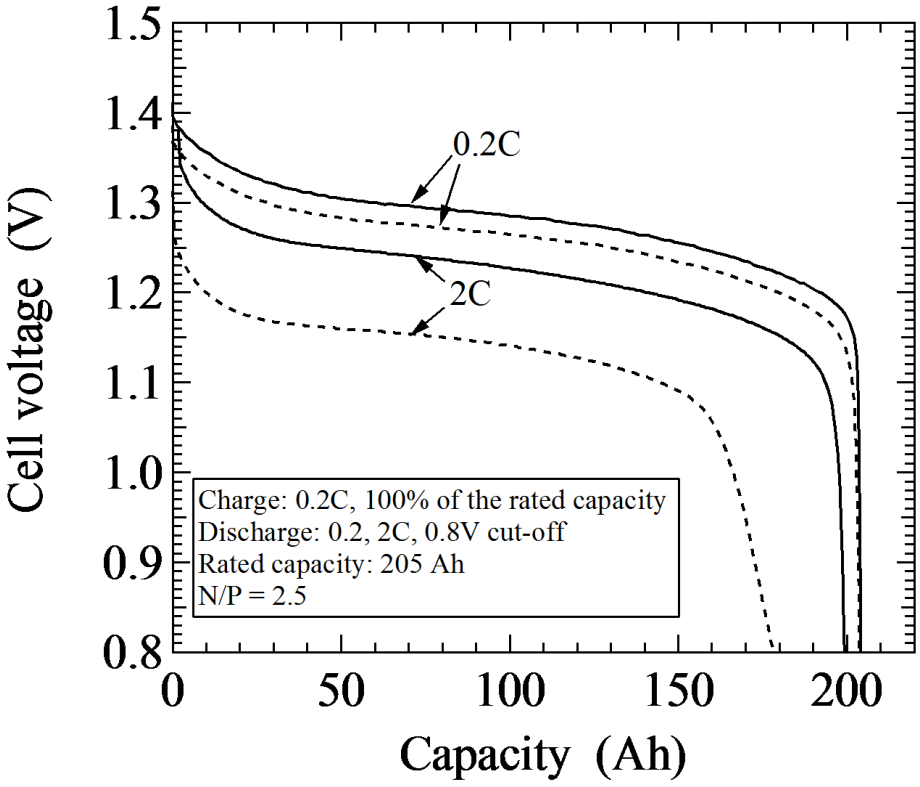

Figure 3.2.8 Discharge curves of single 205Ah GIGACELL-type cells. Solid and dashed lines correspond to alloy#1 and $MmNi_{3.7}Co_{0.7}Mn_{0.3}Al_{0.3}$ as negative alloy, respectively. N/P = 2.5.

Figure 3.2.8 shows the discharge curves of the single 205Ah cells. At the 0.2C rate (= 41A) discharge, the voltage and discharge capacity were almost equivalent to each other. At the 2C rate (= 410A) discharge, the Co-free cell maintained a 1.25V voltage and 97%

Ah-efficiency. On the other hand, the cell containing the $MmNi_{3.7}Co_{0.7}Mn_{0.3}Al_{0.3}$ alloy (dashed line) exhibited a 1.15V discharge and 90% Ah-efficiency. The voltage of the former one is higher by 100mV than that of the latter one. The combination of the Co-free materials and GIGACELL structure would be suitable for industrial use as a high-power, large-sized battery with a long cycle-life.

3.2.4 Conclusion

The use of the Co-free alloy#1 as the negative electrode effectively improved the high-rate discharge and suppressed the self-discharge of the Ni-MH battery. Moreover, the carbon-coated $Ni(OH)_2$, which was prepared using a fluid-bed coating method, exhibited a good cycle-life performance that was comparable to the conventional CoOOH-coated one. The GIGACELL-type Ni-MH cell consisting of these Co-free materials exhibited long cycle-life performances. Good high-rate characteristics were maintained in the GIGACELL-type cell with a 205Ah rating.

References

[1] T. Sakai, I. Uehara, H. Ishikawa, J. Alloys. Compd., 293-295 (1999) 762.

[2] K. Nishimura, K. Tsutsumi, Powder Science and Engineering. 39(7) (2007) 1.

[3] K. Tsutsumi, J. Jpn. Inst. Energy, 87(7) (2008) 506.

[4] M. Oshitani, H. Yufu, K. Takashima, S. Tsuji, Y. Matsumaru, J. Electrochem. Soc., 136 (1989) 1590.

[5] T. Sakai, H. Yoshinaga, H. Miyamura, N. Kuriyama, H. Ishikawa, J. Alloys. Compd., 180 (1992) 37.

[6] T. Sakai, J. Jpn. Inst. Energy, 89 (2010) 420 (in Japanese).

[7] K. Kadir, T. Sakai, I. Uehara, J. Alloys. Compd., 257 (1997) 115.

[8] K. Kadir, N. Kuriyama, T. Sakai, I. Uehara, J. Alloys. Compd., 284 (1999) 145.

[9] K. Kadir, T. Sakai, I. Uehara, J. Alloys. Compd., 287 (1999) 264.

[10] K. Kadir, H. Tanaka, T. Sakai, I. Uehara, J. Alloys. Compd., 289 (1999) 66.

[11] K. Kadir, T. Sakai, I. Uehara, J. Alloys. Compd., 302 (2000) 112.

[12] T. Sakai, K. Kadir, M. Nagatani, H. Takeshita, H. Tanaka, N. Kuriyama, I. Uehara, Abstract of the 40th Battery Symposium, Kyoto, Japan, 1999, p. 133.

[13] J. Chen, N. Kuriyama, H. Takeshita, H. Tanaka, T. Sakai, M. Haruta, Electrochem. Solid State Lett. 3(6) (2000) 304.

[14] H. Pan, Y. Liu, M. Gao, Y. Lei, Q. Wang., J. Electrochem. Soc, 150(5) (2003) A565.

[15] T. Kohno, H. Yoshida, F. Kawashima, T. Inaba, I. Sakai, M. Yamamoto, M. Kanda, J. Alloys. Compd., 311 (2000) L5.

[16] S. Yasuoka, Y. Magari, T. Murata, T. Tanaka, J. Ishida, H. Nakamura, T. Nohma, M. Kihara, Y. Baba, H. Teraoka, J. Power Sources, 156 (2006) 662.

[17] T. Ozaki, M. Kanemoto, T. Kakeya, Y. Kitano, M. Kuzuhara, M. Watada, S. Tanase,

T. Sakai, J. Alloys. Compd, 446-447 (2007) 620.

[18] T. Ozaki, M. Kanemoto, T. Kakeya, Y. Kitano, M. Kuzuhara, M. Watada, S. Tanase, T. Sakai, ITE Letters on Batteries, New Technologies & Medicine, 8(4), 394 (2007).

[19] M. Kanemoto, T. Ozaki, T. Kakeya, D. Okuda, M. Kodama, R. Okuyama, GS-Yuasa Technical Report, 8 (2011) 22.

[20] F. Izumi, T. Ikeda, Mater. Sci. Forum, 321-324 (2000) 198.

Chapter 4

Development of fiber-type $Ni(OH)_2$ electrodes for nickel-metal hydride battery

4.1 Fiber-type $Ni(OH)_2$ electrode for nickel-metal hydride battery: Super high-rate charge/discharge and long cycle-life performances

4.1.1 Introduction

For more than two decades, nickel-metal hydride (Ni-MH) batteries have made progress and are widely used as power sources of consumer electronic devices, as well as hybrid electric vehicles (HEVs). In particular, the demand for the Ni-MH battery in HEVs has been increasing because of its superior properties of high-power capability, long cycle-life, reliability and safety [1-3]. Moreover, large-sized Ni-MH batteries have been developed for a battery-driven light rail vehicle (LRV; 600 V – 200Ah unit), and battery power system for railways (BPS; 750V – 150Ah unit) [4- 6]. In order to realize the widespread use of these large-sized batteries, further high-power capabilities are required.

At the end of the 1920s, the high-power discharge performance of the nickel positive electrode was improved by Ackermann's invention of the sintered nickel electrode [7, 8]. In the 1980s, a paste-type electrode was developed in order to increase the energy density of the nickel positive electrode [9, 10]. The latter electrode is comprised of a spherical $Ni(OH)_2$ powder which is loaded on a porous nickel substrate. Zinc is coprecipitated with the $Ni(OH)_2$ to prevent the formation of γ-NiOOH, which produces electrode swelling and capacity decay [11]. The $Ni(OH)_2$ particles are coated with $Co(OH)_2$ in order to increase in the utilization efficiency [10, 12]. The $Co(OH)_2$ is transformed into CoOOH having a high electrical conductivity during the charging process. Recently, Higuchi et al. reported that pretreatment, discharging before the initial activation, improves the $Co(OH)_2$-coated $Ni(OH)_2$ electrode performances such as high-rate discharge and cycle durability [13]. Meanwhile, a high amount of $Co(OH)_2$

with a thick deposition layer not only has a low specific area, but also hinders the diffusion of protons from the surface to the interior of the $Ni(OH)_2$ particles [14].

In recent studies of $Ni(OH)_2$, several new particle shapes, such as a ribbon- and board-like one [15], tube-type one [16] and large pseudo-single crystal [17], have been synthesized. Moreover, the $Ni(OH)_2$ thin film [18] and $Ni(OH)_2$/carbon composite [19] were prepared by a liquid phase deposition method. These new materials are expected to be candidates for use as the $Ni(OH)_2$ electrode for future batteries.

For further improvement of the high-power performance, the electrodes need to have a high electronic conductivity as well as a low electrochemical impedance. In this study, a carbon fiber-type $Ni(OH)_2$ electrode was developed for the Ni-MH battery. This electrode exhibits a high discharge capacity and long cycle-life without the CoOOH coating. Moreover, excellent high-rate charge and discharge characteristics are observed. The phase compositions in the charge and discharge states have been examined by the synchrotron X-ray diffraction (XRD) method.

4.1.2 Experimental

In order to prepare the fiber-type $Ni(OH)_2$ electrodes, a carbon fiber-tow (Toho Tenax Co., Ltd.) with 3000 single fibers was used for the collector substrate. The carbon fibers with the diameter of 6 μm were plated with 0.2 ~ 0.3 μm thickness by metallic nickel. A commercially available electroless plating reagent (Topchemi alloy B-1; Okuno chemical industries., Ltd.) was used. As shown in Fig. 4.1.1, the end of the fiber-tow was fixed by inserting it between two nickel-foam pieces, and a lead wire for electrical contact was spot-welded to the nickel-foam piece. The $Ni(OH)_2$ was electrodeposited [20, 21] from a 0.5 ~ 1.0 mol/*l* nickel nitrate aqueous solution at the current density of 5 ~ 25 mA/cm^2 for 5 ~ 30 minutes. The electrode was immersed in

the 5M NaOH solution at 353 K for 30 minutes to remove the nitrate ions remaining on the deposited $Ni(OH)_2$. The amount of $Ni(OH)_2$ was determined from the weight difference before and after the deposition. The nominal capacities were calculated using 289 mAh/g as the one-electron exchange for the β-$Ni(OH)_2$/β-NiOOH couple reaction. The size of the fiber-type electrode, which was modified by $Ni(OH)_2$, was about 3cm (length) ×1.3 cm (width) × 0.005 cm (thickness).

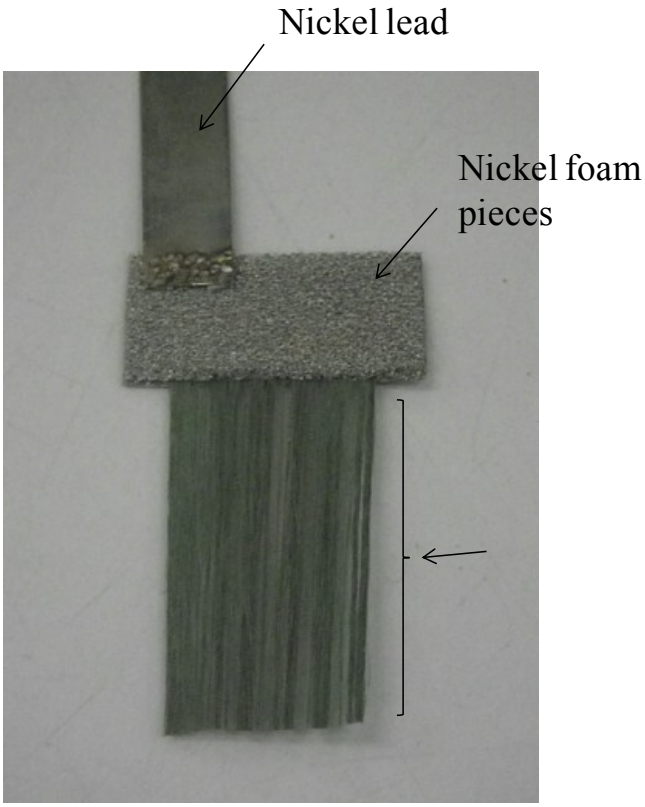

Figure 4.1.1 Photograph of the fiber-type substrate.

To prepare the test cells, the fiber-type $Ni(OH)_2$ electrode was held between two $MmNi_{3.7}Co_{0.7}Mn_{0.3}Al_{0.3}$ alloy electrodes (Mm: mishmetal) through a non-woven polypropylene separator. The alloy capacities were in significant excess compared to that of the fiber-type $Ni(OH)_2$ electrode. The electrolyte was 30wt. % KOH with $30gL^{-1}$LiOH. The cell was charged and discharged at the 0.1C rate during the first 10

cycles for activation. The charge/discharge curves were recorded using a computer-controlled charge/discharge system (BLS series, Keisokuki Center Co., Japan) equipped with a thermostatic chamber at 298 K. In this paper, the value of 1.0 for the number of exchanged electrons (NEE) per one nickel atom is defined as 100% (= 289 mAh/g) of the depth of charge (DOC). The cells were charged in the range of 110 – 150% of the DOC, that is, 1.1 – 1.5 of the NEE.

The electrochemical impedance spectra (EIS) were measured by a frequency response analyzer (SI 1280B, Solartron, UK) after charging to 1.1 of the NEE.

The morphologies of the fiber-type $Ni(OH)_2$ electrode were observed by a scanning electron microscope (SEM, JSM-6390, JEOL DATUM, Ltd., Japan).

The phase compositions of the samples were characterized by X-ray diffraction (XRD) using the beam line BL19B2 at the synchrotron radiation facility, SPring-8, Japan. A large Debye-Scherrer camera was used to detect the fine diffraction patterns. The wavelengths were calibrated to λ = 0.7010(2) Å using CeO_2 as the standard. The fiber-type electrodes were cut into small pieces, then loaded into glass capillaries with a 0.3 mmϕ inner diameter. The structural analysis was carried out using the Rietveld program, RIETAN-2000 [22].

4.1.3 Results and Discussion

4.1.3.1 Preparation of the fiber-type $Ni(OH)_2$ electrode and charge/discharge tests using the Ni-MH cell.

Approximately 18 ~ 23 mg of $Ni(OH)_2$ was electrodeposited on the 3000 carbon fibers with a 3 cm length. Figure 4.1.2 shows that the surface of each single fiber was coated with a $Ni(OH)_2$ layer of 1.5 ~ 2.5μm thickness. The capacities per unit-volume and per electrode-weight were estimated to be 280 ~ 340 mAh/cm^3 and 180 ~ 200

mAh/g, respectively. The latter values are greater than that of the paste-type one [10]. Table 4.1.1 summarizes the specification of the fiber-type electrodes. Table 4.1.2 shows the fiber-type electrodes contained in the Ni-MH test cells.

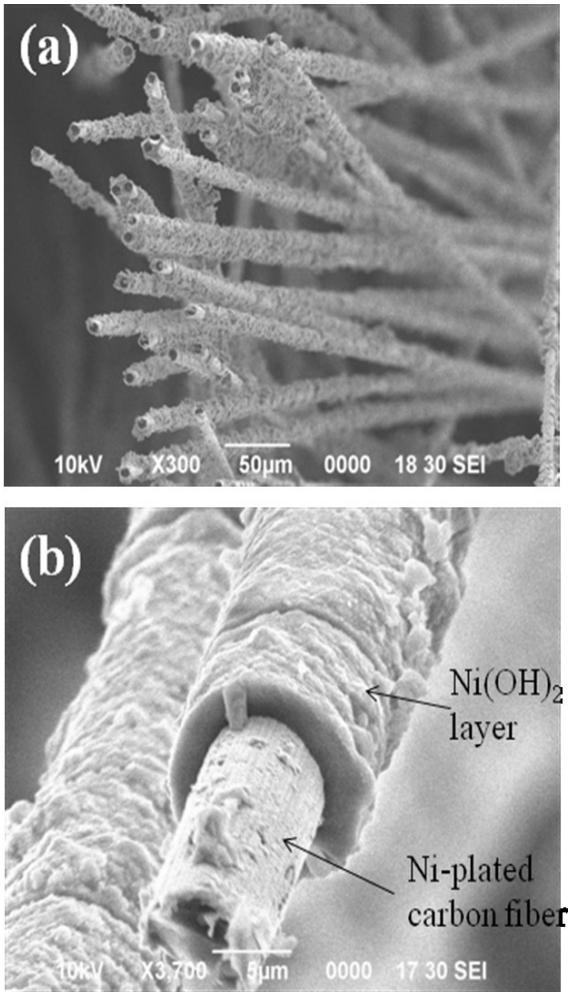

Figure 4.1.2 SEM photographs of the fiber-type electrode (a) image of a number of single fibers and (b) expanded view of a single fiber.

Figure 4.1.3 shows the 1C-rate charge/discharge curve of cell#1 after repeating 100 cycles. An approximate 1.3V discharge voltage and 1.05 (= 303mAh/g) NEE was observed during the discharge process after charging to 1.1 of the NEE.

Table 4.1.1 Specification of the fiber-type electrode for the Ni-MH test cells.

Number of carbon fibers	3000
Length of carbon fibers (cm)	3
Weight of nickel plated carbon fibers (g)	0.011
Weight of electrodeposited $Ni(OH)_2$ (g)	0.018 ~ 0.023
Capacity of the fiber-type electrode (mAh)	5.2 ~ 6.6
Capacity per unit volume (mAh/cm^3)	280 ~ 340
Capacity per electrode weight (mAh/g)	180 ~ 200

*Nominal capacities were calculated using 289 mAh/g as the one-electron exchange in the β-$Ni(OH)_2$/β-NiOOH couple reaction.

Table 4.1.2 Fiber-type electrodes in the Ni-MH test cells.

	fiber electrode	capacity (mAh)
Cell #1	No-coating	5.49
Cell #2		5.72
Cell #3		6.60
Cell_co#1	CoOOH coating	5.20
cell_co#2		6.10

Figure 4.1.4 shows the capacity retention of cell#2 at 298 K. No remarkable capacity decay is observed during 2000 cycles. The average voltage was 1.24 V for the cycles less than 200. The voltage then began to fade, and the average voltages remained at about 1.15V after 700 cycles. The inset shows the discharge curves. At the 100th cycle, the curve displays plateau region and the voltage significantly drops at the end of the discharge. Meanwhile, at the 2000th cycle, the voltage gradually decreases during the discharge process. These characteristics suggest that the internal resistance of cell#2 increases during the cycling.

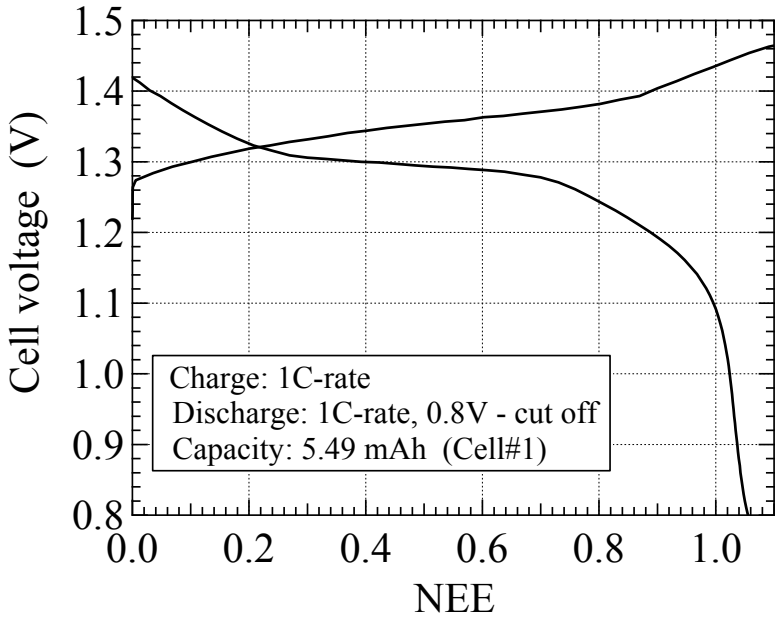

Figure 4.1.3 1C rate charge/discharge curve of cell#1.

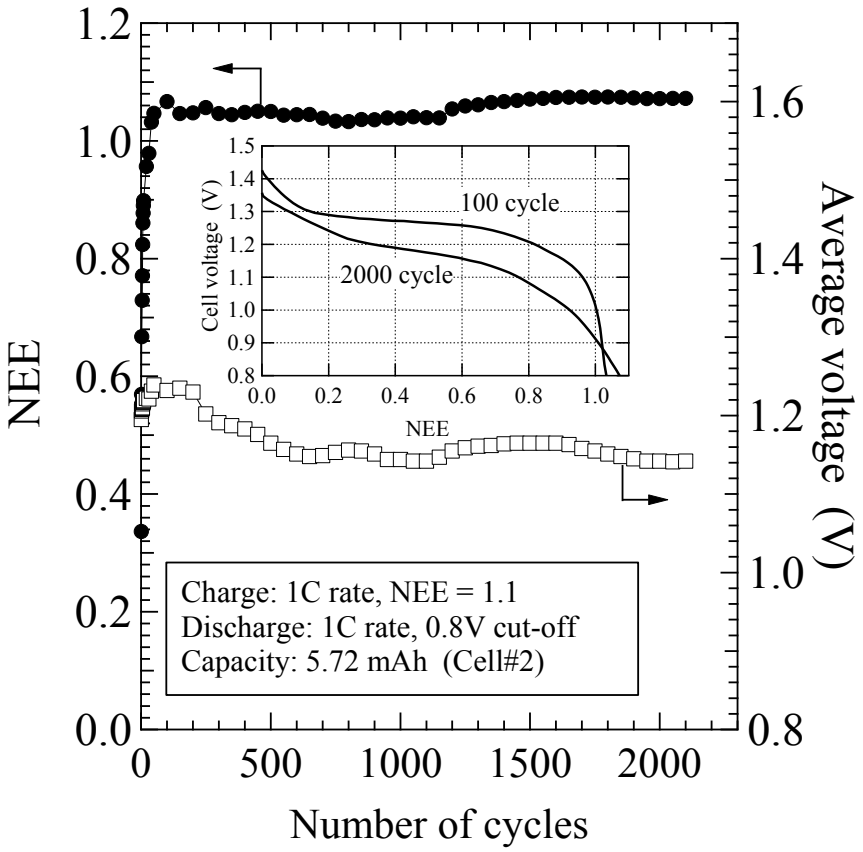

Figure 4.1.4 Cycle-life performance of cell#2.

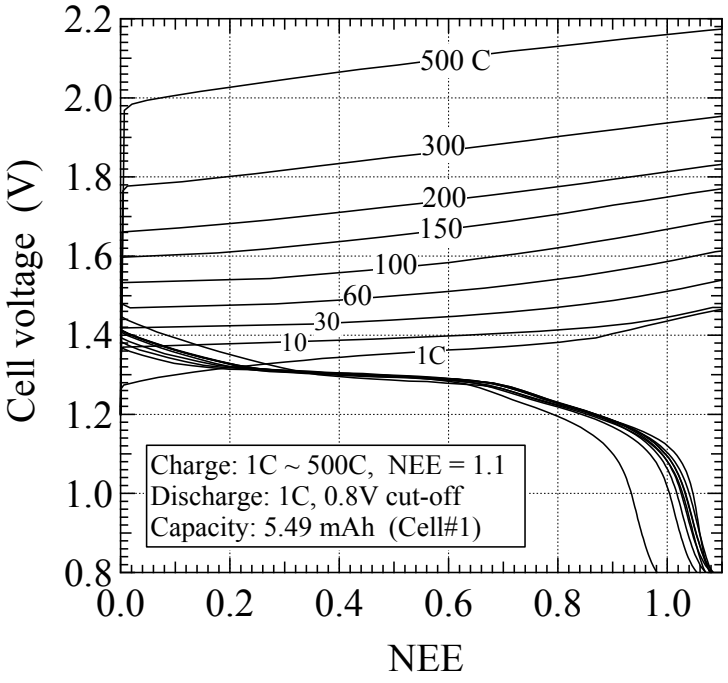

Figure 4.1.5 High-rate chargeability of cell#1 at various currents to 1.1 of the NEE, and discharged at the 1C rate to a 0.8 V cut-off voltage.

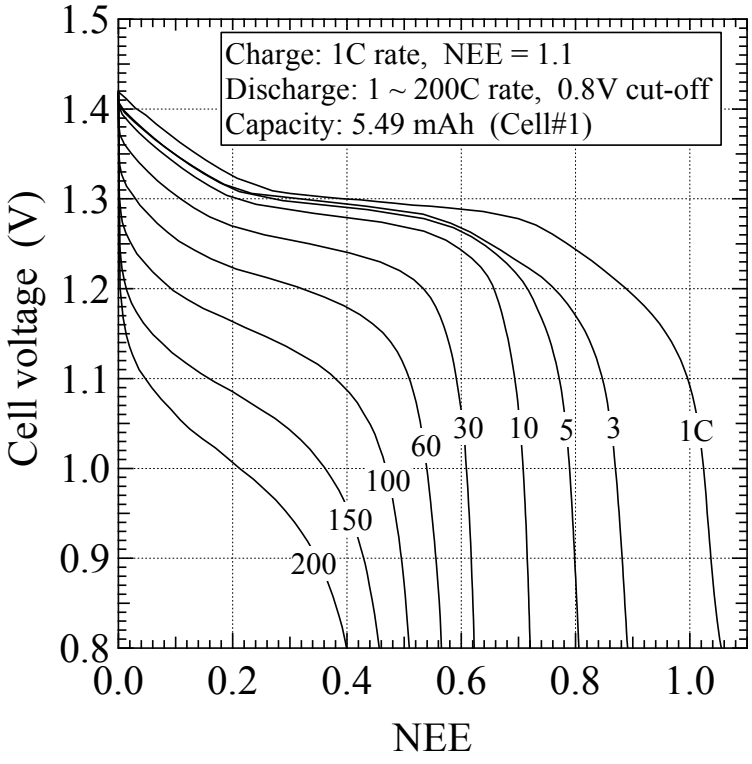

Figure 4.1.6 High-rate dischargeability of cell#1 at various currents after charging to 1.1 of NEE at the 1C rate.

Figure 4.1.5 shows the high-rate charging of cell#1. After charging to 1.1 of the NEE at a current ranging from the 1 - 500C rate, the cell was discharged at the 1C rate to a 0.8V cut-off voltage. An approximate 0.98 (= 283 mAh/g) NEE was obtained, even if the cell was charged at the 500C rate.

Figure 4.1.6 shows the high-rate discharging of cell#1. After charging to 1.1 of the NEE at the 1C rate, the cell was discharged at various currents ranging from the 1 to 200C rate. Even at the 100C rate, an approximate 1.15V discharge voltage and 0.5 NEE were delivered.

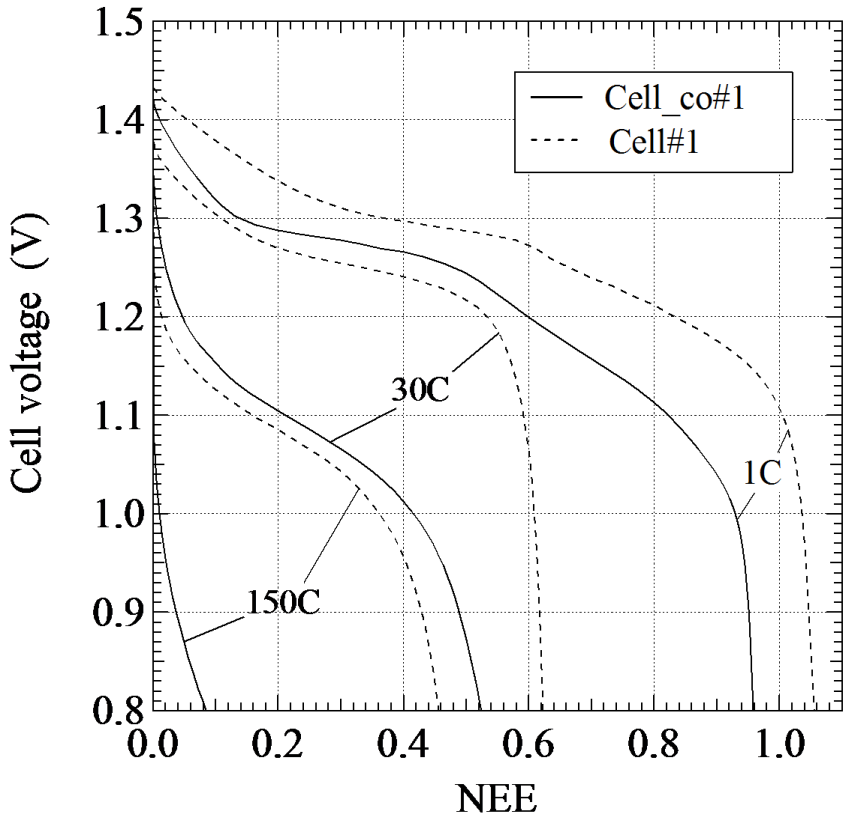

Figure 4.1.7 High-rate dischargeability of cell_co#1 (solid lines) and cell#1 (dashed lines) at various currents.

In order to form the CoOOH layer, the fiber-type $Ni(OH)_2$ electrode was alternately immersed in a cobalt nitrate solution and NaOH solution, and then dried at 378 K for 1 hour. Figure 4.1.7 shows the high-rate discharge of cell_co#1. This cell exhibited a lower discharge voltage than cell#1, especially at the high-rate discharge. The internal resistance of cell_co#1 is estimated to be approximately 7 mΩ·Ah from the voltage vs. current (*I*-*V*) plots at the 10-second discharge, which is 2.3 times higher than that of cell#1. This result suggests that the high-rate discharge performance of the fiber-type $Ni(OH)_2$ electrode is degraded by the CoOOH coating.

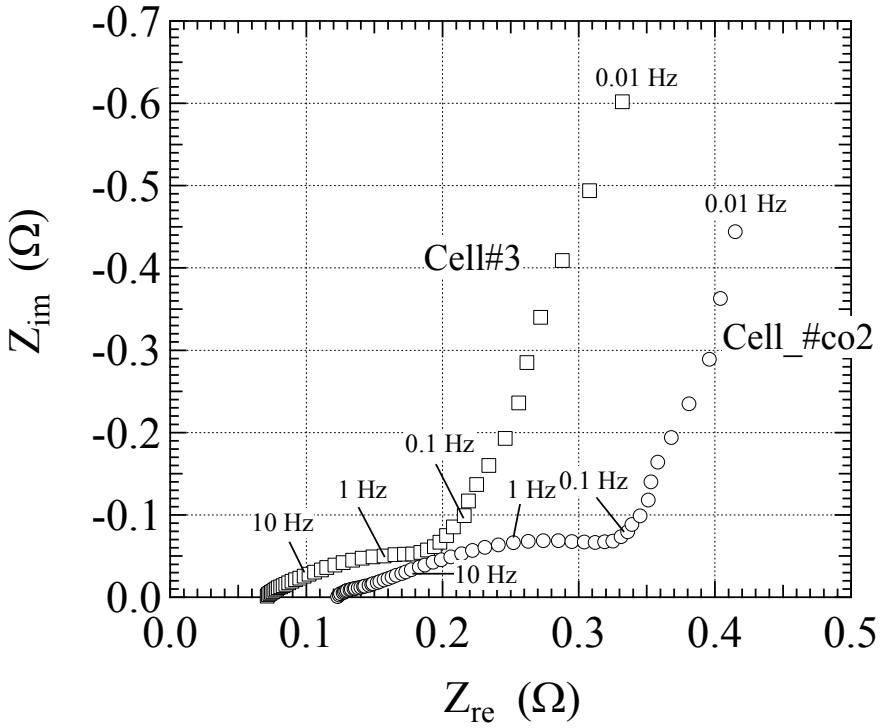

Figure 4.1.8 Electrochemical impedance spectra (EIS) of cell#3 (□) and cell_co#2 (○) at the 1.1 NEE.

Figure 4.1.8 shows the electrochemical impedance spectra (EIS) for cell#3 and cell_co#2 after charging to 1.1 of the NEE. Both spectra show a depressed semicircle resulting from the charge transfer resistance (R_{ct}) at a high frequency, and a slope resulting from the Warburg impedance (Z_W) in the low frequency region. The Cell#3 exhibited a lower R_{ct} than that of cell_co#2. In the frequency region greater than about 0.1 Hz (= 10s), the EIS includes information about the electrochemical reaction. This result suggests that the internal resistances obtained at the 10-second discharge in Fig. 7 reflect the difference in the electrochemical reactions between cell#3 and cell_co#2.

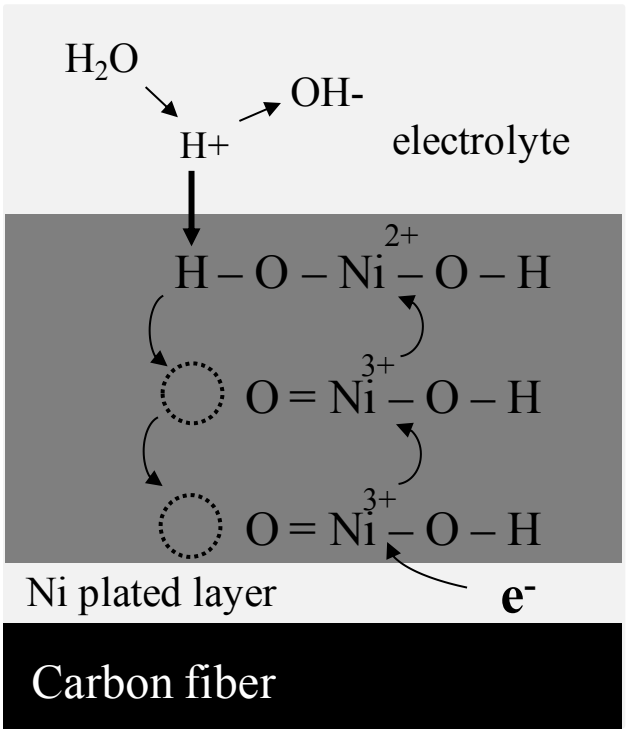

Figure 4.1.9 Schematic views of the discharge reaction mechanism of the fiber-type $Ni(OH)_2$ electrode.

Figure 4.1.9 shows a schematic view of the discharge reaction mechanism of the fiber-type electrode in the test cells. An electron is supplied from the nickel-plated fiber

on the inner side of the NiOOH layer, and a proton diffuses in the NiOOH layer through the NiOOH/electrolyte interface. In the CoOOH-coated fiber-type electrode, the state of the electron path would be equivalent to the non-coated fiber-type electrode. Meanwhile, the CoOOH layer on the NiOOH/electrolyte interface is different for both electrodes. The results of Figs. 7 and 8 suggest that the CoOOH reduces the specific area which participates in the electrochemical reaction of the fiber-type $Ni(OH)_2$ electrode.

4.1.3.2 XRD patterns of the fiber-type $Ni(OH)_2$ electrodes.

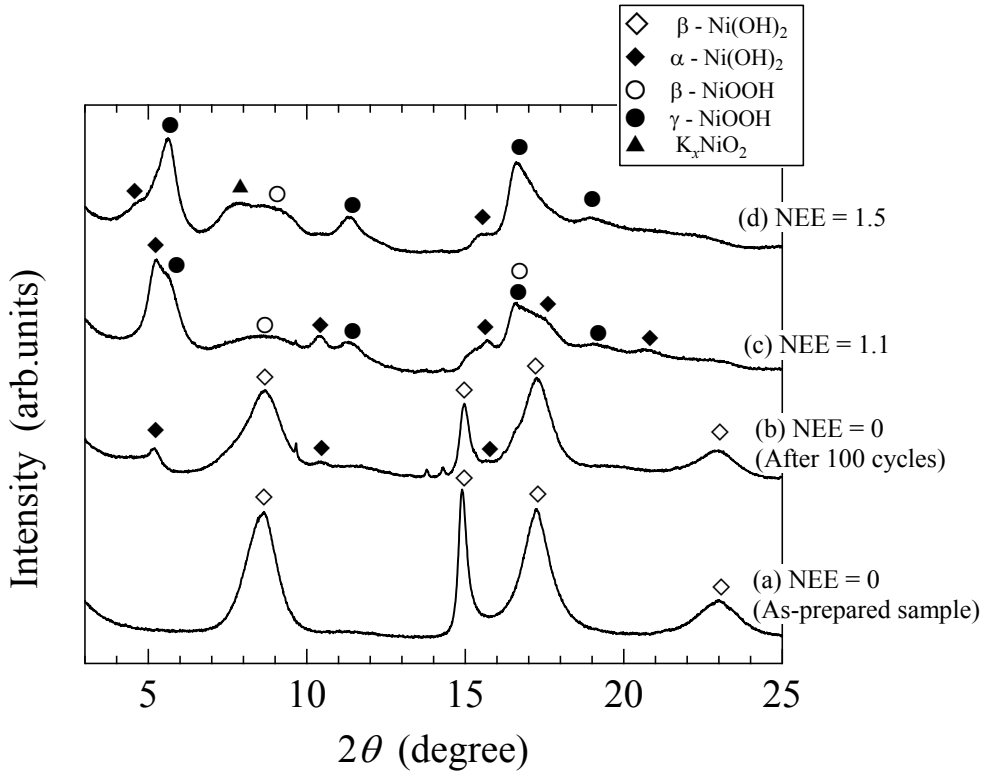

Figure 4.1.10 Synchrotron XRD patterns of the fiber-type $Ni(OH)_2$ electrodes at various NEEs; (a) NEE = 0 (as-prepared sample), (b) NEE = 0 (after 100 cycles), (c) NEE = 1.1, (d) NEE = 1.5.

Figure 4.1.10 shows the synchrotron XRD patterns of the fiber-type $Ni(OH)_2$ electrodes. The as-prepared sample consists of β-$Ni(OH)_2$. At the 0 of the NEE after 100 cycles, α-$Ni(OH)_2$ was found in addition to β-$Ni(OH)_2$. After charging to 1.1 of the NEE, the β-NiOOH, γ-NiOOH and α-$Ni(OH)_2$ phases were observed. After charging to 1.5 of the NEE, a monoclinic phase, which could be composed of K_xNiO_2 [23, 24], was found in addition to the β-NiOOH, γ-NiOOH and α-$Ni(OH)_2$ phases.

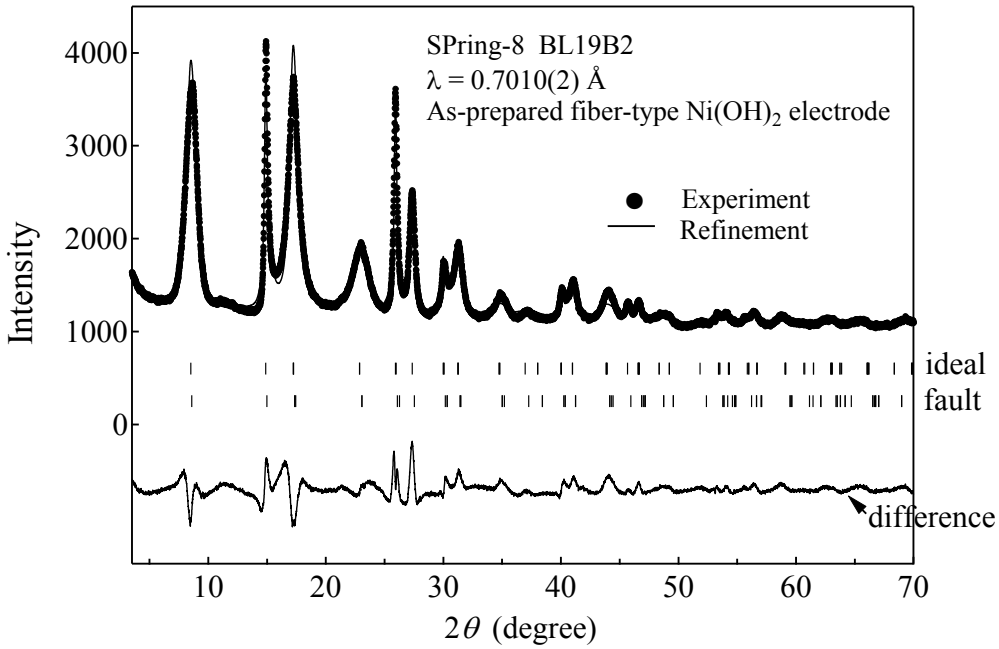

Figure 4.1.11 Synchrotron XRD pattern and the Rietveld refinement results of the as-prepared fiber-type $Ni(OH)_2$ electrode.

Figure 4.1.11 shows an XRD pattern with the Rietveld refinement of the as-prepared fiber-type $Ni(OH)_2$ electrode. For the refinement, a model containing a stacking fault [25-27] was used, in which the β-$Ni(OH)_2$ contains two types of phases, namely, the ideal phase and fault one. The nickel atom is shifted from the (0, 0, 0) site for the ideal phase to the (2/3, 1/3, 0) site for the fault one. The abundance of the fault phase was

around 30 wt.%, indicating that the fiber-type $Ni(OH)_2$ electrode contains many stacking faults compared to the spherical $Ni(OH)_2$ particle [27]. Table 4.1.3 summarizes the refinement results for the various NEEs.

Table 4.1.3 Phase components, R values, mass fractions and cell parameters obtained from the Rietveld refinements using the synchrotron XRD data of the carbon fiber-type $Ni(OH)_2$ at the various NEEs.

(a) NEE = 0 (As-prepared sample); R_{wp} = 4.79, R_p = 3.55, R_e = 2.69

Phases	Ideal/fault	R_B (%)	R_F (%)	(wt. %)	Space Group	*Cell parameter* (Å)	Volume (Å^3)
β-$Ni(OH)_2$	Ideal	1.76	0.89	67	P-3m1 (No.164)	*a* = 3.138(1) *c* = 4.698(2)	40.1
	Fault	2.12	1.06	33	P-3m1 (No.164)	*a* = 3.120(2) *c* = 4.648(3)	39.2

(b) NEE = 0 (After 100 cycles); R_{wp} = 3.12, R_p = 2.27, R_e = 2.81

Phases	Ideal/Fault	R_B (%)	R_F (%)	(wt. %)	Space Group	*Cell parameter* (Å)	Volume (Å^3)
β-$Ni(OH)_2$	Ideal	1.85	0.84	53	P-3m1 (No.164)	*a* = 3.122(1) *c* = 4.666(2)	39.4
	Fault	3.53	1.70	28	P-3m1 (No.164)	*a* = 3.112(1) *c* = 4.635(3)	38.9
α-$Ni(OH)_2$	Ideal	1.70	0.84	17	R-3m (No.166)	*a* = 3.068(4) *c* = 23.86(6)	194.6
	Fault	1.25	0.75	2	R-3m (No.166)	*a* = 3.03(2) *c* = 23.17(1)	185.3

(b) NEE = 1.1; R_{wp} = 2.88, R_p = 2.14, R_e = 2.72

	Phases	R_B (%)	R_F (%)	(wt. %)	Space Group	*Cell parameter* (Å)	Volume (Å^3)
β-NiOOH	Ideal	1.72	0.82	14	P-3m1 (No.164)	*a* = 2.841(7) *c* = 4.830(7)	33.8
	Fault	1.45	0.65	16	P-3m1 (No.164)	*a* = 2.821(6) *c* = 4.850(8)	33.4
α-$Ni(OH)_2$	Ideal	1.31	0.74	14	R-3m (No.166)	*a* = 3.047(2) *c* = 23.22(1)	186.8
	Fault	1.47	0.73	4	R-3m (No.166)	*a* = 3.060(5) *c* = 23.15(5)	187.8
γ-NiOOH	Ideal	2.10	1.03	44	R-3m (No.166)	*a* = 2.794(2) *c* = 20.85(1)	141.1
	Fault	1.72	1.01	8	R-3m(No.166)	*a* = 2.816(3) *c* = 21.22(1)	145.8

(c) NEE = 1.5; R_{wp} = 2.91, R_p = 2.13, R_e = 2.72

	Phases	R_B (%)	R_F (%)	(wt. %)	Space Group	*Cell parameter* (Å)	Volume (Å^3)
β-NiOOH	Ideal	1.77	1.19	1	P-3m1 (No.164)	*a* = 2.812(5) *c* = 4.756(4)	33.5
	Fault	0.82	0.48	9	P-3m1 (No.164)	*a* = 2.989(3) *c* = 4.668(5)	33.4
α-$Ni(OH)_2$	Ideal	1.90	1.05	10	R-3m (No.166)	*a* = 3.017(2) *c* = 25.55(2)	201.5
	Fault	2.80	1.57	3	R-3m (No.166)	*a* = 3.026(2) *c* = 26.44(2)	209.8
γ-NiOOH	Ideal	1.20	0.54	51	R-3m (No.166)	*a* = 2.814(1) *c* = 21.72(3)	144.1
	Fault	1.64	0.83	16	R-3m (No.166)	*a* = 2.8381(9) *c* = 21.31(1)	146.0
$K_x NiO_2$	-	1.58	0.72	10	C2/m (No.12)	*a* = 4.84(1) *b* = 2.918(5) *c* = 5.65(1) *β* = 113.2(2)	73.5

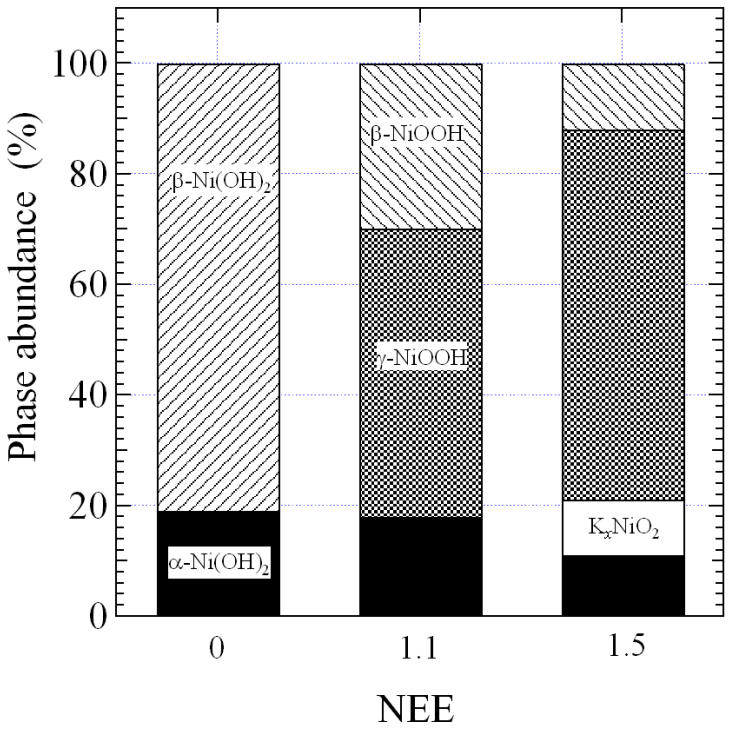

Figure 4.1.12 The phase abundance of the fiber-type electrodes at various NEEs: 0, 1.1 and 1.5.

Figure 4.1.12 shows the phase abundances for each phase at the various NEEs. The abundance of the α-$Ni(OH)_2$ phases remained constant value during charging to 1.1 of the NEE, indicating that the α-$Ni(OH)_2$ hardly participates in the reaction. The β-$Ni(OH)_2$ phases were transformed into β-NiOOH and γ-NiOOH ones during the charging to the 1.1 NEE. After charging to 1.5 the NEE, the mass fractions of the α-$Ni(OH)_2$ phases decreased to around 10 wt.%. A part of the α-$Ni(OH)_2$ phases could be charged and transformed into the γ-NiOOH or K_xNiO_2 phases. The K_xNiO_2 phase could be formed by overcharge of the γ-NiOOH phase.

It is considered that a charge reaction arises from the inner side of the active-material layer near the carbon fiber, and gradually progresses towards the outside. The β-$Ni(OH)_2$ and α-$Ni(OH)_2$ possibly exist in the inside and the outside of the

active-material layer as shown in Figs. 4.1.13(a) and 4.1.13(b). As shown in Fig. 4.1.13(c), the real fiber-type electrode after cycling is composed of $Ni(OH)_2$ fixed on the inner fiber and outer layer separated from the inner fiber.

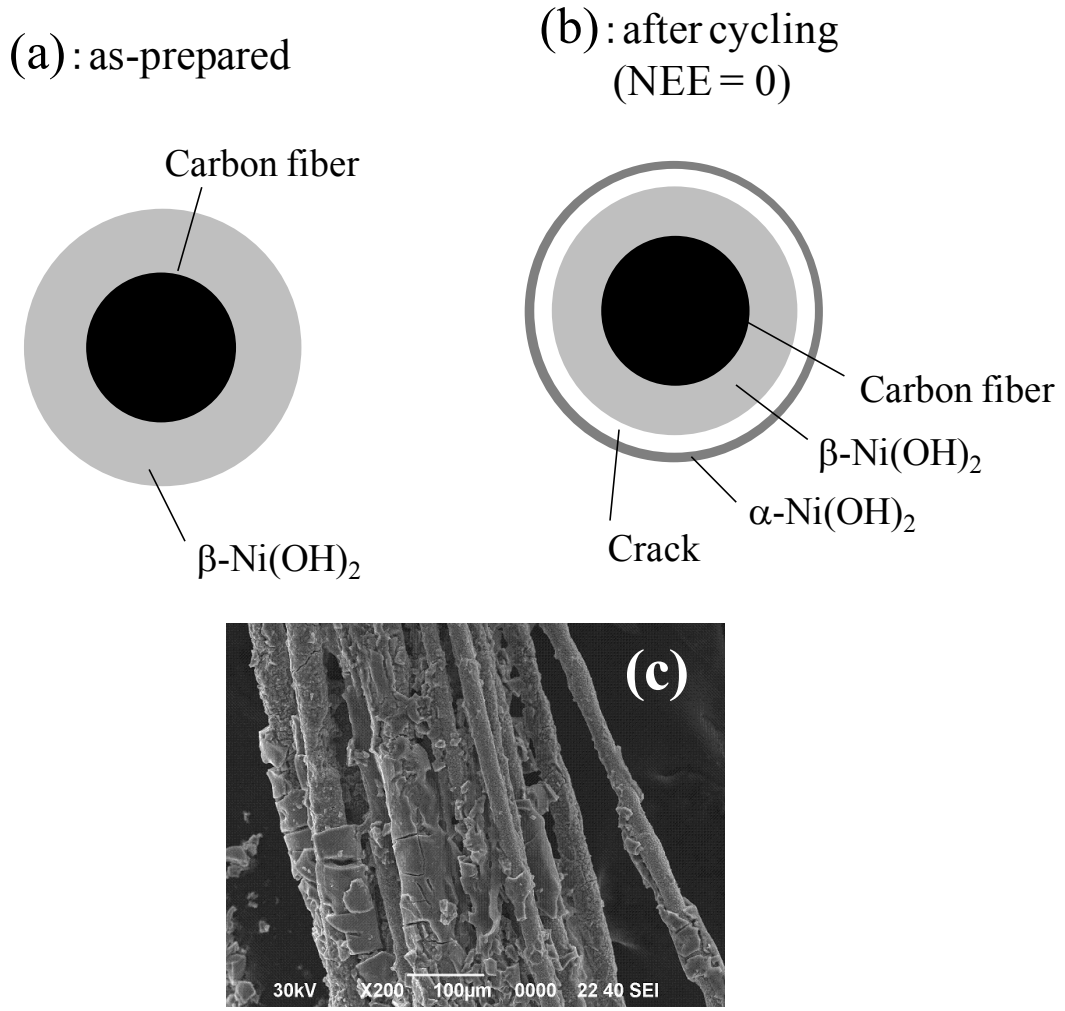

Figure 4.1.13 Schematic views of cross-sections of the (a) as-prepared electrode, (b) the electrode after cycling, and (c) SEM photographs of a fiber-type electrode after cycling.

Figure 4.1.14 shows the average cell volumes for the various NEEs, which were obtained by the linear combination of the cell volumes multiplied by the abundance for each phase. The expansion ratio, {V(NEE= 1.1) – V(NEE=0)}/V(NEE = 0), is

estimated to be approximately 8 %, a value which is much lower than the other ratios, such as {V(γ-NiOOH) – V(β-Ni(OH)$_2$)}/V(β-Ni(OH)$_2$) of ~ 20% and {V(γ-NiOOH) – V(β-NiOOH)}/V(β-NiOOH) of ~ 40%.

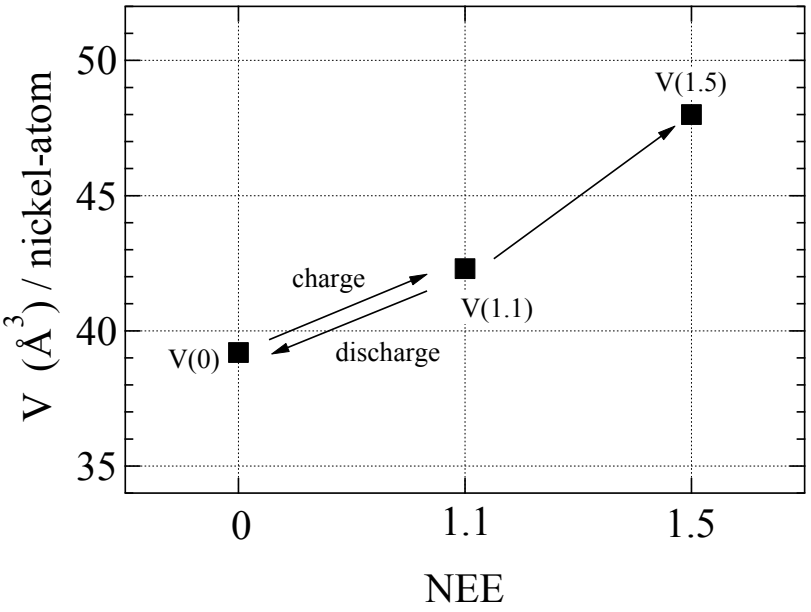

Figure 4.1.14 (a) The change in average cell volumes at various NEEs: V(0), V(1.1) and V(1.5) for NEE = 0, 1.1 and 1.5, respectively.

The reason for the low expansion ratio would be related to the fact that the contraction degree of the β-Ni(OH)$_2$ → β-NiOOH transformation and the expansion degree of the β-NiOOH → γ-NiOOH transformation offset each other. The low expansion at the 1.1 NEE would permit a good capacity retention for the fiber-type electrode in spite of containing a large amount of the γ-NiOOH phase. Meanwhile, the repeated expansion/contraction during the charge/discharge cycles should gradually weaken the contact between the active-material layer and carbon fiber, causing the increased internal resistance. This is extrapolated to be the reason for the voltage decrease in Fig. 4. The 0.8V cut-off, which is a general cut-off voltage value for the

Ni-MH cell [28], enabled the fiber-type electrode to maintain the discharge capacity as shown in the inset of Fig.4. If the cut-off voltage is considered to be a higher value, e.g. 1.0V, the discharge capacity is found to be reduced at the 2000th cycle.

On the other hand, the expansion ratio, {V(1.5)-V(0)}/V(0), was estimated to be approximately 23%. The inner layer would be expanded by forming a total of 77 wt.% of the γ-NiOOH and K_xNiO_2 phases, and the α-$Ni(OH)_2$ is also charged by perhaps contacting the expanded inner layer. At the 1.5 NEE, the capacity and voltage was found to decrease during several tens of cycles. In order to produce a long cycle-life for the fiber-type electrode, it is necessary to limit the charge capacity so that the state occurs when the outer layer is not charged.

For the conventional paste-type electrode, the coprecipitation of the Zn [11] and CoOOH-coating [10, 12] is indispensable for suppressing the formation of γ-NiOOH, which produces electrode swelling and capacity decay. For the fiber-type $Ni(OH)_2$ electrode, it was found that pure $Ni(OH)_2$, which easily forms γ-NiOOH, exhibits good electrode performances. However, in order to apply this electrode to practical batteries, improving the voltage retention during several thousands of cycles is an important subject. A further study in this area is now in progress.

4.1.4 Conclusion

The fiber-type $Ni(OH)_2$ electrode was prepared by the electrodeposition of pure $Ni(OH)_2$ on nickel-plated carbon fibers. The Ni-MH cell containing the fiber-type $Ni(OH)_2$ electrode can get a higher-rate performance due to good mass transport of the electrolyte. The CoOOH coating, which is indispensable for the conventional paste-type electrode, degraded the electrochemical reactivity of the fiber-type $Ni(OH)_2$ electrode.

A comparatively long cycle-life occurred due to low volume expansion of the

active-material layer during charging. Meanwhile, a high volume expansion with overcharge affects the cycle-life during several tens of cycles.

References

[1] T. Sakai, I. Uehara and H. Ishikawa, *J. Alloys. Compd*., **293-295**, 762 (1999).

[2] A. Taniguchi, N. Fujioka, M. Ikoma and A. Ohta, *J. Power Sources*, **100**, 117 (2001).

[3] K. Shinyama, Y. Magari, K. Kumagae, H. Nakamura, T. Nohma, M. Takee and K. Ishiwa, *J. Power Sources*, **141**, 193 (2005).

[4] K. Tsutsumi, *J. Jpn. Inst. Energy*, **87(7)**, 506 (2008).

[5] Y. Oku, *Kawasaki Technical Review,* **169**, 10 (2009).

[6] *High-capacity Fully Sealed Nickel-Metal Hydride Battery [GIGACELL®]*, Kawasaki Heavy Industries, Ltd (2010).

[7] S. U. Falk, A. J. Salkind, *Alkaline Storage Batteries*, p. 30, John Wiley & Sons, Inc, New York, (1969).

[8] A. Fleischer, *J. Electrochem. Soc.*, **94**, 289 (1948).

[9] I. Matsumoto, M. Ikeyama, T. Iwaki and H. Ogawa, *Denki Kagaku oyobi Kogyo Buturi Kagaku*, **54**, 159 (1986).

[10] M. Oshitani, H. Yufu, K. Takashima, S. Tsuji and Y. Matsumaru, *J. Electrochem. Soc.*, **136**, 1590 (1989).

[11] M. Oshitani, M. Watada, H. Yufu and Y. Matsumaru, *Denki Kagaku oyobi Kogyo Buturi Kagaku*, **57**, 480 (1989).

[12] M. Yano, T. Ogasawara, Y. Baba, M. Tadokoro and S. Nakahori, *Electrochemistry,* **69**, 858 (2001).

[13] E. Higuchi, T. Mizuta and H. Inoue, *Electrochemistry,* **78**, 420 (2010).

[14] C. Shao-an, W. Leng, Z. Jianqing and C. Chunan, *J. Power Sources,* **101,** 248 (2001).

[15] D. Yang, R. Wang, M. He, J. Zhang and Z.Liu, *J. Phys. Chem. B,* **109**, 7654 (2005).

[16] W. Li, S. Zhang, J. Chen, *J. Phys. Chem. B,* **109**, 14025, (2005).

[17] L. Gourrier, S. Deabate, T. Michel, M. Paillet, P. Hermet, J-L. Bantignies and F. Henn, *J. Phys. Chem. C,* **115**, 15067 (2011).

[18] S. Deki, A. Hosokawa, A.B. Béléké and M. Mizuhata, *Thin Solid Films,* **517**, 1546 (2009).

[19] A.B. Béléké, A. Hosokawa, M. Mizuhata and S. Deki, J. Ceram. Soc. Japan, **117**, 392 (2009).

[20] S. Yoshizawa, Z. Takehara and M. Kato, *Denki Kagaku* **35**, 559 (1966).

[21] Y. Sasaki and T. Yamashita, *Denki Kagaku,* **56**, 668 (1988).

[22] F. Izumi, T. Ikeda, *Mater. Sci. Forum,* **321-324**, 198 (2000).

[23] P. Oliva, J. Leonaridi, J.F. Laurent, C. Delmas, J.J. Braconnier, M. Figlarz, F. Fievet and A. De Guibert, *J. Power Sources,* **8**, 229 (1982).

[24] L. Viciu, J.W.G. Bos, H.W. Zandbergen, Q. Huang, M.L. Foo, S. Ishiwata, A.P. Ramirez, M. Lee, N.P. Ong and R.J. Cava, *Phys. Rev. B,* **73**, 174104 (2006).

[25] C. Delmas and C. Tessier, *J. Mater. Chem*., **7**, 1439 (1997).

[26] C. Tessier, P. H. Haumesser, P. Bernard, and C. Delmas, *J. Electrochem. Soc*., **146**, 2059 (1999).

[27] M. Morishita, S. Ochiai, T. Kakeya, T. Ozaki, Y. Kawabe, M. Watada, S. Tanase and T. Sakai, *J. Electrochem. Soc.*, **155(12)**, A936 (2008).

[28] M. Yao, K. Okuno, T. Iwaki, M. Kato, K. Harada, J.J. Park, S. Tanase, T. Sakai, *Electrochem. Solid-State Lett.,* **10(3)** A56 (2007).

4.2 Fiber-type $Ni(OH)_2$ electrode with α/γ phase transformation: high-capacity and high-voltage performances of nickel-metal hydride battery

4.2.1 Introduction

Nickel-metal hydride (Ni-MH) batteries are being widely used in various consumer electronic devices and hybrid electric vehicles (HEVs) [1-3]. Their applications have also been extended to various industrial equipment such as a battery-driven light rail vehicle (LRV), a battery power system for railways (BPS) and a power-grid for a renewable energy source. For this trend, large-scale battery systems with the capacity of 200 ~ 400kWh were developed and verification tests have been conducted at various locations in Japan [4-7]. Further progress in performance, such as the power, cycle-life, safety and cost, is required in order to realize the widespread use of the large-scale battery system.

At present, a paste-type electrode is typically used for the positive electrode of the Ni-MH batteries [8, 9]. This electrode is comprised of a spherical β-$Ni(OH)_2$ powder which is loaded on a porous nickel substrate. The coprecipitation of the Zn [10] and CoOOH-coating [9,11,12] is indispensable for improving the discharge capacity and suppressing the formation of γ-NiOOH, which produces electrode swelling and capacity decay.

$Ni(OH)_2$ has two polymorphs, namely, α-$Ni(OH)_2$ and β-$Ni(OH)_2$. The α-$Ni(OH)_2$, involving the α-$Ni(OH)_2$/γ-NiOOH transition, has received much attention as a high-capacity active material for the positive electrode of advanced Ni-MH batteries. In general, the pure α-$Ni(OH)_2$ is unstable in an alkali electrolyte, being easily transformed into β-$Ni(OH)_2$. To stabilize the α-$Ni(OH)_2$ structure, partial substitution of the nickel in the $Ni(OH)_2$ by other elements, such as Co [13], Fe [14], Mn [15-17], Al [18], and Zn [19] have been carried out. Detailed structural analyses of the Mn or Al substituted

α-$Ni(OH)_2$ were reported [20, 21]. Substitution by trivalent Al ions over 20mol% stabilizes the α-$Ni(OH)_2$ structure. In recent studies, several new Al-substituted materials, such as the α-$Ni(OH)_2$ thin film [22] and α-$Ni(OH)_2$/carbon composite [23], were developed by a liquid phase deposition method.

Recently, a fiber-type electrode with β-$Ni(OH)_2$ was prepared by electrodeposition [24]. The Ni-MH cell containing the fiber-type $Ni(OH)_2$ electrode can obtain a better high-rate performance. In this electrode, more than 50wt% of the active material was easily transformed into γ-NiOOH during charging. In this study, fiber-type α-$Ni(OH)_2$ electrodes were prepared by electrodeposition in a 20mol% Al-added nickel nitrate solution. Their charge and discharge behaviors, such as the high-rate charge/discharge and cycle-life performances, were investigated. The phase compositions in the charge and discharge states have been investigated by the synchrotron X-ray diffraction (XRD) method.

4.2.2 Experimental

In order to prepare the fiber-type electrodes, a carbon fiber-tow (Toho Tenax Co., Ltd.) with 3000 single fibers was used as the collector substrate. The carbon fibers with an average diameter of 6 μm were plated with 0.2 ~ 0.3 μm metallic nickel. A commercially available electroless plating reagent (Top chemi alloy B-1; Okuno Chemical Industries., Ltd.) was used. The end of the fiber-tow was fixed by inserting it between two nickel-foam pieces, and a lead wire for electrical contact was spot-welded to the nickel-foam piece [24].

Al-substituted fiber-type $Ni(OH)_2$ electrodes were prepared using the electrodeposition method [25, 26] for the nickel-plated carbon fibers. The aqueous solution consisted of Al nitrate and Ni nitrate with the molar ratio of 80 : 20. An

Al-substituted $Ni(OH)_2$ was electrodeposited from the 0.5 ~ 1.0 mol/*l* solution at the current density of 5 ~ 30 mA/cm^2 for 5 ~ 30 minutes.

Meanwhile, a pure $Ni(OH)_2$ (without Al addition) was also electrodeposited from a pure nickel nitrate aqueous solution on the nickel-plated carbon fibers. The fiber-type pure $Ni(OH)_2$ electrode was used as the reference for the comparison.

The electrodes were immersed in a 5M NaOH solution at 353 K for 30 minutes to remove the nitrate ions remaining on the deposited $Ni(OH)_2$. The amount of active material was determined from the weight difference before and after the deposition. An approximate 14 ~ 20 mg electrodeposit was obtained on the carbon fibers.

The dimensions of the fiber-type electrode, which were modified by the active material, were about 3cm (length) ×1.3 cm (width) × 0.005 cm (thickness).

Inductively coupled plasma atomic emission spectroscopy (ICP-AES) was used to obtain the aluminum substitution ratio in the electrodeposited $Ni(OH)_2$.

To prepare the test cells, the fiber-type electrode was held between two $MmNi_{3.7}Co_{0.7}Mn_{0.3}Al_{0.3}$ alloy electrodes (Mm: mishmetal) separated by a non-woven polypropylene separator. The alloy capacities were in significant excess compared to that of the fiber-type electrode. The electrolyte was 30wt.% KOH with $30gL^{-1}$LiOH. The cell was charged and discharged at the 0.1C rate during the first 10 cycles for activation. The charge/discharge curves were recorded using a computer-controlled charge/discharge system (BLS series, Keisokuki Center Co., Japan) equipped with a thermostatic chamber at 298 K.

The phase compositions of the samples were characterized by X-ray diffraction (XRD) using the beam line BL19B2 at the synchrotron radiation facility, SPring-8, Japan. A large Debye-Scherrer camera was used to detect the fine diffraction patterns. The wavelengths were calibrated to λ = 0.7010(2) Å using CeO_2 as the standard. The

fiber-type electrodes were cut into small pieces, then loaded into glass capillaries with a 0.3 mmϕ inner diameter. The structural analysis was carried out using the Rietveld program, RIETAN-2000 [27].

4.2.3 Results and Discussion

4.2.3.1 Analysis of the electrode structure and charge/discharge tests using the Ni-MH cell.

Figure 4.2.1 shows that the surface of each single fiber was coated with a flaky-shaped $Ni(OH)_2$ layer of 2 ~ 4μm thickness. The ICP-AES analysis showed that the electrodeposited nickel hydroxide on the carbon fiber contained approximately 20mol% Al. This fiber-type electrode was labeled the 20%Al fiber-type $Ni(OH)_2$ electrode or electrode_A. The fiber-type pure $Ni(OH)_2$ electrode, which was prepared as the reference, was labeled the electrode_B. In order to investigate the effect of the Al addition, the battery performances of electrode_B were compared to those of electrode_A. For electrode_A, the capacities per unit-volume and per electrode-weight were estimated to be 230 ~ 260 mAh/cm^3 and 160 ~ 170mAh/g, respectively. These values are comparable or lower than those of electrode_B. Table 4.2.1 summarizes the specifications of the fiber-type electrodes contained in the Ni-MH test cells.

Figure 4.2.2 shows the 1C-rate discharge curves of cell_A-1 and cell_B-1 after 100 cycles. Cell_A-1 and cell_B-1 exhibited 305mAh/g and 303mAh/g discharge capacities, respectively, after charging to 318mAh/g. For cell_A-1, a wide plateau region was observed in the discharge curve. Cell_B-1 exhibited a sloping discharge voltage compared to cell_A-1. In electrode_A, 20mol% of the Ni was substituted by Al, namely,

Table 4.2.1 Specifications of the fiber-type electrodes in the Ni-MH test cells

cell	Electrode-type	Number of carbon fibers	Length of carbon fibers (cm)	Weight of nickel plated carbon fibers (g)	Active material	Electro-deposited weight (g)	(*1) Measured capacity (mAh/g)	(*1) Actual discharge capacity (mAh)	(*1)Number of exchange electron (NEE)	Capacity per unit volume (mAh/cm^3)	Capacity per electrode weight (mAh/g)
Cell_A-1	A	3000	3	0.011	20%Al substituted $Ni(OH)_2$	0.0160	305	4.88	1.64(*2)	258	171
Cell_A-2						0.0156	310	4.75	1.67(*2)	233	169
Cell_B-1	B				$Ni(OH)_2$	0.0190	303	5.76	1.05(*3)	282	183
Cell_B-2						0.0198	304	6.01	1.03(*3)	293	186

(*1) Discharge capacities at the 1C rate after charging to 318mAh/g at the 1C rate.

(*2) The NEE values of electrode_A were calculated by considering the Ni contents on $Ni_{0.8}Al_{0.2}(OH)_2$ and phase abundance of the γ-NiOOH in the charged state.

(*3)The NEE values of electrode_B were calculated by dividing the measured capacity by the 289mAh/g on the one electron exchange for $Ni(OH)_2$/NiOOH transformation

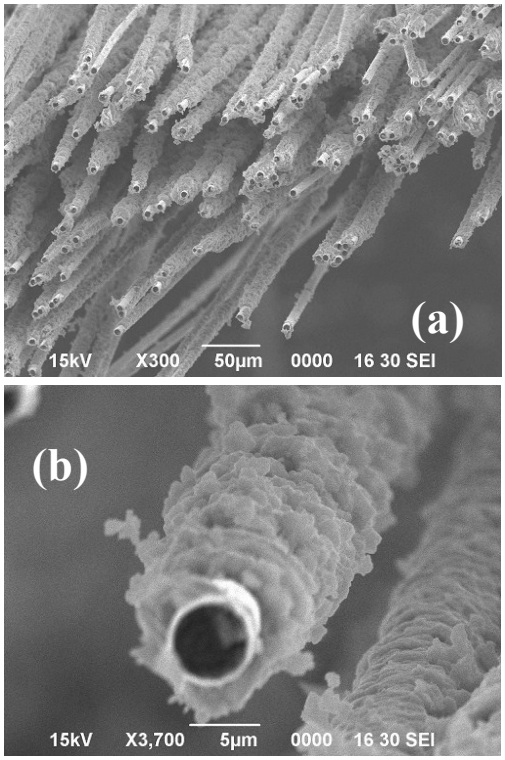

Figure 4.2.1 SEM photographs of the 20%Al fiber-type $Ni(OH)_2$ electrode (a) image of a number of single fibers, and (b) expanded view of a single fiber.

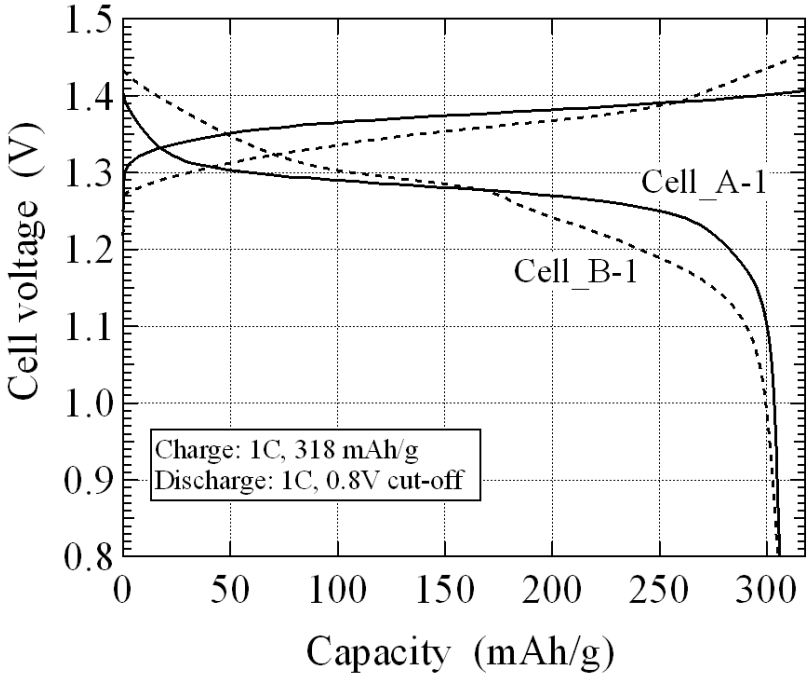

Figure 4.2.2 1C rate charge/discharge curves of cell_A-1 (solid lines) and cell_B-1 (dashed lines).

$Ni_{0.8}Al_{0.2}(OH)_2$ was formed. The nickel content of the electrode_A was 20% less than that of electrode_B. Nevertheless, cell_A-1 exhibited a discharge capacity comparable to cell_B-1. These results suggest that the number of exchange electrons (NEE) of electrode_A is greater than that of electrode_B.

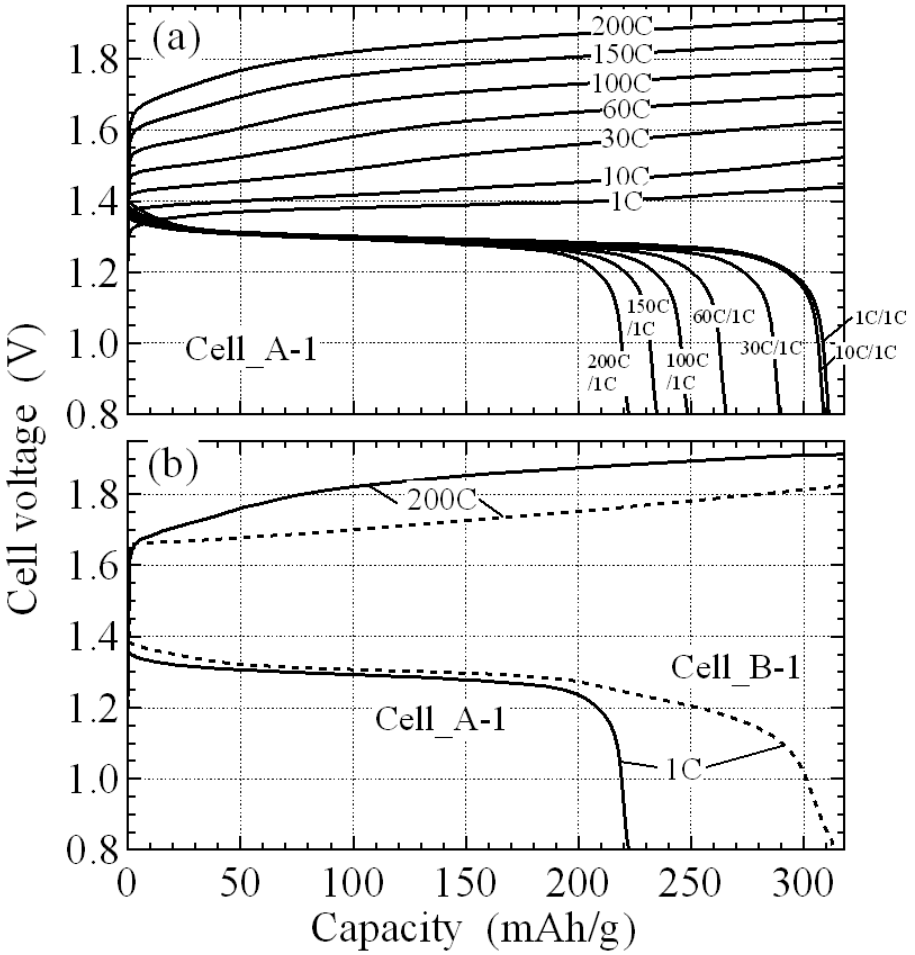

Figure 4.2.3 (a) High-rate chargeability of cell_A-1 at various currents to 318mAh/g, discharged at the 1C rate to a 0.8 V cut-off voltage, and (b) 1C-rate discharge curves after 200C-rate charging for cell_A-1 (solid line) and cell_B-1 (dashed line).

Figure 4.2.3(a) shows the high-rate charging of cell_A-1. After charging to 318mAh/g at a current ranging from the 1 - 200C rate, the cell was discharged at the 1C rate to a 0.8V cut-off voltage. The discharge capacity gradually decreased with the

increasing charging rate. Figure 4.2.3(b) shows the 1C-rate discharge curves for cell_A-1 and cell_B-1 after the 200C-rate charging. The former one exhibited an approximate 220mAh/g discharge capacity, while the latter one was 310mAh/g. This result suggests that the high-rate discharge performance of the fiber-type $Ni(OH)_2$ electrode is degraded by the Al addition.

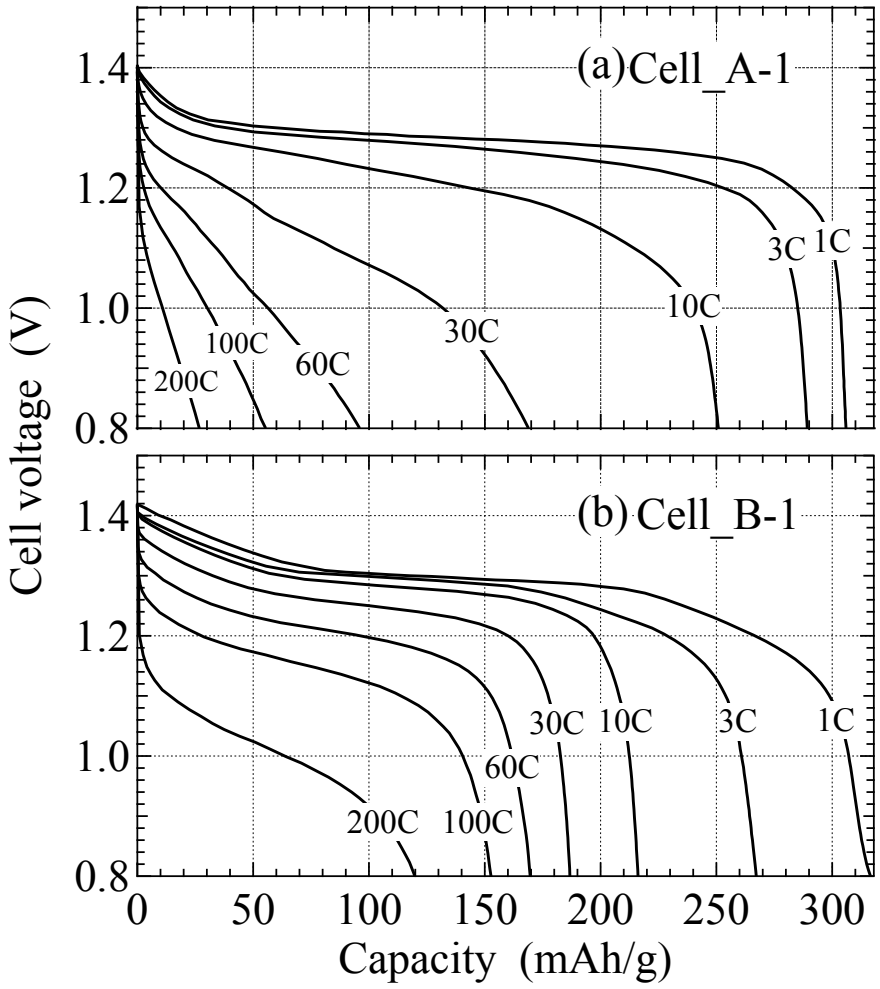

Figure 4.2.4 High-rate dischargeability of (a) cell_A-1 at various currents after charging to 318mAh/g at the 1C rate, and (b) cell_B-1 at various currents.

Figures 4.2.4(a) and (b) show the high-rate discharging of cell_A-1 and cell_B-1, respectively. After charging to 318mAh/g at the 1C rate, the cells were discharged at

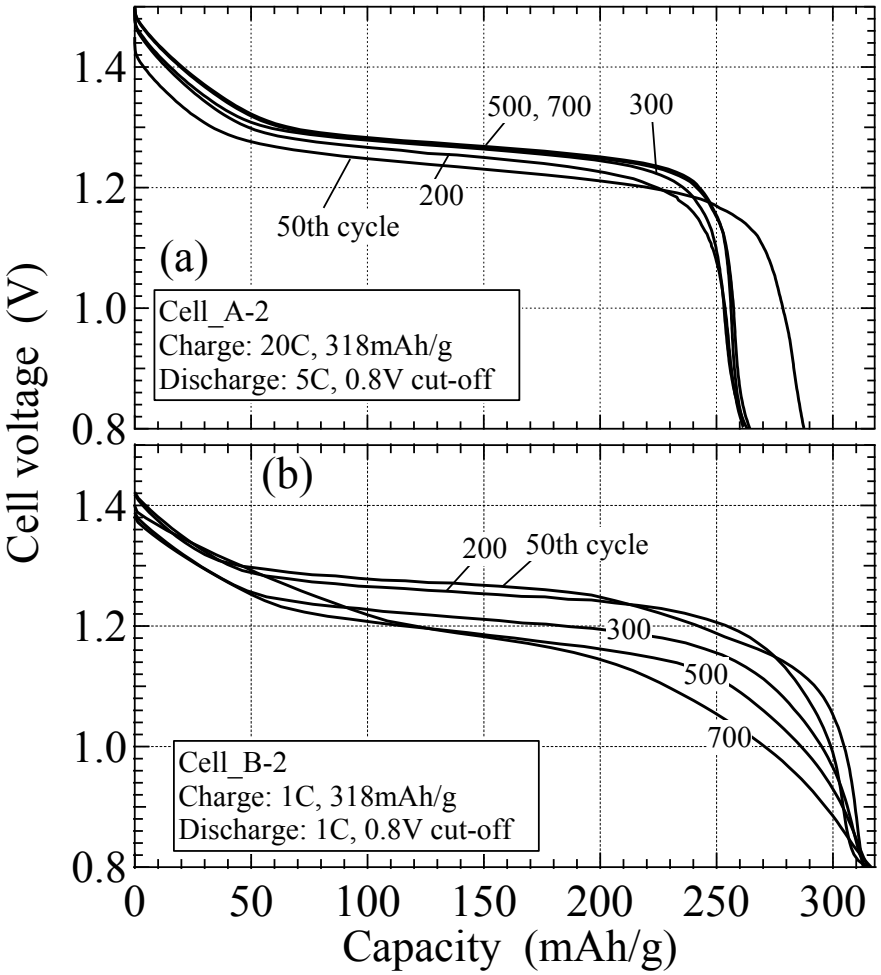

Figure 4.2.5 Cycle-dependent discharge curves of (a) cell_A-2 and (b) cell_B-2 at the 50th, 200th, 300th, 500th and 700th cycles.

various currents ranging from the 1 to 200C rate. At a rate lower than 30C, the capacity of cell_A-1 is comparable or greater than that of cell_B-1. Overall, cell_A-1 exhibited a lower discharge voltage than cell_B-1, especially at the higher rate. The internal resistances of cell_A-1 and B-1 were estimated to be approximately 1300mΩ and 600mΩ, respectively, from the voltage vs. current (*I*-*V*) plots at the 10-second discharge. The resistance value is affected by the battery capacity. For example, in our experiments using the large-sized Ni-MH battery "GIGACELL®" [4 - 7], the resistance value for the 100Ah-cell became approximately 0.2mΩ, while that for the 1Ah-cell became

approximately 20mΩ. In order to compare the internal resistances between these cells, the internal resistance value has to be normalized by multiplying the capacity (Ah) and the resistance value (mΩ). In this case, the internal resistance of cell_A-1 was estimated to be approximately 6.0mΩ·Ah, which is 1.9 times higher than that of cell_B-1 (3.1 mΩ·Ah). These results suggest that the high-rate discharge performance of the fiber-type $Ni(OH)_2$ electrode is degraded by the 20% Al addition.

Figure 4.2.5(a) shows the cycle-dependent discharge curves for cell_A-2 at the 5C-rate. After charging to 318mAh/g at the 20C rate, the cell was discharged at the 5C rate. In addition, the remaining capacity was discharged at the 1C-rate during every cycle. The discharge capacity at the 5C rate (total 5C+1C) was 290mAh/g (310mAh/g) at the 50th cycle. The discharge capacity then began to fade after 50 cycles. At the 200th cycle, the discharge capacity at the 5C rate (total 5C+1C) decreased to 260mAh/g (290mAh/g). This capacity value was maintained from the 200th to 700th cycle. Meanwhile, the discharge voltage maintained the initial characteristics with a wide plateau region and high voltage value even at the 700th cycle. In the case of cell_B-2, no remarkable capacity decay was observed during the 700 cycles, but the voltage faded as shown in Fig. 4.2.5(b). These cycling data suggest that the capacity retention was degraded, while the voltage retention was improved by the 20% Al addition for the fiber-type $Ni(OH)_2$ electrode.

4.2.3.2 XRD patterns of the 20%Al fiber-type $Ni(OH)_2$ electrodes

Figure 4.2.6 shows the synchrotron XRD patterns of the fiber-type 20%Al-$Ni(OH)_2$ electrodes. The as-prepared sample consisted of α-$Ni(OH)_2$. After charging to 318 mAh/g, the γ-NiOOH and α-$Ni(OH)_2$ phases were observed. After the charge/discharge cycles, the discharged electrode consisted of α-$Ni(OH)_2$.

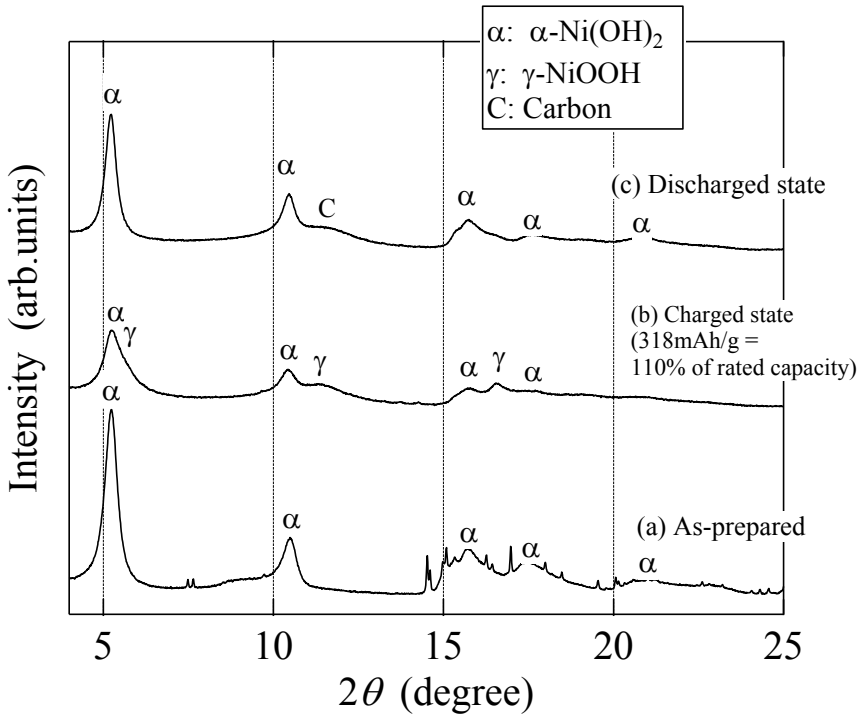

Figure 4.2.6 Synchrotron XRD patterns of the 20%Al fiber-type $Ni(OH)_2$ electrodes (electrode_A) at various states; (a) as-prepared sample, (b) after charging to 318mAh/g, and (c) discharged sample after 50 cycles.

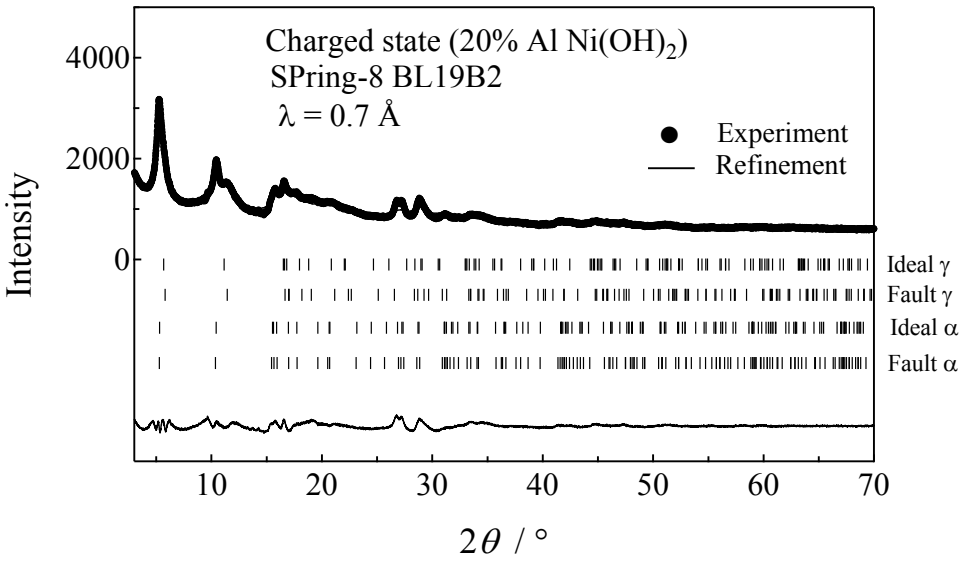

Figure 4.2.7 Synchrotron XRD pattern and the Rietveld refinement results of the 20%Al fiber-type $Ni(OH)_2$ electrode.

Figure 4.2.7 shows a synchrotron XRD pattern with the Rietveld refinement of the 20%Al-$Ni(OH)_2$ electrode in the charged state after 50 cycles. Table 4.2.2 summarizes the refinement results for the charged and discharged states. For the refinement, a model containing a stacking fault [28, 29, 21] was used, in which the α-$Ni(OH)_2$ contains two types of phases, namely, the ideal phase and fault one. The nickel atom is shifted from the (0, 0, 0) site for the ideal phase to the (2/3, 1/3, 0) site for the fault one. The abundance of the fault phase was around 30wt%, which is equivalent to that of the pure fiber-type $Ni(OH)_2$ electrode [24], but is greater than those (20wt%) of the spherical $Ni(OH)_2$ particles [21].

Approximately 80% of the α-$Ni(OH)_2$ phases was transformed into γ-NiOOH during the charging to 318 mAh/g. In addition, the ICP-AES analysis indicated that the $Ni_{0.8}Al_{0.2}(OH)_2$ was formed in electrode_A. The 80mol% nickel would contribute to the electron exchange during charging and discharging. Furthermore, as shown in table 4.2.2(b), approximately 80% of its active material was transformed into γ-NiOOH during charging to 318mAh/g. For the 305mAh/g discharge capacity in Fig. 2, the number of exchanged electrons (NEE) per one nickel atom was estimated to be NEE = 1.64, corresponding to the 3.64 nickel oxidation state in the γ-NiOOH phase. This value is within the range of the previously reported ones of 3.3 – 3.7 [30]. For the total 290mAh/g (5C+1C) discharge capacity at the 700th cycle, the NEE value was estimated to be 1.56. On the other hand, for electrode_B, the NEE values are simply calculated by dividing the discharge capacity by 289mAh/g as the one-electron exchange for the β-$Ni(OH)_2$/β-NiOOH couple reaction. These NEE values are summarized in Table 4.2.1.

Our group (M.Morishita and T. Sakai *et al.*) previously reported the electrode performances of the paste-type α-$Ni(OH)_2$ contained in the Ni-foam substrate [20, 21].

These are examples showing that the Al or Mn-substituted $Ni(OH)_2$ particles are used for the most generally employed electrode structure. They reported that Al-substituted $Ni(OH)_2$ with the α/γ transformation exhibited a higher discharge voltage and capacity than the conventional $Ni(OH)_2$ with the β/β transformation. On the other hand, discharge capacity decrease after 50 cycles.

In reference [21], the NEE value reached 1.41 at the 20th cycle, and then decreased to 1.26 at the 50th cycle. The NEE values are lower than those of the fiber-type electrodes. The capacity retention between the 20th and 50th cycles was estimated to be 89%. Meanwhile, for the fiber-type electrode, the capacity retention between the 50th and 700th cycles was estimated to be 94%. These results suggest that the fiber-type electrode structure is more suitable for the long cycle-life performance than the conventional paste-type one.

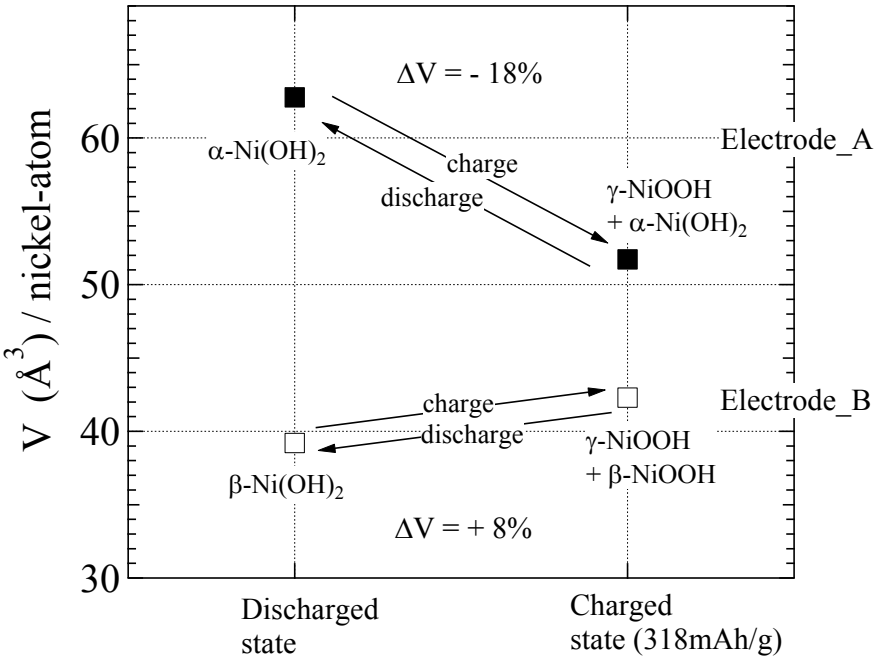

Figure 4.2.8 The change in average lattice volumes of electrodes_A and _B in the charged and discharged states.

Figure 4.2.8 shows the average cell volumes for the charged and discharged states, which were obtained by the linear combination of the cell volumes multiplied by the abundance of each phase. For electrode_A, the volume of the active material layer contracted during charging. The volume change (ΔV) from the α-$Ni(OH)_2$ to γ-NiOOH + α-$Ni(OH)_2$ was estimated to be approximately –18%. During discharging, the active-material layer returned to the original volume. Namely, the volume of the active material does not expand more than the original size. On the other hand, for electrode_B, the volume change from the β-$Ni(OH)_2$ to γ-NiOOH + β-NiOOH was estimated to be approximately ΔV= +8% as previously reported [24].

Figure 4.2.9 shows a schematic view of the cross-sections for the fiber-type electrodes during the charge/discharge process. For electrode_A, the volume-contraction of the active-material layer during charging maintains a good contact between the active-material and the carbon-fiber substrate. This is suggested to be the reason for the good voltage retention during the cycle-life performances of cell_A-2. Meanwhile, the greater volume-change (ΔV = -18%) could cause partial separation of the active material, especially located on the outside of the layer during cycling. The active material, which contributes to the discharge capacity, would decrease during the cycling. This is suggested to be the reason for the capacity decay of cell_A-2. For electrode_B, a small expansion during charging (ΔV = +8%) would allow for the good capacity retention of the fiber-type electrode. Meanwhile, repeated expansions during cycling could weaken the contact between the active material layer and carbon fiber, and the voltage gradually decreases as shown in Fig. 4.2.5(b).

For electrode_B, more than 50wt% of the active-material was transformed into the γ-NiOOH phase during charging [24]. Regardless of the Al addition, the γ-NiOOH phase mainly contributes to the discharge performances of the fiber-type electrodes. The

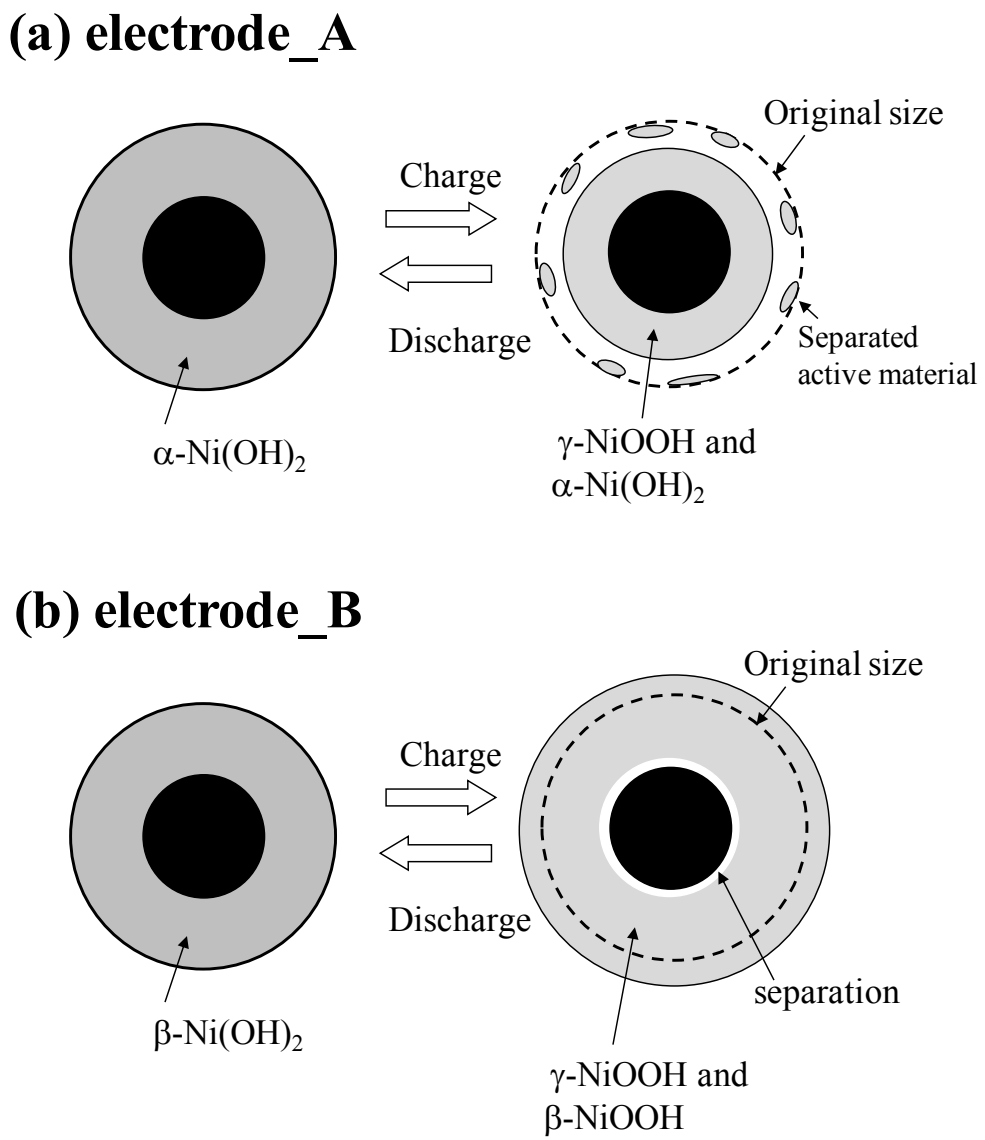

Figure 4.2.9 Schematic views of cross-sections of the fiber-type electrode during charging and discharging for (a) electrode_A and (b) electrode_B.

difference in the high-rate performances between electrode_A and electrode_B could be related to the Al addition, which causes a decrease in the amount of Ni present in the active material, rather than the γ-NiOOH formation. Namely, the internal resistance of electrode_A could be increased by the Al addition. Further investigation in this area is now in progress.

4.2.4. Conclusion

The fiber-type α-$Ni(OH)_2$ electrode was prepared by electrodeposition in a 20mol% aluminum nitrate-added nickel nitrate solution. The discharge curve of the Ni-MH cell containing the 20%Al fiber-type $Ni(OH)_2$ electrode exhibited a wider plateau region than that of the cell containing the pure $Ni(OH)_2$ one. Better high-rate charge/discharge performances were obtained for the pure $Ni(OH)_2$ electrode than for the 20%Al substituted $Ni(OH)_2$ one. During the cycling test, the 20%Al fiber-type electrode exhibited a better voltage retention than the pure $Ni(OH)_2$ one. For the capacity retention, the pure $Ni(OH)_2$ one was better than the 20%Al fiber-type one.

Meanwhile, for the 20%Al substituted $Ni(OH)_2$ with α/γ transformation, the fiber-type electrode structure is more suitable for long cycle-life performances than the generally employed paste-type electrode.

References

[1] T. Sakai, I. Uehara and H. Ishikawa, *J. Alloys. Compd*., 293-295, 762 (1999).

[2] A. Taniguchi, N. Fujioka, M. Ikoma and A. Ohta, *J. Power Sources*, 100, 117 (2001).

[3] K. Shinyama, Y. Magari, K. Kumagae, H. Nakamura, T. Nohma, M. Takee and K. Ishiwa, *J. Power Sources*, 141, 193 (2005).

[4] K. Tsutsumi, *J. Jpn. Inst. Energy*, 87(7), 506 (2008).

[5] Y. Oku, *Kawasaki Technical Review,* 169, 10 (2009).

[6] *High-capacity Fully Sealed Nickel-Metal Hydride Battery [GIGACELL®]*, Kawasaki Heavy Industries, Ltd. (2010).

[7] K. Ishikawa, *Large scale secondary battery for electrical power storage,* chapter 4, p. 113, Nikkan Kogyo Shinbun, Ltd., Tokyo, Japan (2011).

[8] I. Matsumoto, M. Ikeyama, T. Iwaki and H. Ogawa, *Denki Kagaku oyobi Kogyo Buturi Kagaku*, 54, 159 (1986).

[9] M. Oshitani, H. Yufu, K. Takashima, S. Tsuji and Y. Matsumaru, *J. Electrochem. Soc.*, 136, 1590 (1989).

[10] M. Oshitani, M. Watada, H. Yufu and Y. Matsumaru, *Denki Kagaku oyobi Kogyo Buturi Kagaku*, 57, 480 (1989).

[11] M. Yano, T. Ogasawara, Y. Baba, M. Tadokoro and S. Nakahori, *Electrochemistry,* 69, 858 (2001).

[12] E. Higuchi, T. Mizuta and H. Inoue, *Electrochemistry,* 78, 420 (2010).

[13] C. Delmas, J.J. Braconnier, Y. Borthomieu, P. Hagenmuller, *Mat. Res. Bull.,* 22, 741 (1987).

[14] L. Demourgues-Guerlou, C. Delmas, *J. Power Sources,* 45, 281 (1993).

[15] L. Demourgues-Guerlou, C. Denage, C. Delmas, *J. Power Sources,* 52, 269 (1994).

[16] L. Demourgues-Guerlou, C. Delmas, *J. Power Sources,* 52, 275 (1994).

[17] L. Guerlou-Demourgues, C. Delmas, *J. Electrochem. Soc.,* 143, 561 (1996).

[18] P. V. Kamath, M. Dixit, L. Indira, A. K. Shukla, V. Ganesh Kumar, N. Munichandraiah, *J. Electrochem. Soc.,* 141, 2956 (1994).

[19] M. Dixit, P. V. Kamath, J. Gopalakrishnan, *J. Electrochem. Soc.,* 146, 72 (1999).

[20] M. Morishita, S. Ochiai, T. Kakeya, T. Ozaki, Y. Kawabe, M. Watada, S. Tanase, T. Sakai, *J. Electrochem. Soc.,* 155, A936 (2008).

[21] M. Morishita, T. Kakeya, S. Ochiai, T. Ozaki, Y. Kawabe, M. Watada, T. Sakai, *J. Power Sources,* 193, 871 (2009).

[22] S. Deki, A. Hosokawa, A.B. Béléké and M. Mizuhata, *Thin Solid Films,* 517, 1546 (2009).

[23] A.B. Béléké, A. Hosokawa, M. Mizuhata and S. Deki, *J. Ceram. Soc. Japan,* 117, 392 (2009).

[24] T. Takasaki, K. Nishimura, T. Mukai, T. Iwaki, K. Tsutsumi, T. Sakai, *J. Electrochem. Soc.,* 159(11), A1891 (2012).

[25] S. Yoshizawa, Z. Takehara and M. Kato, *Denki Kagaku* 35, 559 (1966).

[26] Y. Sasaki and T. Yamashita, *Denki Kagaku,* 56, 668 (1988).

[27] F. Izumi, T. Ikeda, *Mater. Sci. Forum,* 321-324, 198 (2000).

[28] C. Delmas and C. Tessier, *J. Mater. Chem*., 7, 1439 (1997).

[29] C. Tessier, P. H. Haumesser, P. Bernard, and C. Delmas, *J. Electrochem. Soc*., 146, 2059 (1999).

[30] R. Barnard, C. F. Randell, F. L. Tye, *J. Appl. Electrochem.,* 10, 109 (1980).

4.3 Nickel-metal hydride battery using fiber-type $Ni(OH)_2$ electrode: electrode manufacturing and battery performance

4.3.1 Introduction

In 1990, the nickel-metal hydride (Ni-MH) battery was commercialized in Japan. The Ni-MH battery was used for consumer applications such as cordless and mobile devices, while the demand for this battery is big, and the amount of the production was increased year by year. At present, the lithium-ion (Li-ion) battery is mainly used for the consumer applications because of the higher energy density. On the other hand, the Ni-MH battery exhibits superior performances such as power, cycle-life, safety. In particular, in the use for taking a severe current momentarily, uniformity scale demand for HEV would be expected. Furthermore, application of large-scale battery system using the high-power and safe Ni-MH battery for social-infrastructure, such as a railway and natural power generation, is expected [3-7].

Nickel hydroxide is generally used as active material of alkaline secondary battery including the Ni-MH battery. One of the technical problems of this material is the expansion and contraction during charge and discharge process. The low electrical conductivity is also the problem. When the positive electrode is produced, adhesion between the active material and the substrate and the conductivity has to be improved. In 1900s, W. Junger developed the Ni-Cd battery using the pocket-type electrodes. In the electrode, the active material powder mixed to graphite was filled in the nickel-plated punched steel [8, 9]. On the other hand, Edison developed a tube-type electrode, which consists of metal tube containing the material alternately laminated nickel hydroxide and nickel foil. And the electric vehicle (EV) was run by using the Edison's Ni-Fe battery. After the 1920s, the sintered nickel electrode was invented, and the high-power performance of the alkaline secondary battery was significantly

improved. In this electrode, active material is chemically impregnated into the porous nickel substrate prepared by sintering process. [8, 10-15]. In the 1980s, a paste-type method was developed in order to iprove the energy density of the nickel positive electrode [9, 10]. In this method, high density spherical $Ni(OH)_2$ powder is loaded on Ni foam substrate. Moreover, the Co-coating technique increased the active material utilization. [16] – 20].

In order to realize the widespread use of Ni-MH battery into the large-scale industrial use, the high-power performance have to be improved. In our previous studies, a fiber-type nickel hydroxide electrode, namely the $Ni(OH)_2$ layer formed on a nickel-plated carbon fiber, was developed [21, 22]. The small sized electrode with a 5mAh rating exhibited super high-rate charge and discharge performances at the 100 ~ 500C rates. In order to construct the larger sized battery using the fiber-type electrode, we constructed a fiber-electrode manufacturing apparatus. A battery with the 350mAh rating was constructed using the produced meter-sized fiber-type electrode. The charge-discharge performance was performed.

4.3.2 Experimental

The fiber-type $Ni(OH)_2$ electrode was prepared by use of a home-made manufacturing equipment as shown in Fig. 1. As the 1st step, 12,000 carbon fiber-tow was sent from a wind-roll to the equipment, and the fiber-tow was spread into a seat with an approximate 4cm width by blowing air.

Then, the spread tow was sent into the first bath and metallic nickel was electroplated on the fibers.

After that, the nickel-plated fiber-tow was sent to the second bath, and the $Ni(OH)_2$ layer was formed on the plated layer. At the third bath, the fiber-type $Ni(OH)_2$ electrode

was immersed in the alkaline solution. Table 1 summarizes the compositions of the bath solutions.

Scanning electron microscope (SEM, S-3000N, HITACHI Co. Ltd) was used for the observation of fiber-type electrode.

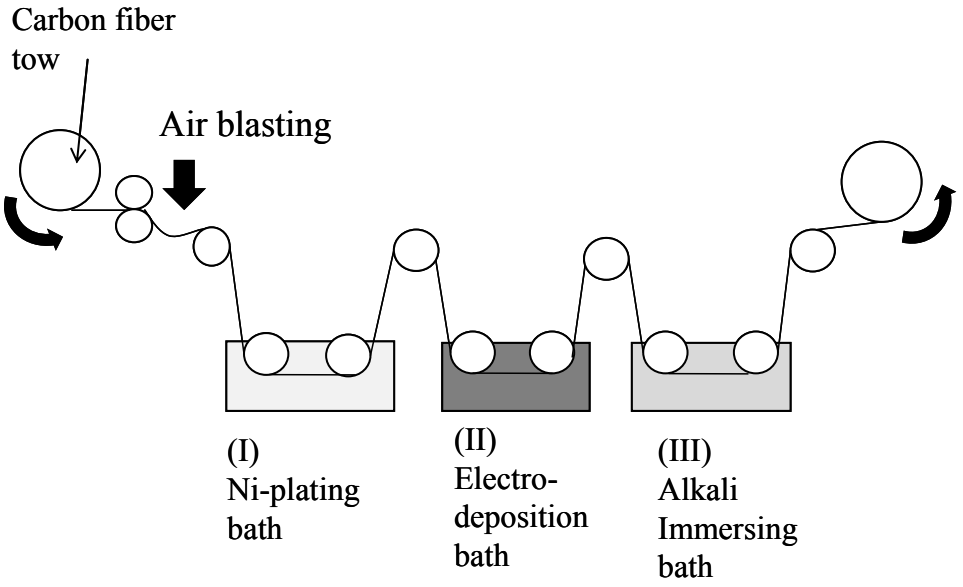

Figure 1. Consecutively manufacturing fiber-type electrode manufacturing system.

Table 1: Bath composition and temperature for the fiber-type electrode manufacturing

Number of bath	Composition	Bath temperature (K)
(I) Nickel plating bath	$Ni(NH_2SO_3)_2$ (450g/L) / H_3BO_4 (30g/L) / $NiCl_2$ (15g/L)	328
(II) $Ni(OH)_2$ deposition bath	$Ni(NO_3)_2 \cdot 6H_2O$ (0.3mol/L)	328
(III) Alkaline bath	NaOH (5mol/L)	333

After cutting in 3.5cm length as shown in Figure 2(a), the fiber-type electrode was lined up in the direction perpendicular to the fiber direction as shown in Figure 2(b). Then, the both terminals of the fibers were clipped by a Ni-foam frame. After the pressing, the positive electrode using fiber-type electrode was gotten. The negative electrode was prepared by the paste-method, namely, the $RE_{0.9}Mg_{0.1}Ni_{3.9}Al_{0.2}$ alloy powder mixed to styrene-butadiene-rubber (SBR; the binder material) and carboxyl

methylcellulose (CMC; thickening agent) was loaded on Ni-foam. The positive and negative electrodes were spirally wounded with a non-woven polypropylene separator as shown in Figure 2(c). The electrode block was inserted into the battery case, and the terminals were connected to get the test cell (Cell#1). The electrolyte was 30wt. % KOH with 30gL^{-1}LiOH. A paste-type positive electrode consisting of $Co(OH)_2$ coated spherical $Ni(OH)_2$ powder (Tanaka Chemical CZ) and CMC was prepared and spirally wounded to construct the test cell (Cell#2) for comparison. Specification of Cell#2 is equivalent to that of Cell#1 except for the positive electrode. Table 2 summarizes the test cell's specifications.

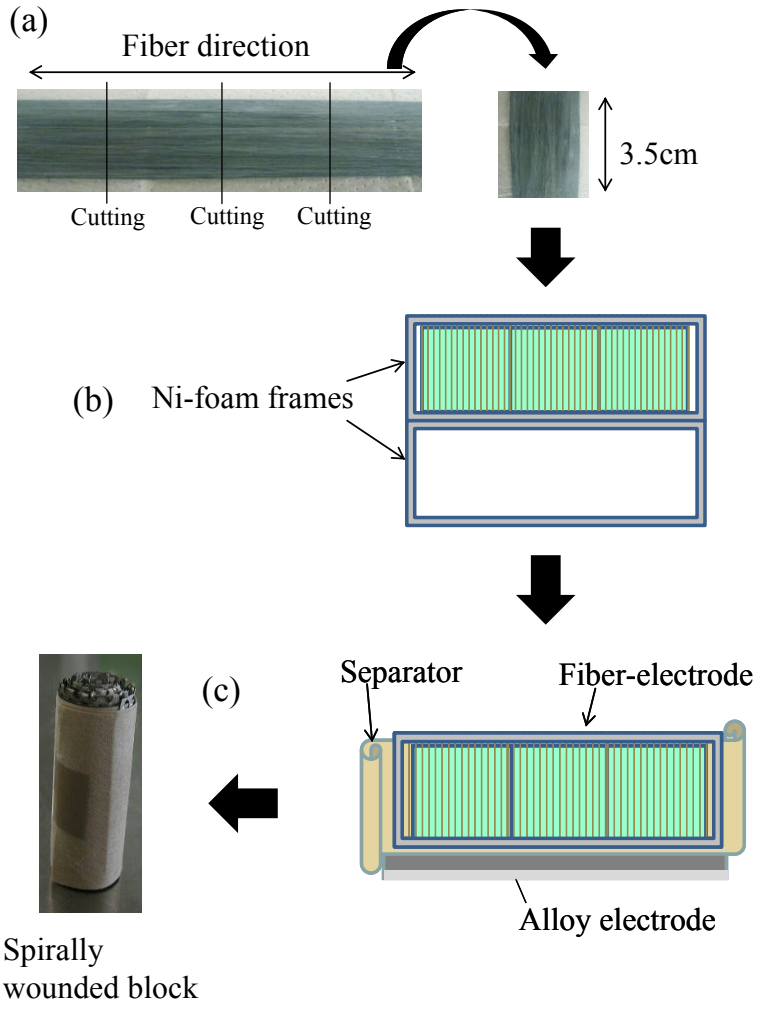

Figure 2(a) the fiber-type electrode 2(b) Ni-foam frames 2(c)Separator and alloy electrode

Table2 : Positive elecrtrode specifications used for cylinder-type cells

	Substrate	$Ni(OH)_2$ loading process	Rated electrode capacity (mAh)	Conductive agent (addition)	thickerning agent (addition)	Capacity per electrode volume (Ah L^{-1})
Cell#1	Ni-plated carbon fiber	Electrodeposition on the Ni-plated carbon fiber	357	-	-	128
Cell#2	Ni-foam	Filling the $Ni(OH)_2$ containig slurry on the Ni-foam	403	CoOOH coating (5wt%)	CMC (0.2wt%)	123

4.3.3 Results and discussion

Figure 3 shows the SEM image of the fiber-type electrode prepared by electrodesposition process. On each carbon fiber, the $Ni(OH)_2$ layer with an approximate 2□m thickness is confirmed.

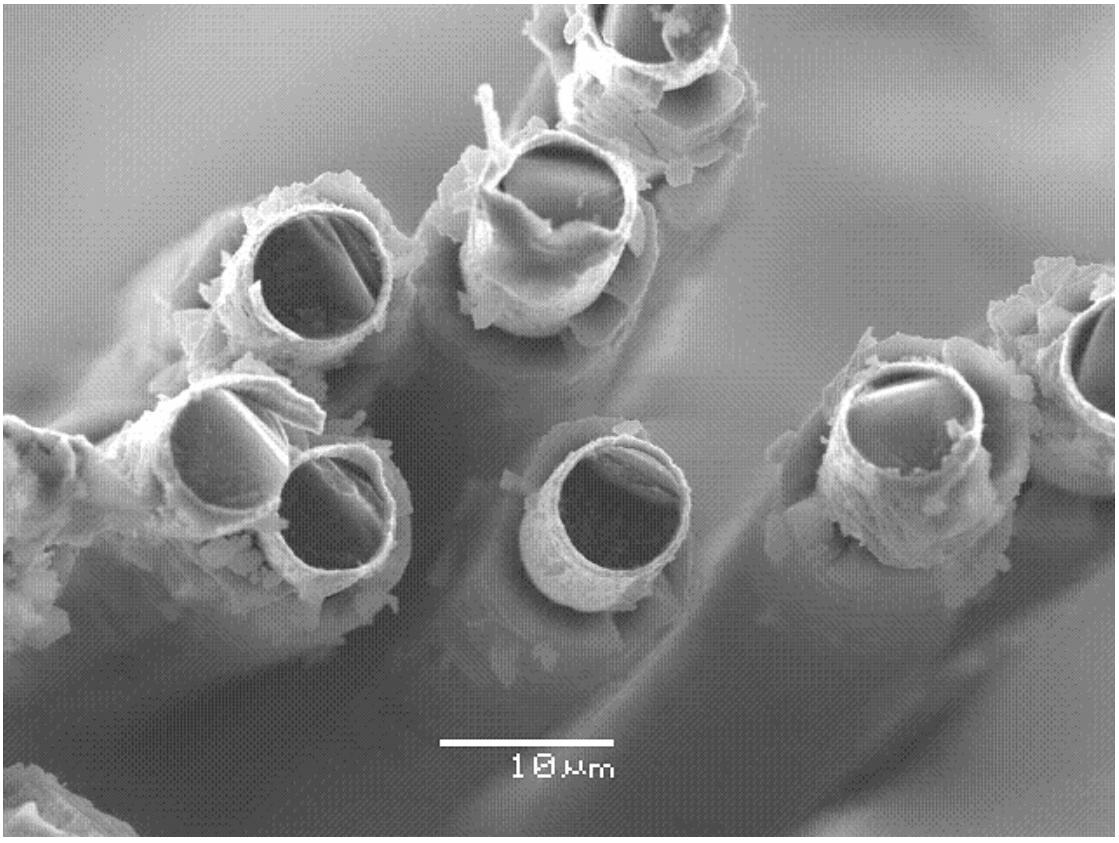

Figure 3 SEM image of the fiber-type electrode prepared by electrodesposition process.

Figure 4 shows the relationship between the elapsed time after the electrodeposition and the deposition weight. Fiber-type electrode obtained by 30 minutes continuous deposition was cut in 70mm length, and their deposition weights were measured. An approximate 3mA/cm^2 deposition current gave the relatively stable deposition in the range of 0.09 ~ 1.0g/70mm. The pH measurement every 5 minutes shows that the pH in the second bath keeps a constant value as shown in Fig. 4(b).

Homogeneous fiber-type electrode was continuously produced using the manufacturing equipment.

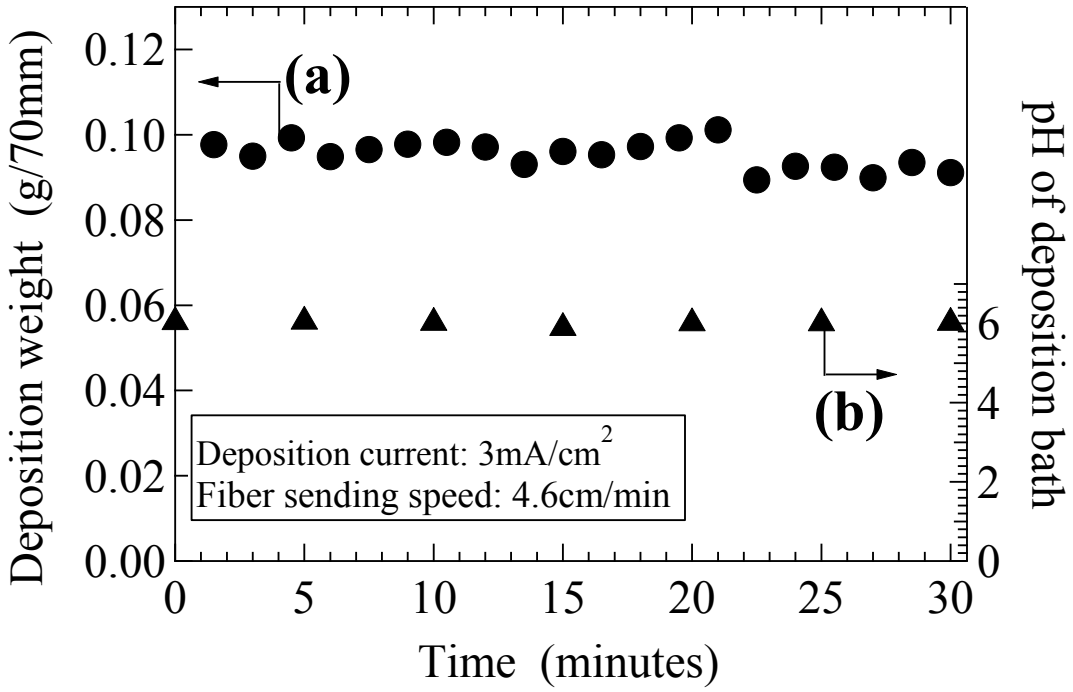

Figure 4 relationship between the elapsed time after the electrodeposition and the deposition weight.

Figure 5(a) shows the high-rate discharge curves for Cell#1 using the fiber-type electrode. After charging to 110% of the rated capacity at the 1C rate, the cell was discharged at various current ranging from the 1 to 70C rate. At the 30C rate discharging, 70% of the rated capacity was delivered. Even at the 70C rate, an approximate 50% was maintained. Figure 5(b) shows the discharge performance of Cell#2 using the paste-type electrode. The capacity reduction with increasing the rate was greater than that of Cell#1.

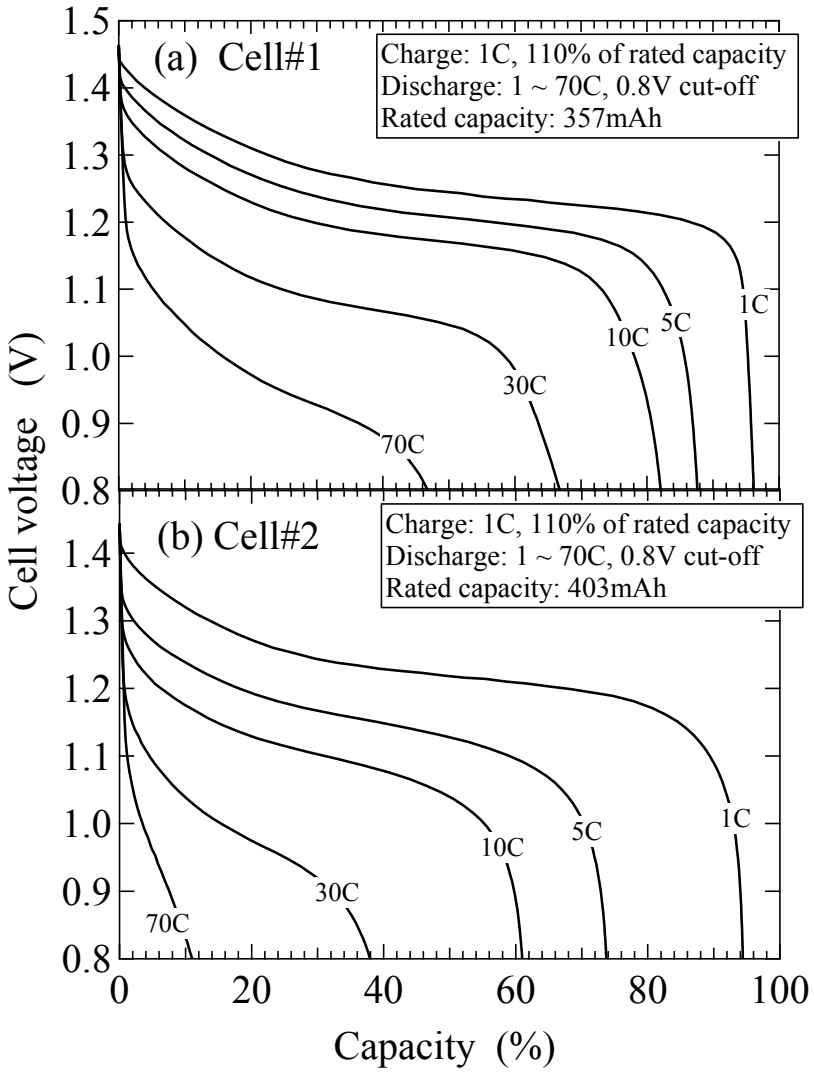

Figure 5(a) High-rate discharge curves for Cell#1 using the fiber-type electrode. 5(b) using the paste-type electrode.

Figure 6 shows the voltage vs. current (*I-V*) plots at the 5second and 10-second discharge for Cell#1 and Cell#2. The voltage value is straightly decreased dependent on the discharge current at the 10~ 70C rates. Table 3 summarizes the internal resistance values obtained from the slope of the line. With increasing the discharge time, Cell#2 exhibited greater voltage drop and internal resistance than Cell#1.

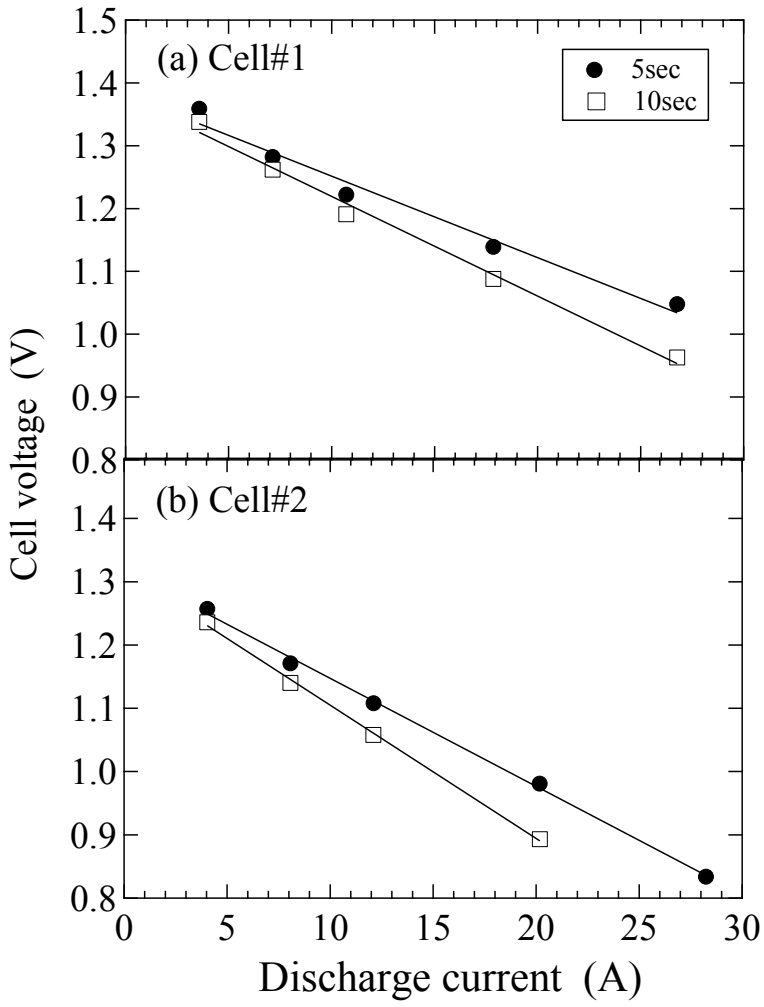

Figure 6 Voltage vs. current (*I-V*) plots at the 5second and 10-second discharge for Cell#1 and Cell#2.

Table 3: Internal resistance (mΩ·Ah)

	5sec	10sec
Cell#1	5.2	5.4
Cell#2	8.5	10.3

The paste-type electrode is obtained by loading the $Ni(OH)_2$ powder with an approximate 10μm diameter on the Ni-foam substrate, and the large energy density per volume with 500 ~ 600 Ah L^{-1} was possible. Generally, in order to obtain a high-power battery using the paste-type electrode, the loading $Ni(OH)_2$ quantity is reduced and the electrode is thinly molded. For Cell#2, the low density with an approximate 120 Ah L-1 permitted the high-rate discharge even at the 70C rate. However, the internal resistance is lower than that of Cell#1, containing the equivalent density of fiber-type electrode. Therefore, for Cell#2, the capacity reduction is greater than that of Cell#1.

The different high-rate performances would be ascribed to the thickness of the active material layers. For the fiber-type electrode, thickness of the $Ni(OH)_2$ layer is approximately 2μm, while for the paste-type one, average diameter of the $Ni(OH)_2$ particle is approximately 10μm. For the latter case, electron and proton would be relatively hard to penetrate inside of the particle detached from the contact area between the substrate and the particle, and the electrochemical reactions would hardly occur.

For the paste-type electrode, some $Ni(OH)_2$ particles are directly collected to the nickel substrate, while the other ones are indirectly collected mediated from the other $Ni(OH)_2$ particles. In order to increase the active material utilization, it is essential to improve the electrical conductivity of the indirectly collected $Ni(OH)_2$. Generally, Co materials such as CoO, $Co(OH)_2$ and CoOOH were coated on the $Ni(OH)_2$ surface. However, the Co material was lain on the interface between the electrolyte and the $Ni(OH)_2$, and the existence of the Co-material layer prevents the ionic conduction, causing internal resistance increasing [21 - 25]. The paste type electrode realized the high-energy density and active material utilization, while the particle size and surface coating would restrict the improvement of the high-rate performance. On the other hand,

the passes of ionic and electronic conduction are separated because the inner nickel layer contribute to the electrical conduction, while the outer periphery of the $Ni(OH)_2$ layer that contact to the electrolyte contribute to ionic conduction. Therefore, the charge and discharge reaction easily occurred compared to the paste-type one, and the high-rate performance was improved.

Generally, a sintered nickel electrode is known as the electrode which is the superior in the high-power performance. This electrode was prepared by the chemical impregnation or electrochemical deposition. [9, 15]. For the latter method, the $Ni(OH)_2$ was directly deposited on the 6 ~ 12μm pore of the sintered nickel substrate by the cathodic polarization in the $Ni(NO_3)_2$ aqueous solution. Then, impurities of the deposited $Ni(OH)_2$ were removed by the chemical conversion treatment in the caustic alkali solution, and there are similarities between the fiber-type electrode and the sintered one on their manufacturing processes. From the microscopic point of view, the sintered nickel layer contribute to the electrical conduction, while the outer periphery of the $Ni(OH)_2$ layer that contact to the electrolyte contribute to ionic conduction. The reaction mechanism is equivalent to that of the fiber-type one.

From the macroscopic point of view, the sintered electrode consists of platy shapes with the 500 ~ 1000mm thickness, while the fiber-type electrode consists of 12000 fibers spread with 4cm width and 50 ~ 150μm thickness. Electrochemical reaction of the fiber-type electrode would proceed more smoothly and show the better high-rate performance than that of the sintered one, because of the thinner electrode structure of fiber-type one. In Ref [10, 11], the high-rate discharge performance of the battery using the sintered nickel electrode is introduced. The batteries consisting of the sintered Ni positive electrode and Cd negative one exhibited less than 0.9V discharge voltage and 50% of the rated capacity at the 18 ~ 20C rate. Meanwhile, in the case of

the fiber-type electrode, 1.1V discharge voltage and 70% of the rated capacity was maintained even at the 30C rate discharge.

The energy density per volume of the fiber-type electrode, which was used for Cell#1 is an approximate 120Ah L^{-1}. The effective density is 100 ~ 300 Ah L^{-1} by considering the previous reports [21, 22]. These values are smaller than the conventional one for the sintered nickel electrode.

The reason for the small density would be ascribed to the space occupying among the fibers. The energy density per volume could be significantly increased if the space was decreased. For example, as shown in Figure.7, the fiber-type electrode, consisting of the $Ni(OH)_2$ layer with the 2μm thickness, is considered. Each fiber was arranged parallel without a gap. The capacity of the fiber-type electrode occupying the space and the space where the fibers occupy (shown as slash-lined area) were calculated as follows

$1.44\times10\text{-}9\bullet n\bullet a$ (L)

$7.21\times10\text{-}7\bullet n\bullet a$ (Ah)

Here, the number of fibers (n) and length of fibers (a) were arbitrary.

The energy density per volume is calculated to be an approximate 500 Ah L^{-1}. In this calculation, the density (3.97g/cm^3) and theoretical capacity (289mAh/g) of β-$Ni(OH)_2$ were used. Although it would be very difficult to remove the space completely, progress of the electrode manufacturing technique would realize the higher-power positive electrode maintaining the energy density equivalent to the sintered one in the future.

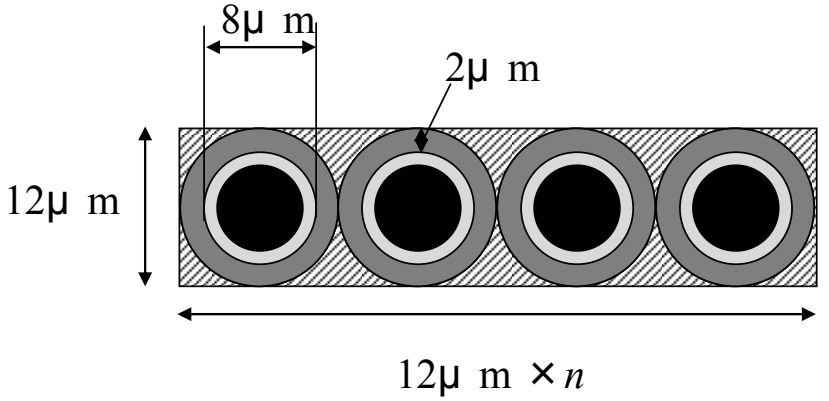

Figure.7 Schematic image of the fiber-type electrode

Figure 8 shows the discharge capacity per electrode weight (= active material + substrate) for Cell#1 and Cell#2. The fiber-type electrode exhibited higher discharge capacity per electrode weight than the paste-type one. For the former case, carbon-based light-weight material is used as the substrate, while for the latter one, the substrate consists of metallic nickel. The difference of nickel quantity occupying the substrate would be the reason.

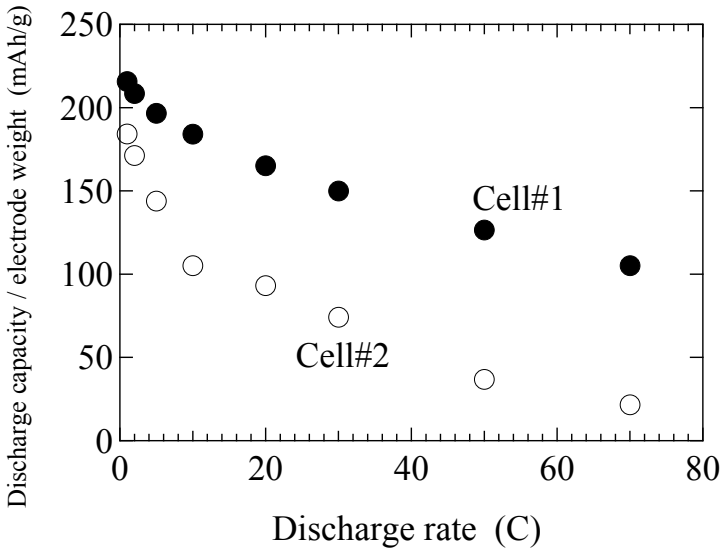

Figure 8 Discharge capacity per electrode weight for Cell#1 and Cell#2.

Figure 9 shows the cycle-life performance of the battery consisting of the spirally rolled fiber-type electrode. The cell construction condition is equivalent to Cell#1. The capacity retention is 90% even after 1400 cycles. The carbon materials were not almost used as the positive conductive material for the alkaline secondary battery because of the low oxidation resistance. As reported in Refs. [23, 24], carbon materials heat-treated more than 2000 degree Celsius exhibited better oxidation resistance, and enables more than 1000 charge and discharge cycles. The carbon fiber used in this study was also heat-treated at more than 2000 degree Celsius. The improved oxidation resistance would improve the cycle-life performance of the fiber-type electrode.

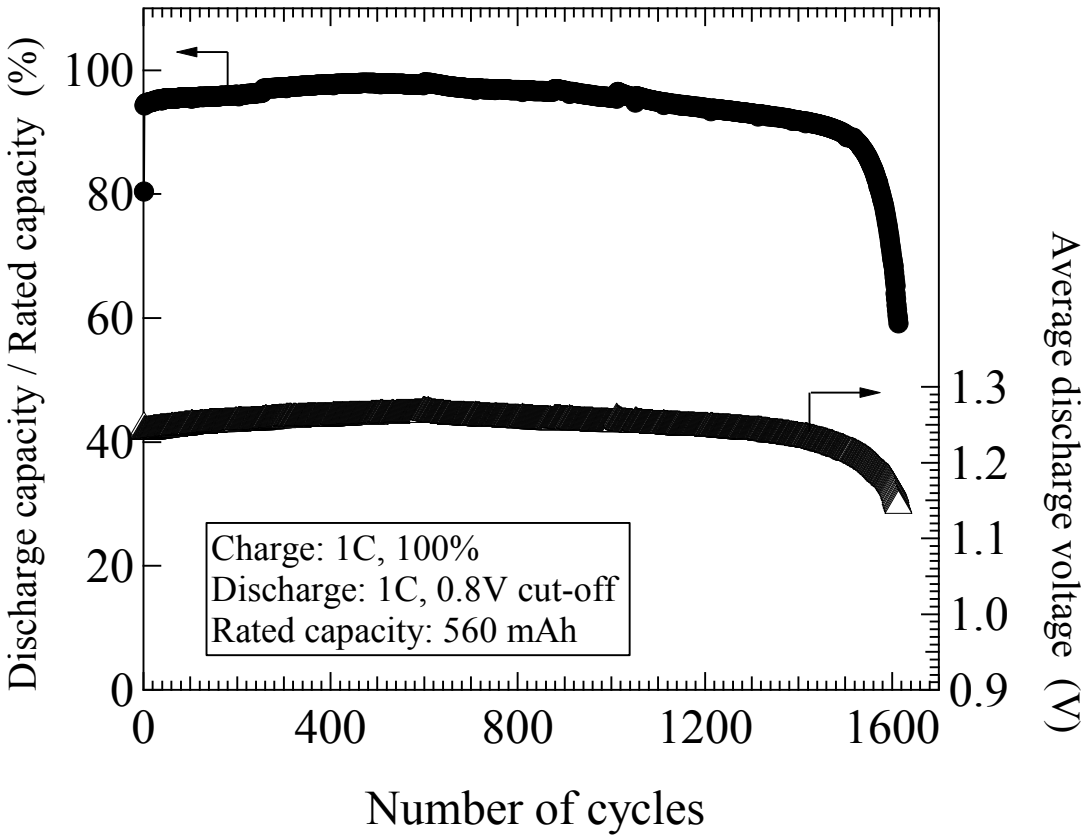

Figure 9 Cycle-life performance of the battery consisting of the spirally rolled fiber-type electrode.

As shown in Fig. 9, spirally rolled fiber-type battery maintained 1.24V average discharge voltage during cycling. In Ref. [21], discharge voltage reduction was reported. The volume expansion and contraction of the active material layer is large and the gradual separation from the substrate and the internal resistance increasing would be the reason for the voltage reduction. It is considered that the difference of the battery structure cause the different battery performances. In the case of Ref [21], the stacked electrodes and separator was put between two acrylic plates, and the four corners were fixed using the bolts and nuts. In this structure, the pressure in the contact area is smaller than that of the spirally wounded structure. Actually, pressure sensitive papers put between the separator and electrode exhibits higher pressure value for the spirally wounded structure than that of the simple-type structure in Ref. [21]. For the former case, overall 2.5MPa pressure was observed, and several 10MPa points were also observed. On the other hand, around 0.2 ~ 0.5MPa was observe in the simple-type cell. Higher pressure in the contact area prevents the active material separation from the substrate and contribute to the improvement of the voltage retention.

4.3.4 Conclusion

The fiber-type electrode was manufactured using the device for consecutively manufacturing fiber-type electrode manufacturing system. Using the meter-sized fiber-type electrode, a spirally wounded structured fiber-type cell with a 350mAh rating (Cell#1) was constructed and the charge and discharge performance was investigated. The cell using a paste-type electrode with the equivalent energy density per volume (Cell#2) was also tested. Cell#1 exhibited superior high-rate discharge performance than Cell#2, and the former internal resistance is half of the latter one.

References

1. T. Sakai, *Funtaigijutsu,* 2(3), 17 (2010) (in Japanese).

2. M. Watada, *Funtaigijutsu,* 2(3), 25 (2010) (in Japanese).

3. K. Nishimura, K. Tsutsumi, *Powder Science and Engineering,* 39(7), 1 (2007).

4. K. Tsutsumi, *Journal of the Japan Institute of Energy,* 87(7), 506 (2008).

5. K. Tsutsumi, T. Matsumura, *Science & Technology in Japan,* 26, 21 (2009).

6. H. Yamazaki, S. Akiyama, T. Hirashima, M. Kataoka, K. Matsuo, *Kawasaki Technical Review,* 170, 16 (2010).

7. K. Ogura, T. Matsumura, C. Tonda, K. Nishimura, M. Kataoka, *Kawasaki Technical Review,* 170, 24 (2010).

8. S. U. Falk, A. J. Salkind, *Alkaline Storage Batteries*, p. 30, John Wiley & Sons, Inc, New York, (1969).

9. Battery enchiridion 3rd Edition(in Japanese)

10. A. Fleischer, *J. Electrochem. Soc.*, 94, 289 (1948).

11. K. Sugita, *Denki kagaku,* 26, 105 (1957).

12. T. Iwaki, M. Fukuda, *Denki kagaku,* 33, 737 (1965).

13. T. Iwaki, K. Kanetsuki, T. Hirai, M. Fukuda, *Denki Kagaku,* 36, 660 (1967).

14. P. K. Ng, E. W. Schneider, *J. Electrochem Soc.,* 133, 17 (1986).

15. “Series on functional chemistry of electrons and ions: Everything about the nickel-hydrogen secondary batteries attracting attention”, NTS Inc. Tokyo, Japan (2001). (in Japanese)

16. I. Matsumoto, M. Ikeyama, T. Iwaki and H. Ogawa, *Denki Kagaku oyobi Kogyo Buturi Kagaku*, 54, 159 (1986).

17. M. Oshitani, H. Yufu, K. Takashima, S. Tsuji and Y. Matsumaru, *J. Electrochem. Soc.*, 136, 1590 (1989).

18. M. Yano, T. Ogasawara, Y. Baba, M. Tadokoro and S. Nakahori, *Electrochemistry (Tokyo, Japan)*, 69, 858 (2001).

19. M. Yao, K. Okuno, T. Iwaki, M. Kato, K. Harada, J-J. Park, S. Tanase, T. Sakai, *Journal of the Electrochemical Society,* 154(7), A709 (2007).

20. E. Higuchi, T. Mizuta and H. Inoue, *Electrochemistry,* 78, 420 (2010).

21. T. Takasaki, K. Nishimura, T. Mukai, T. Iwaki, K. Tsutsumi, T. Sakai, *J. Electrochem. Soc.,* 159(11), A1891 (2012).

22. T. Takasaki, K. Nishimura, T. Mukai, T. Iwaki, K. Tsutsumi, T. Sakai, *J. Electrochem. Soc.,* 160(4), A1 (2013).

23. T. Takasaki, K. Nishimura, M. Saito, H. Fukunaga, T. Iwaki and T. Sakai, *J. Alloys. Compd.,* (2013) in press.

24. T. Takasaki, K. Nishimura, M. Saito, T. Iwaki, T. Sakai, *Electrochemistry*, 81(7), 553 (2013).

25. C. Shao-an, W. Leng, Z. Jianqing and C. Chunan, *J. Power Sources,* 101, 248 (2001).

Chapter 5

General conclusion

General conclusion

The Ni-MH battery is one of the promising candidates as the future energy storage device for various industrial applications, because of the high-power, large-energy density, long cycle-life, reliability, safety and low environmental load. However, the battery materials are very expensive and it would prevent the widespread use of this battery. Development of rare-metal free, in particular Co-free electrodes, which maintains high performance, have to be developed in order to decrease costs. Moreover, the electrode and battery structures, which enhance the high-power performance, should be investigated and developed for further applications.

1. The active material powder was granulated with ORCB, Ni-CF and EVA, and the granulated particles were sandwiched between two nickel-foam pieces to form plate-like electrodes for the Ni-MH battery. The positive electrode with the 5wt% of ORCB, Ni-CF and EVA as additives exhibited the highest discharge capacity. The battery test using the GIGACELL®-type single cells showed that the cycle-life performance was influenced by the separator compression. At a 0.2mmt separator thickness, no remarkable capacity loss was observed for 2000 cycles. The repulsive force dependent on the separator compression would suppress the electrolyte absorption of the electrode and dry out the separator, contributing to an improved cycle-life performance. Heat generation must be minimized when the scale of a battery is expanded. A new method was found for reducing the internal resistance of a Ni-MH battery. The structure of collecting current only by the contact of electrodes rather than having them welded was called GIGACELL, and it was verified that even if the scale of the battery is expanded, the internal resistance is sustained at a certain value.The temperature increase of the battery was kept small by sending air through the structure with a

cooling fan.Performance tests verified that this GIGACELL structure is a battery structure which is suitable for large cells.A lot of improvements were made to resolve the dispersion in the internal resistance of cells, and there is no dispersion in the commercialized GIGACELL of today. The high-performance battery has become one of the key components for environmental protection and its sustainability. KHI has developed a large-sized high-power Ni-MH battery, called the GIGACELL®. This battery shows a great potential for various industrial applications, such as LRV, BPS for railways and stabilization of the power grid. The GIGACELL® will significantly contribute to energy savings and reduction CO_2 emissions in future social-infrastructures. The GIGACELL® is viewed as a competitive candidate for next generation energy storage system.

2. $RE_{0.9}Mg_{0.1}Ni_xAl_{0.2}$ alloys (RE: rare earth, x = 3.9 ~ 4.3) were prepared for producing a low self-discharge nickel-metal hydride (Ni-MH) battery. The alloys contains 4 phases, such as $CaCu_5$-type (1:5H), Ce_2Ni_7-type (2:7H), Ce_5Co_{19}-type (5:19R) and Pr_5Co_{19}-type (5:19H) ones. The phase abundance of the 1:5H one increased with the increasing x value. The capacity retention during the electrochemical test has a correlation to the abundance of the 1:5H phase. Based on the battery test using a cylinder-type sealed cell, the cell using alloy#1 as the negative material exhibited better self-discharge characteristics than that using the conventional $Mm(Ni,Co,Mn,Al)_5$-type alloy. A carbon-coated $Ni(OH)_2$ was prepared by spraying a carbon dispersion onto $Ni(OH)_2$ particles using a fluid-bed coating apparatus. The overcharge and overdischarge performances of the CB-coated $Ni(OH)_2$ are comparable or better than those of the conventional CoOOH-coated one. The CoOOH conductive network is easily damaged by any overdischarge treatment. A Co-free Ni-MH battery consisting of these Co-free

electrodes would combine several good battery characteristics, such as a low self-discharge and overdischarge resistance. The GIGACELL-type Ni-MH cell consisting of these Co-free materials exhibited long cycle-life performances. Good high-rate characteristics were maintained in the GIGACELL-type cell with a 205Ah rating.

3. The fiber-type $Ni(OH)_2$ electrode was prepared by the electrodeposition of pure $Ni(OH)_2$ on nickel-plated carbon fibers. The Ni-MH cell containing the fiber-type $Ni(OH)_2$ electrode can get a higher-rate performance due to good mass transport of the electrolyte. The CoOOH coating, which is indispensable for the conventional paste-type electrode, degraded the electrochemical reactivity of the fiber-type $Ni(OH)_2$ electrode. A comparatively long cycle-life occurred due to low volume expansion of the active-material layer during charging. Meanwhile, a high volume expansion with overcharge affects the cycle-life during several tens of cycles. Meanwhile, the fiber-type α-$Ni(OH)_2$ electrode was prepared by electrodeposition in a 20mol% aluminum nitrate-added nickel nitrate solution. The discharge curve of the Ni-MH cell containing the 20%Al fiber-type $Ni(OH)_2$ electrode exhibited a wider plateau region than that of the cell containing the pure $Ni(OH)_2$ one. Better high-rate charge/discharge performances were obtained for the pure $Ni(OH)_2$ electrode than for the 20%Al substituted $Ni(OH)_2$ one. During the cycling test, the 20%Al fiber-type electrode exhibited a better voltage retention than the pure $Ni(OH)_2$ one. For the capacity retention, the pure $Ni(OH)_2$ one was better than the 20%Al fiber-type one. Meanwhile, for the 20%Al substituted $Ni(OH)_2$ with α / γ transformation, the fiber-type electrode structure is more suitable for long cycle-life performances than the generally employed paste-type electrode. The

fiber-type electrode was manufactured using the device for consecutively manufacturing fiber-type electrode manufacturing system. Using the meter-sized fiber-type electrode, a spirally wounded structured fiber-type cell with a 350mAh rating was constructed and the charge and discharge performance was investigated. The cell using a paste-type electrode with the equivalent energy density per volume was also tested. The spirally wounded structured fiber-type cell exhibited superior high-rate discharge performance than the Cell with a paste-type electrode , and the former internal resistance is half of the latter one.

PUBLICATIONS

1. **Introduction of large-sized nickel-metal hydride battery GIGACELL® for industrial applications**

   Kazuya Nishimura, Tomoaki Takasaki, Tetsuo Sakai

   Journal of Alloys and Compounds,580,S353-S358,2013

2. **Development of Ni-MH battery with a new structure suitable for scaling-up and verification test**

   Kazuya Nishimura, Tomoaki Takasaki, Tetsuo Sakai

   Studies in Scence and Technology,Volume 2,Number 2, 33-36,2013

3. **Development of high-capacity $Ni(OH)_2$ electrode using granulation process**

   Kazuya Nishimura, Tomoaki Takasaki, Tetsuo Sakai

   Studies in Scence and Technology,Volume 2,Number 2, 27-32,2013

4. **Nickel-metal hydride battery using fiber-type $Ni(OH)_2$ electrode: electrode manufacturing and battery performance**

   Kazuya Nishimura, Shiori Katsura, Tomoaki Takasaki, Tetsuo Sakai

   Electrochemistry,82(1),1-5,2014

5. **Cobalt-free nickel-metal hydride battery for industrial application**

   Tomoaki Takasaki, **Kazuya Nishimura**, Makoto Saito, Hiroshi Fukunaga, Tsutomu Iwaki, Tetsuo Sakai,

   Journal of Alloys and Compounds,580,S378-S381,2013

6. **Cobalt-free materials for nickel-metal hydride battery: self-discharge suppression and overdischarge-resistance improvement**

   Tomoaki Takasaki, **Kazuya Nishimura**, Makoto Saito, Tsutomu Iwaki, Tetsuo Sakai,

   Electrochemistry, **81(7)**, 553-558, 2013.

7. **Fiber-type $Ni(OH)_2$ electrode with α/γ phase transformation: high-capacity and high-voltage performances of nickel-metal hydride battery**

   Tomoaki Takasaki, **Kazuya Nishimura**, Takashi Mukai, Tsutomu Iwaki, Kaduo Tsutsumi, Tetsuo Sakai,

   Journal of the Electrochemical Society, **160(4)**, A564-A568, 2013.

8. **Fiber-type $Ni(OH)_2$ electrode for nickel-metal hydride battery: Super high-rate charge/discharge and long cycle-life performances**

   Tomoaki Takasaki, **Kazuya Nishimura**, Takashi Mukai, Tsutomu Iwaki, Kaduo Tsutsumi, Tetsuo Sakai,

   Journal of the Electrochemical Society, **159(11)**, A1891-A1896, 2012.

9. **Preparation and electrode performance of fiber-type Cu-Sn negative electrode for Li-ion battery**

   Jinhan Yao, Tomoaki Takasaki, **Kazuya Nishimura**, Takashi Mukai, Tetsuo Sakai

   Journal of the Electrochemical Society, **160(6)**, A980-A984, 2013.

10. **$LiMn_{0.97}Al_{0.03}O_2$ based carbon fiber electrode possessing high-rate capabilities for Li-ion batteries**

Jinhan Yao, **Kazuya Nishimura**, Takashi Mukai, Tomoaki Takasaki, Kaduo Tsutsumi, Kondo-Francois Aguey Zinsou, Tetsuo Sakai,

ECS Electrochemistry letter, **1(6)**, A83-A86, 2012.

11. **X-ray diffraction characterization and battery performances of fiber-type Li-Mn-O electrode for Li-ion battery**

    Jinhan Yao, Tomoaki Takasaki, **Kazuya Nishimura**, Takashi Mukai, Tetsuo Sakai,

    Electrochemistry,82,(2014) in press.

12. **Lithium manganese aluminum oxide-based full Li-ion battery using carbon fibers as current collectors**

    Jinhan Yao, J.Xie, **Kazuya Nishimura**, Takashi Mukai, Tomoaki Takasaki, Kaduo Tsutsumi,Tetsuo Sakai,

    Ionics,19,1849-1853,2013.

Acknowledgement

The present thesis is a collection of the author's studies that have been carried out at Kawasaki Heavy Industries, Ltd., Kobe University and The National Institute of Advanced Industrial Science and Technology (AIST).

The author would like to gratefully thank Professor Tetsuo Sakai for fruitful supervision and solicitous care. Without this patient instruction, this work could not be fulfilled.

The author wishes to thank Professor Minoru Mizuhata and Professor Qiang Xu for their kind reviewing and valuable comments.

The author sincerely acknowledges valuable discussion and unselfish help of Dr. Tomoaki Takasaki belongs to GIGACELL battery center of Kawasaki Heavy Industries, Ltd. during two years.

The author would like to thank Dr. Kaduo Tsutsumi who was involved in the design and development of the "GIGACELL®" together.

I gratefully appreciate Kawasaki Heavy Industries, Ltd. For giving me the opportunity for this study, financial and helpful supports.

This work would for sure have been impossible to finish without understanding and support which was given to me by my parents and the members of the family. Many deep thanks to all of you.

Kazuya Nishimura

January 2014

In Akashi City, Hyogo, Japan

Doctor Thesis, Kobe University
“Studies on high-power and rare-metal-free nickel-metal hydride batteries for Industrial applications”,178 pages
Submitted on January, 2014
The date of publication is printed in cover of repository version published in Kobe University Repository Kernel.